May 1999 • NREL/SR-520-26127

Subcontractor Report

Photocharge Transport and Recombination Measurements in Amorphous Silicon Films and Solar Cells by Photoconductive Frequency Mixing

Final Subcontract Report
13 May 1994 — 15 January 1998

R. Braunstein, Y. Tang, S. Dong, J. Liebe,
G. Sun, and A. Kattwinkel
University of California
Los Angeles, California

National Renewable Energy Laboratory
1617 Cole Boulevard
Golden, Colorado 80401-3393

NREL is a U.S. Department of Energy Laboratory
Operated by Midwest Research Institute • Battelle • Bechtel

Contract No. DE-AC36-98-GO10337

May 1999 • NREL/SR-520-26127

Photocharge Transport and Recombination Measurements in Amorphous Silicon Films and Solar Cells by Photoconductive Frequency Mixing

Final Subcontract Report
13 May 1994 — 15 January 1998

R. Braunstein, Y. Tang, S. Dong, J. Liebe, G. Sun, and A. Kattwinkel
University of California
Los Angeles, California

NREL Technical Monitor: B. von Roedern

Prepared under Subcontract No. XAN-4-13318-10

National Renewable Energy Laboratory
1617 Cole Boulevard
Golden, Colorado 80401-3393

NREL is a U.S. Department of Energy Laboratory
Operated by Midwest Research Institute • Battelle • Bechtel

Contract No. DE-AC36-98-GO10337

NOTICE

Available to DOE and DOE contractors from:
Office of Scientific and Technical Information (OSTI)
P.O. Box 62
Oak Ridge, TN 37831
Prices available by calling 423-576-8401

Available to the public from:
National Technical Information Service (NTIS)
U.S. Department of Commerce
5285 Port Royal Road
Springfield, VA 22161
703-605-6000 or 800-553-6847
or
DOE Information Bridge
http://www.doe.gov/bridge/home.html


Printed on paper containing at least 50% wastepaper, including 20% postconsumer waste

Preface

The prime candidate material for thin-film photovoltaic high efficient solar cells for large-scale power generation is hydrogenated amorphous silicon and alloys. The objectives of the technology in this field are to achieve stable and efficient units for cost effective bulk-power generation. The strategy in this field is to optimize amorphous thin-film growth for greater efficiency and the reduction of light-induced instability. Material preparation efforts of amorphous semiconductors have concentrated on the reduction of "Urbach" edges, sub-bandgap absorption, and the density of deep defects to the end to maximize the photoconductive gain of the material. Most material efforts have been to optimize mobility-lifetime product ($\mu\tau$) as measured by steady state photoconductivity which does not determine μ and τ separately. To evaluate various photocharge transport models, it is essential that a simultaneous determination of the mobility and lifetime be performed so as to predict the performance of solar cells. We have developed a photomixing technique to separately determine the mobility and lifetime to characterize materials to predict solar cell performance and to allow the testing of new materials and devices in actual solar cell configurations. The present program formed part of the NREL High-Bandgap Alloy Team, the Metastability and the Mid-bandgap Alloy Teams. Various groups were concerned with material synthesis and device fabrication. The UCLA Group performed photoconductive frequency mixing measurements on these material and solar cell devices to determine the optimum growth conditions for photocharge transport. The continuous feedback of the results of the UCLA Group to the synthesis groups relating to material properties to device performance gave insight into the light-induced degradation mechanisms.

Table of Contents

List of Figures

List of Tables

Executive Summary

The continuous decay of electron drift mobility in intrinsic a-Si:H, a-SiGe:H and a-SiC:H upon light soaking was investigated by the photomixing technique. The photoconductivity, lifetime and drift mobility in intrinsic hydrogenated amorphous silicon (a-Si:H) and hydrogenated amorphous silicon carbide (a-SiC:H) while light-soaking were determined using a photomixing technique. In addition to the decay of the photoconductivity and electron lifetime, continuous decay of the electron drift mobility was found during the light soaking process (Staebler-Wronski effect). Experimental data were fitted to a stretched exponential law. Different stretched-exponential parameters for photoconductivity, lifetime and drift mobility were obtained, which indicates the production of defects with different generation kinetics upon light soaking.

The effects of deposition conditions on transport properties of intrinsic a-Si:H, a-SiGe:H and a-SiC:H films were investigated by the photomixing technique. By using the photomixing technique, we have determined the electron drift mobility, lifetime and the conduction band Urbach energy (~ 0.1 eV below the band edge) as a function of preparation techniques. We have found that for the a-Si:H films with increasing deposition temperature, the lifetime (at 480 K) increases, both the drift mobility (at 480 K) and the Urbach energy decrease; and for the a-SiC:H films with increasing hydrogen dilution ratio, both the drift mobility (at 480 K) and the lifetime (at 480 K) increase, and the Urbach energy shows a tendency to decrease.

By using the photomixing technique, we have found that the drift mobility (μ_d) of intrinsic hydrogenated amorphous silicon (a-Si:H) films produced by both glow discharge and hot wire techniques increases with increasing electric field, while the lifetime (τ) decreases with increasing electric field, and the $\mu\tau$ product is essentially independent of the electric field.

Photoemission in air were performed on a-Si:H, a-SiC:H and transparent conducting oxide layers, and revealed inhomogeneities of composition or surface contamination.

The transport properties of intrinsic hydrogenated amorphous silicon samples with the hydrogen content ranging from over 10% to less 1%, which were produced by hot-wire technique at NREL, were systematically studied by the photomixing technique. The effects of deposition conditions on transport properties were investigated as a function of substrate temperature ($290^0C \leq T_s \leq 400^0C$). It was found that with increasing substrate temperature, the lifetime, the drift mobility and the photoconductivity decreased but the Urbach energy (~ 0.1 eV below the conduction band) increased. These results indicate that for the a-Si:H films with increasing deposition temperature, the density of positively charged, negatively charged, and neutral defects all show a tendency to increase in agreement with the results observed by other workers employing other measurement

techniques. The continuous degradation of photoconductivity, lifetime and drift mobility were found during light soaking which obey different stretched-exponential laws which indicates the production of defects with different generation kinetics upon light soaking.It was found that the drift mobility (μ_d) of these samples increases, the lifetime (τ) decreases with increasing electric field, while the mt product is essentially independent of the electric field in the range of 1000 V/cm - 10,000V/cm. The electric field dependence of mobility ($\Delta\mu$) /μ_0/ (ΔE) in the as-grown or/and annealed states are always larger than that in the light soaked state. This electric field dependence of mobility can be explained by the existence of long-range potential fluctuations. Employing a model for potential fluctuations, whose range can be determined employing a model which we have developed.

Preliminary photomixing measurements were performed on Schottky structure, from which such parameters as the products of the thickness of depletion layer and absorption coefficient, barrier potential and transit time were obtained.

Introduction

The research pursued during the past three years under NREL subcontract XAN-4-13318-10 were part of a collaboration with members of the NREL Wide-bandgap Alloy Team and the Metastability and Mid-bandgap Alloy Team. The tasks were concerned with the characterization of the photoconductivity of a-Si:H, a-SiC:H, and a-SiGe:H layers so as to deconvolute the mobility-lifetime products into mobility and response time. In addition the changes of the above parameters in detail as a function of light induced degradation were investigated. The continuous decay of the electron drift mobility in intrinsic a-Si:H, a-SiC:H, and a-SiGe:H upon light soaking was investigated by the technique of photomixing. In addition the effect of deposition temperature and hydrogen dilution on the transport properties of intrinsic a-Si:H and a-SiC:H was also investigated. The dominant approach to accomplish the tasks of the present phase of the program is the technique of photoconductive frequency to separately determine the drift mobility and recombination time. In the following sections the theory of the photoconductive frequency mixing (photomixing), the experimental configuration and the results of the light degradation studies and the characterization of the photocurrent properties of a-Si:H and a-SiC:H prepared by various growth techniques are presented.

Light degradation studies reveal in addition to the decay of the photoconductivity and electron lifetime, continuous decay of the electron drift mobility during the light soaking process. In addition to the generation of defects as recombination centers, defects as charged scattering centers can also be generated upon light soaking. Different generation kinetics for these two kinds of defects were found through stretched-exponential-law analysis.

The effects of deposition temperature and hydrogen dilution ratio an the transport properties of a-Si:H and a-SiC:H were investigated. Our results, together with previous results of other workers, indicate that for the a-Si:H films with increasing deposition temperature, the density of negatively charged defects increases and the density of positively charged and neutral defects decreases; and for the a-SiC:H films with increasing hydrogen dilution ratio, the density of positively charged, negatively charged, and neutral defects all shows a tendency to decrease. The photomixing technique, which can experimentally determine both the drift mobility and lifetime, together with subgap absorption, can provide information not only for the density of midgap defects, but also for the charge state profile of midgap defects.

We observed an electric field dependence of the drift mobility which varies for different sample preparation which lead to the development of a model which accounts for the long range potential fluctuations.

Photoemission measurements to revealed inhomogeneities of composition or surface contaminates.

Photomixing technique for separate determination of mobility and lifetime

We have developed a photomixing technique that allows us to determine both drift mobility and lifetime[1-5]. In the present section we details of the theory and experimental setup of the photomixing technique.

The photomixing technique employed is based on the idea of heterodyne detection for photoconductors. When two similarly polarized monochromatic optical beams of slightly different frequencies are incident upon a photoconductor, the generation rate of electron-hole pairs and therefore the photocurrent produced, when a dc bias is applied, will contain components resulting from the square of the sum of the incident electrical fields. Consequently, a photocurrent composed of a dc and a microwave current due to the beat frequency of the incident fields will be produced; these two photocurrents allow a determination of the mobility and lifetime of the photogenerated carriers.

In the present work, instead of using two lasers, the multiple longitudinal modes of a single laser were used. In this case several microwave signals or photomixing signals with different frequencies can be generated due to the beating of the various laser longitudinal modes. Fig. 1 shows photomixing signals obtained with a Spectra-Physics 125A HeNe laser (20 mW) on a commercial EG&G FND100 diode. The frequencies of the photomixing signals are: 84 MHz, 168 MHz, 252MHz,... 1.092 GHz. This is consistent with the fact that the frequencies (fm) of the longitudinal modes of the laser are given by the following: f_m=mc/2L, where m is an integer, L is the length of the laser cavity and c is the speed of light in the cavity. The variation of the intensity of each frequency component is due to the intensity distribution of the laser modes and the frequency roll-off of the diode. The signal at 252 MHz was the one mostly used, since it has highest intensity.

The phenomenon of photoconductivity originates from the generation of electron-hole pairs to delocalized states by optical excitations. The electron-hole pair generation rate G is proportional to the square of the total electrical field (E) of the incident light, which is the superposition of the electrical fields (E_m) of all the incident beams, i.e.,

$$E = \sum_{m=1}^{l} E_m \exp(i w_m' t + i\Phi_m), \tag{1}$$

where ω_m', ϕ_m are the angular frequency and the initial phase constant, respectively, of the m^{th} optical beam (or mode), and l is the total number of the optical beams (or modes).

If longitudinal modes of a laser are used, then

$$w_m' = w_1' + 2p(m-1)\frac{c}{2L} = w_1' + (m-1)w_{0,} \tag{2}$$

where ω_1' is the lowest frequency of the laser modes, m is an integer, L is the length of the laser cavity, and c is the speed of light in the cavity. For the Spectra-Physics 125 A laser used, ω_0=84 MHz.

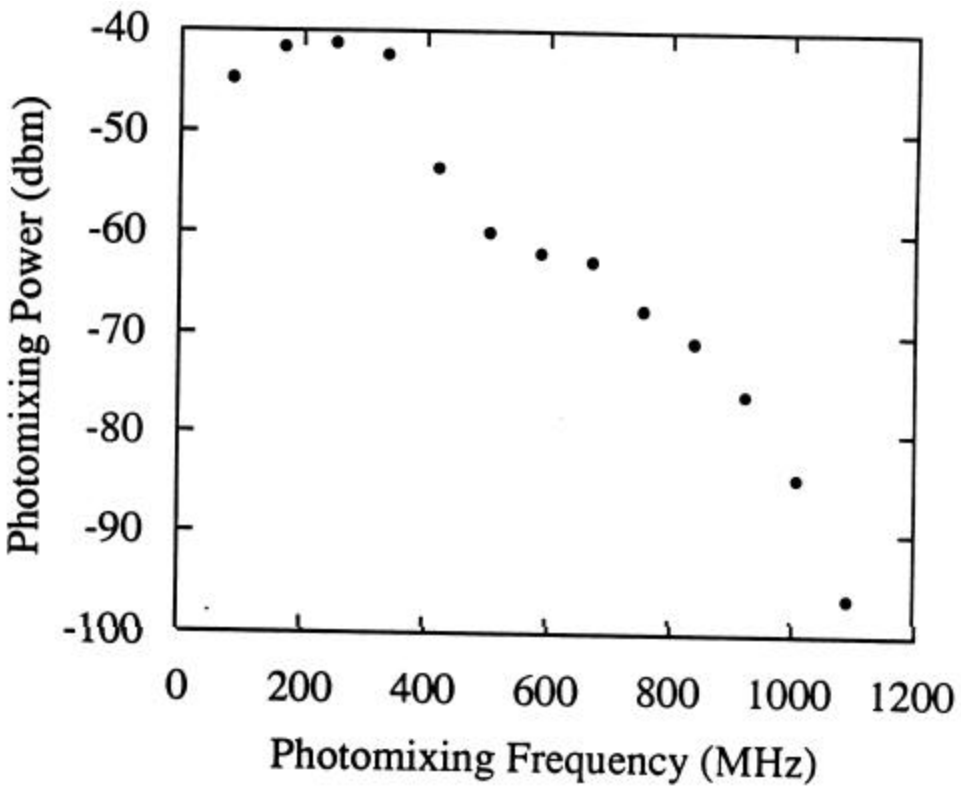

Figure 1. Photomixing signals obtained with a commercial EG&G FND100 diode. The incident laser power was about 20 mW and the dc bias was 90V (back biased). The frequencies of the photomixing signals are: 84MHz, 168MHz, 252MHz, … 1.092GHz. The 252 MHz was the one mostly used, since it has highest intensity. 1 dbm=1mW.

The total generation rate (G) and the generation rate of the m^{th} optical beam (or mode) (G_m) are proportional to the square of the corresponding electrical field, i.e.: $G=C|E|^2$ and $G_m=C|E_m|^2$, where C is a proportionality constant.

The total generation rate G can be further expressed as:

$$
\begin{aligned}
G &= C\Big|\sum_{m=1}^{l} E_m \exp(i w_m' t + i\Phi_m)\Big|^2 \\
&= C\sum_{m=1}^{l} |E_m|^2 + 2C\,\mathrm{Re}\Big(\sum_{m=1}^{l}\sum_{j=1}^{l} E_m . E_j \exp[\, i(w_m' - w_j')t + i(\Phi_m - \Phi_j)]\Big), \\
&= C\sum_{m=1}^{l} |E_m|^2 + 2C\,\mathrm{Re}\Big(\sum_{m=1}^{l-1}\sum_{j=1}^{l-m} E_m . E_j \exp[\, i(w_{j+m}' - w_j')t + i(\Phi_{j+m} - \Phi_j)]\Big)
\end{aligned}
\qquad (3)
$$

With $E_{j+m}.E_j=|E_{j+m}|.|E_j|\cos(\alpha_{j+m,j})$, where $\alpha_{j+m,j}$ is the angle between the two electric fields, which can also take into account the dynamic correlation between the two laser modes. If longitudinal modes of a laser are used, then from Eq.(2): $\omega'_{j+m}-\omega_j'=m\omega_0=\omega_m$. Therefore, the total generation rate G can be rewritten as:

$$G=\sum_{m=1}^{l} G_m + 2\,\mathrm{Re}\Big(\sum_{m=1}^{l-1}\Big(\sum_{j=1}^{l-m}\sqrt{G_{j+m}G_j}\cos(\alpha_{j+m,j})\exp(i\Phi_{j+m}-i\Phi_j)\Big)\exp(iw_m t)\Big). \tag{4}$$

The second term on the right hand side of the above equation has to be further evaluated, since the phase constants are unknown. First we evaluate the following quantity:

$$\begin{aligned}\Big|\sum_{j=1}^{l-m}\sqrt{G_{j+m}G_j}\cos(\alpha_{j+m,j})\exp(i\Phi_{j+m}-i\Phi_j)\Big|^2 &= \sum_{j=1}^{l-m} G_{j+m}G_j\cos^2(\alpha_{j+m,j}) \\ +2\sum_{j'=1}^{l-m}\sum_{j=1}^{l-m}\sqrt{G_{j'+m}G_{j'}G_{j+m}G_j}\cos^2(\alpha_{j+m,j})&\cos(\Phi_{j'+m}-\Phi_{j'}+\Phi_{j+m}-\Phi_{j)}\end{aligned} \tag{5}$$

For a laser without mode locking, the phase differences are random. Therefore, on the average, the second term on the right hand side of the above equation is much smaller than the first term and thus can be neglected to the first order. Consequently,

$$\sum_{j=1}^{l-m}\sqrt{G_{j+m}G_j}\cos(\alpha_{j+m,j})\exp(i\Phi_{j+m}-i\Phi_j)=\sqrt{\sum_{j=1}^{l-m}G_{j+m}G_j\cos^2(\alpha_{j+m,j})}\exp(i\delta_m), \tag{6}$$

where δ_m is a certain phase constant.

By defining

$$G_0=\sum_{m=1}^{l} G_m \quad and \quad \lambda_m=\sqrt{\sum_{j=1}^{l-m}G_{j+m}G_j\cos^2(\alpha_{j+m,j})}\,/\,G_0$$

and with the understanding that only the real part of the generation rate G should be considered, G can be rewritten as

$$G=G_0+2G_0\sum_{m=1}^{l-1}\lambda_m\exp(iw_m t+i\delta_m). \tag{7}$$

G_0, the total dc generation rate, can be determined by the total power of the incident optical beams and can be measured by a conventional photodetector. λ_m, the effective modulation indices, can be determined by a Fabry-Perot interferometer. For a nearly linearly polarized laser beam, $\cos(\alpha_{j+m,j})\cong 1$.

In general, especially for amorphous semiconductors and insulators, there are four processes involved in the phenomenon of photoconductivity (Fig. 2): (1) photo-generation, (2) recombination, (3) trapping -- charge carriers are trapped to the localized states inside the band gap, (4) thermal emission -- trapped charge carriers are thermally emitted back to the extended states. The rate equation for photo-generated electrons, which are often the dominant carriers, in the conduction band in given by [2, 3, 6, 7]:

$$\frac{dn}{dt} = G_0 + 2G_0 \sum_{m=1}^{l-1} l_m \exp(i w_m t + i d_m) - \int_0^{E_d} \frac{dn_T(E)}{dt} dE - \frac{n}{t}. \qquad (8)$$

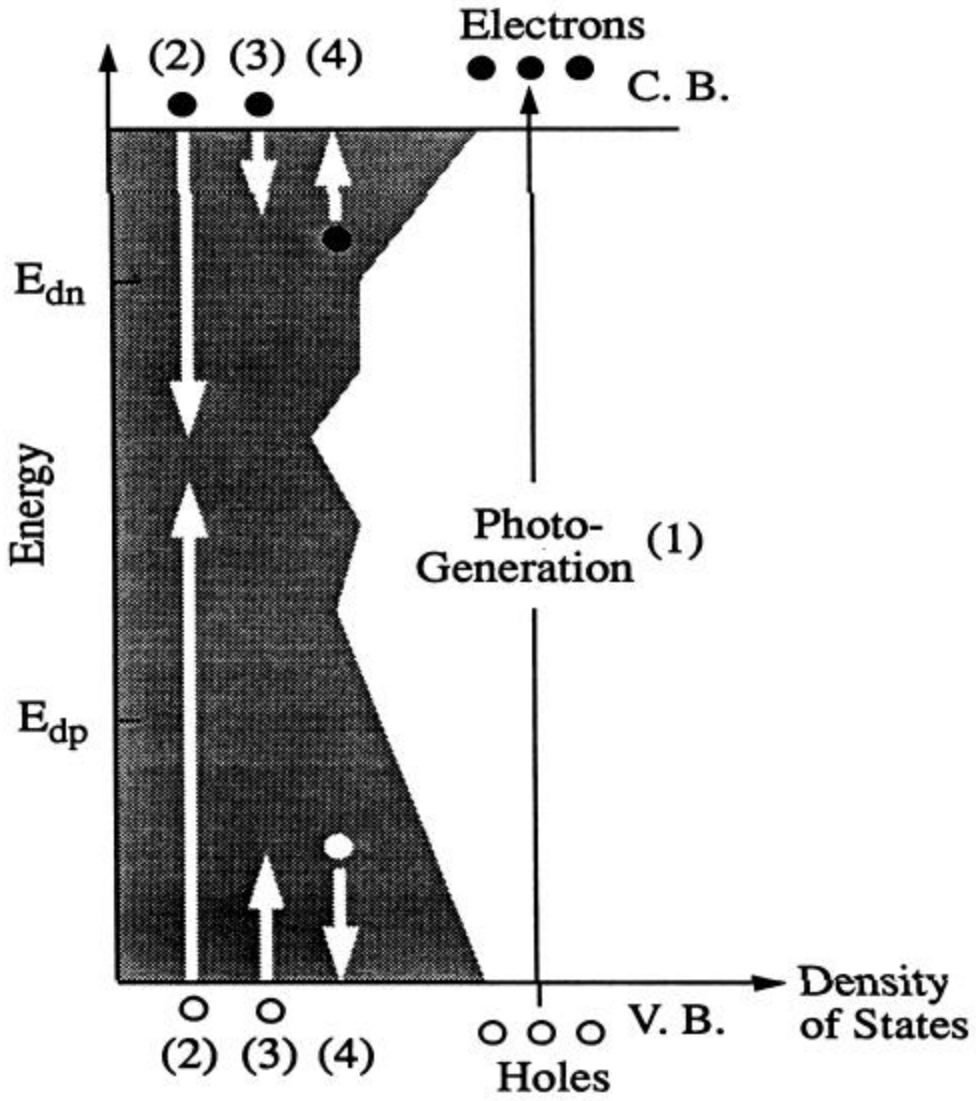

Figure 2. Schematic diagram of the photo-generation (1), recombination (2), trapping (3) and thermal emission (4) processes. Only mono-molecular recombination is considered, since it is usually the recombination process with highest probability. Edn and Edp are demarcation energies for electrons and holes.

The first term on the right is the dc generation term, the second term is the ac generation from the beating of the various laser longitudinal modes with the difference frequencies of ω_m, the integral describes the number of trapped electrons in localized states below the conduction band and above the electron demarcation level E_d due to the trapping and thermal emission processes, and the last term represents the recombination of mobile electrons with trapped holes at a constant recombination rate $1/\tau_R$.

The trapped electron rate equation is given by[7]

$$\frac{dn_T(E)}{dt} = nK[N_T(E) - n_T(E)] - N_c K n_T \exp(-\frac{E}{kT}) \tag{9}$$

where $n_T(E)$ is the density of electrons in the localized states, N_c is the effective number of states in the extended state transport band, N_T is the density of states for the conduction band tail, K is the capture rate; the first term on the right represents the trapping and the second represents the thermal emission of electrons from localized gap states.

Exact solutions for Eqs. (8) and (9) can be obtained[6,7] in the form of

$$n = n_0 \sum_{m=1}^{l-1} n_m \exp(i\omega_m t) \quad wth \qquad n_0 = \tau_R G_0 \quad and \quad n_m = \frac{2 l_m G_0}{(A^2 + B^2)^{1/2}} \exp(i\Phi_m)$$

where, for simplicity the mixing frequency ω_m has been replaced by ω,

$$A = \frac{1}{\tau_R} + \int_0^{E_d} \frac{D^2 K}{1 + \exp[(E_{fn} - E)/kT]} \times \frac{\exp[(E_{fn} - E)/kT]}{D^2 + \{1 + \exp[(E_{fn} - E)/kT\}^2} N_T(E) dE, \tag{10}$$

$$B = \omega(1 + \frac{1}{n_0} \int_0^{E_d} \frac{\exp[(E_{fn} - E)/kT]}{D^2 + \{1 + \exp[(E_{fn} - E)/kT]\}^2} N_T(E) dE), \tag{11}$$

$$and \quad D = \frac{\omega}{N_c K \exp(-E_{fn}/kT)}, \quad E_{fn} = kT \ln(N_c / n_0), \quad and \quad E_\omega = kT \ln(N_c K / \omega).$$

In the above equations E_{fn} is the quasi-Fermi level for electrons and E_ω is a frequency-dependent demarcation energy. Their physical meanings become clear if we rewrite the last two of the above equations as $n_0 = N_c \exp(-E_{fn}/kT)$ and $\omega = N_c K \exp(-E_\omega/kT)$.

Thus, roughly speaking, above E_ω the carriers are in quasi-thermal equilibrium since their thermal emission frequencies are higher than the mixing frequency ω, while those below

E_ω are in deep traps with concomitant emission frequencies less than the mixing frequency ω.

When a dc bias is applied, the resulting dc and root-mean-square ac conductivities are given by[2]

$$\sigma_{dc} = eG_0\mu_0\tau_R, \tag{12}$$

$$\sqrt{<\sigma_{ac}^2>} = \sqrt{2}eG_0\mu_0\frac{l}{\sqrt{A^2+B^2}}. \tag{13}$$

In the case of no trapping, the above equation becomes

$$\sqrt{<\sigma_{ac}^2>} = \sqrt{2}eG_0\mu_0\frac{l}{\sqrt{\omega^2+1/\tau_R^2}}. \tag{14}$$

Comparing the last two equations, one can see that in general the quantity

$$\mu_0\sqrt{\omega^2+1/\tau_R^2}/\sqrt{A^2+B^2}$$

plays the same role in the case of trapping as the extended state mobility μ_0 in the case of no trapping, thus the former can be identified as an effective mobility or drift mobility (μ_d), i.e.,

$$\mu_d = \mu_0\frac{\sqrt{\omega^2+1/\tau_R^2}}{\sqrt{A^2+B^2}} \tag{15}$$

For our photomixing frequency of 252 MHz, ωis about 1.58 GHz (corresponding to a time scale of 630 ps). Since the recombination lifetime τ_R is usually greater than 10 ns, thus $\omega^2\tau_R^2 >> 1$, therefore the above equation can be simplified to

$$\mu_d = \mu_0\frac{\omega}{\sqrt{A^2+B^2}}. \tag{16}$$

From Eqs. (13) and (16) one can see that the drift mobility (μ_d) is an experimentally measurable quantity with no need for any detailed knowledge of trapping and thermal emission, i.e.:

$$\mu_d = \omega\sqrt{<\sigma_{ac}^2>}/(\sqrt{2}eG_0 l), \tag{17}$$

where λ (= 7.05%) is an effective modulation index. Attention is focused on electrons, since they have more dominant contributions to transport in intrinsic a-Si:H and a-SiC:H samples than holes.

The root-mean-square ac photoconductivity was determined through the measurement of the power of the ac or photomixing signal using a Tektronix 492P spectrum analyzer. The drift mobility μ_d can thus be obtained from Eq. (17) and the lifetime t corresponding to μ_d can be written as

$$t = \frac{m_0 t_R}{m_d} = \frac{s_{dc}}{eG_0 m_d}. \tag{18}$$

The photomixing process for single crystalline materials is a special case of the above discussion such that the trapping term in Eq. (8) can be set to zero. In this case, the integrals in the Eqs. (10) and (11) are zero, and Eqs. (17) and (18) give the drift mobility μ_d which is equal to the extended state mobility μ_0 and the recombination lifetime τ_R respectively. In the case of amorphous or polycrystalline materials, the drift mobility μ_d usually is less than the extended state mobility μ_0, but approaches to μ_0 at high frequency or high temperature limit according to Eqs. (10) and (11).

The absolute values for mobility and lifetime can be obtained through the measurement of the absolute values of the microwave photomixing signal and the generation rate.

To see the temperature dependence of the transport properties under trapping, one can use the following approximations for A and B in Eq. (16):

$$A \approx \frac{1}{t_R} + \int_{E_w}^{E_{fn}} KN_T(E)dE, \quad B \approx w + \frac{p}{2} kTKN_T(E_w),$$

if D >> 1 or the frequency-dependent demarcation energy E_ω is well above the quasi-Fermi level E_{fn}, which is true in our case. Therefore, further considering that the recombination effect (the $1/\tau_R$ term in the expression for A) can be proven to be negligible:

$$\begin{aligned} m_d &= m_0 \frac{w}{\sqrt{[w + \frac{p}{2} kTKN_T(E_w)]^2 + [eKN_T(E_w)]^2}} \\ &= m_0 \frac{w}{\sqrt{[w/[KN_T(E_w)] + \frac{p}{2} kT]^2 + e^2 Kg_c}} \exp(kT \frac{\ln(N_c K / w)}{e} \end{aligned} \tag{19}$$

where the distribution of tail states is given by: $N_T = g_c \exp(-E/\varepsilon)$, and g_c is the density of states in the conduction band and e is the spread of the band tail.

Thus by measuring the dc and the ac photoconductivities at a single photomixing frequency as a function of temperature, μ_0, K and ε can be determined through curve fitting according to Eq. (19). The recombination lifetime τ_R is then given by:

$$t_R = \frac{s_{dc}}{eG_0 m_0}.$$

It is interesting to point out that when $\varepsilon > kT$ and the photomixing frequency is much less than certain "trapping frequencies", i.e., $\omega << (\pi/2)kTKN_T(E_\omega)$ and $\omega << \varepsilon K N_T(E_\omega)$, explicit dispersive transport can be obtained from Eq. (19): $\mu_d \mu\, \omega^{1-kT/\varepsilon}$.

Experimental setup of photomixing

The block diagram of the experimental setup for photomixing is shown in Fig. 3. The dc photo-signal was measured by a Keithley 617 Programmable Digital Electrometer, and the photomixing signal, i.e., the ac photo-signal, was measured by a Tektronix 492P Spectrum Analyzer with a frequency range of 50 KHz to 220 GHz. The dc and the ac signals were separated by a low pass filter and a high pass filter, which are incorporated in a bias tee, that was connected to a three stub tuner. By tuning the stub tuner, the reflection of the photomixing signal, which is in the microwave range, from the Spectrum Analyzer can be reduced to nearly zero, and thus the true measurements of the photomixing signal can be achieved. All the equipment were controlled by an IBM PC through a National Instruments Lab-PC card.

Measurements in the temperature range from 80K to 330K were performed with a Janis double vacuum jacket dewar (model 8 DT) and a Lake Shore temperature controller (model DRC 80C). Measurements from 150K to 450K were performed with a vacuum dewar and a software emulated temperature controller constructed in house.

The light sources used for photomixing and light soaking are included in the optical setup, the details of which are show in Fig. 4.

A Spectra-Physics 125A He-Ne laser was used as the light source for photomixing, and a 600 W or a 1000 W tungsten halogen lamp was used as the light source for light soaking measurements. In ordinary photomixing measurements the tungsten halogen lamp was turned off, only the laser beam was focused onto the sample. In light soaking measurements, the light from the tungsten halogen lamp was focused onto the sample, the laser beam can also be focused onto the sample for photomixing measurements in situ with light soaking. In this case the light from the lamp and the laser beam were combined together by a mirror with a hole in the middle.

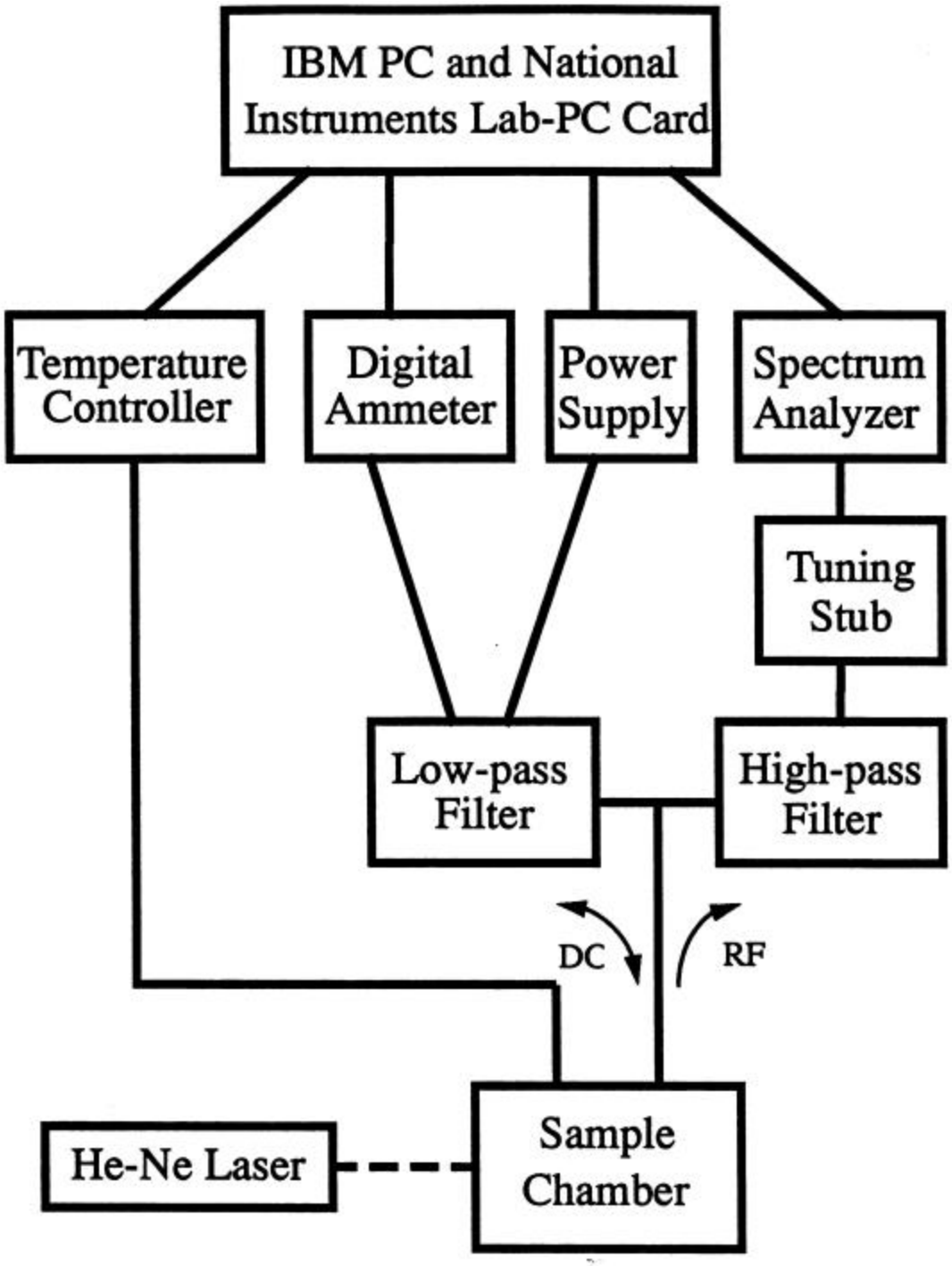

Figure 3. Block diagram of the experimental setup for photomixing.

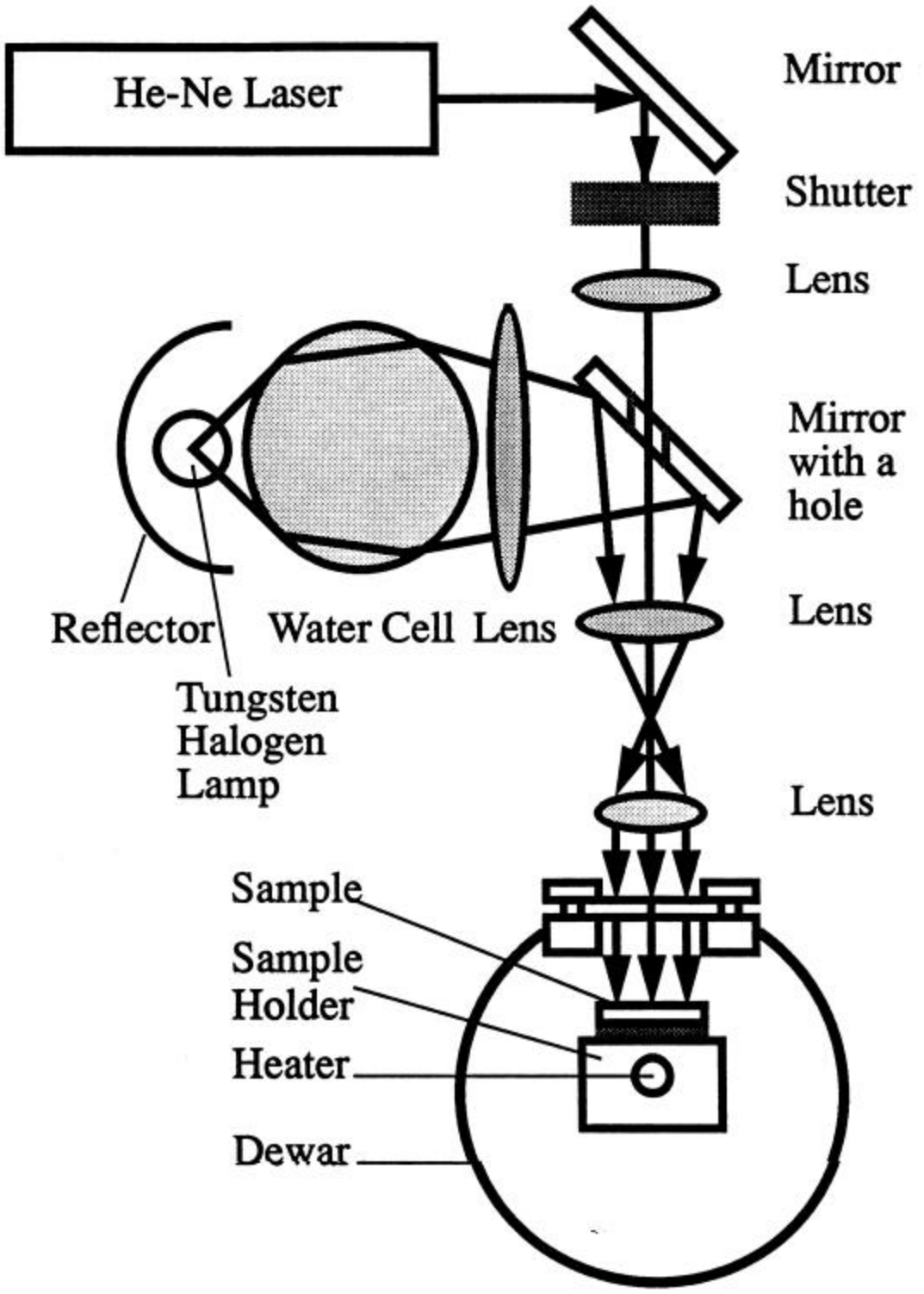

Figure 4. The optical setup for photomixing and light soaking

Results and analysis

The following are the photovoltaic materials studied utilizing the photomixing technique to determine the mobilities and lifetimes in the annealed and under light soaked conditions.

1. Continuous decay of drift mobility in intrinsic a-Si:H and a-SiC:H

2. Effect of deposition on transport properties of intrinsic a-Si:H and a-SiC:H

3. Mobility and lifetime in annealed and light soaked conditions for glow discharge and hot-wire intrinsic a-Si:H

4. Electric field dependence measurements of mobility

5. Electric field dependence of mobility of compensated a-Si:H samples.

6. Photoelectron emission in are from amorphous semiconductors and transport conducting oxides

7. Light induced degradation and the continuous decay of photoconductivity, lifetime and drift mobility of hot-wire intrinsic a-Si:H

8. Temperature dependence measurements and Urbach energy of intrinsic a-Si:H films produced by the hot-wire technique

9. Mobility and lifetime in as-grown, annealed and light soaking conditions of hot-wire intrinsic a-Si:H

10. Electric field dependence of mobility of hot-wire intrinsic a-Si:H films

11. Photomixing measurements on solar cell devices

12. Hot-wire a-SiGe:H alloys

13. Atomic force microscopy study of the surface morphology of hot-wire a-Si:H and the correlation with electrical properties

14. Diluted and undiluted a-Si:H and Electron Cyclotron Resonance produced a-Si:H

15. Spacial dependence of lifetime. Photoconductivity, range and depth of the potential in annealed undiluted a-Si:H

16. Determination of the built-in electric field near Contacts to $CuInSe_2$

1. Continuous decay of drift mobility in intrinsic a-Si:H and a-SiC:H upon light soaking

The intrinsic a-Si:H, provided by the National Renewable Energy Laboratory (NREL), was deposited by glow discharge on Corning 7059 glass at a substrate temperature of 250 C. The sample was 1. 3 μ thick with co-planar chromium contacts. The hydrogen content was about 10%. Measurements were performed at room temperature. The sample was annealed for a few hours before the measurements. The light source for light soaking was a Tungsten Halogen lamp yielding a light intensity of about 2.5 sun at the sample surface and the photomixing signal was obtained by using a He-Ne laser (632.8 nm).

Fig. 5 a-d show the σ_{dc} photoconductivity , power of the photomixing signal P_{mix}, lifetime τ and drift mobility μ_d for the intrinsic a-Si:H sample versus light soaking time. In addition to the decay of the dc photoconductivity and lifetime, continuous decay of the drift mobility can be seen due to light soaking, which reveals a new phenomenon for the Staebler-Wronski effect.

For intrinsic a-Si:H the drift mobility is determined by the trapping of electrons into the conduction band tail and the scattering of electrons by the intrinsic disorder. Both enhanced trapping and scattering can result in the decay of the drift mobility. A question of interest is: which one is the dominant mechanism for the decay of the drift mobility upon light soaking.

The concentration of defects generated by light soaking is usually about $10^{16}cm^{-3}$ for dangling bonds, located near the mid-gap, at saturation level[8] and about $10^{18}cm^{-3}$ for the light induced defects in the valence band tail[9]. Thus it is conceivable that the conduction band tail, with integrated concentration of states of $10^{19}cm^{-3}$, would not be altered by these defects, especially since the frequency dependent demarcation energy E_ω for the photomixing process is about 0.1eV below the conduction band edge,[2,3] where the density of states for the conduction band tail is high ($\sim 10^{20}cm^{-3}eV^{-1}$). Therefore the enhanced scattering has to be the dominant mechanism for the light induced decay of the drift mobility. In order for the light generated defects ($\sim 10^{18}cm^{-3}$) to compete with the intrinsic neutral scatters due to disorder ($\sim 10^{22}cm^{-3}$) of much greater population so as to reduce the drift mobility, part of the light generated defects can be charged so that they can have much greater scattering cross sections and may form long-range potential fluctuations. Without significant changes for trapping, the lifetime t and the drift mobility μ_d are thus proportional to the recombination lifetime τ_R and the extended state mobility μ_0. Therefore

$$\frac{1}{t} \mu \frac{1}{t_R} = N_r s_r n \tag{20}$$

$$\frac{1}{m} \mu \frac{1}{m_0} \mu N_s s_s n \tag{21}$$

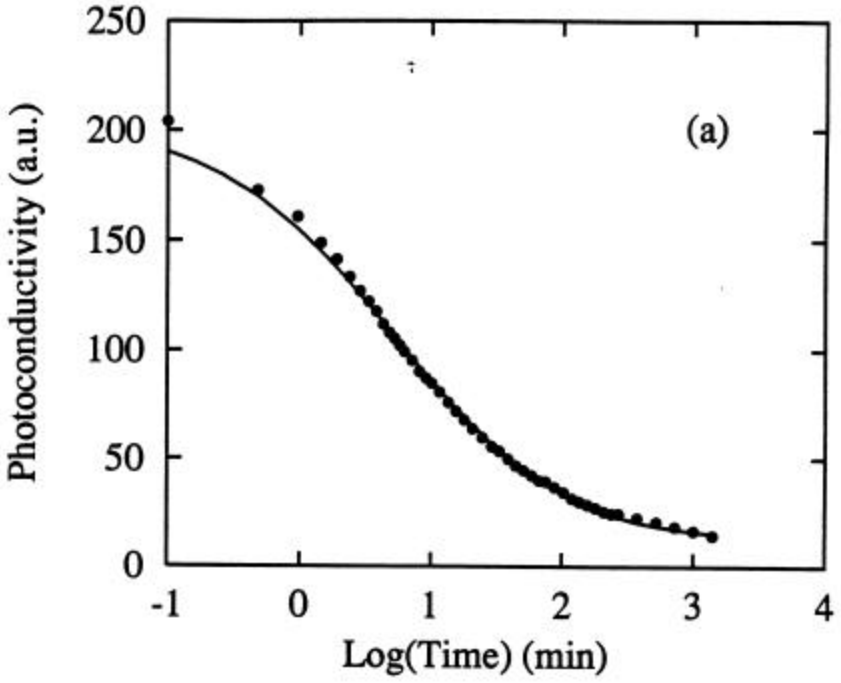

Figure 5(a). The dc photoconductivity for the intrinsic a-Si:H sample versus light soaking time. The solid line is curve fit to the stretched exponential law (Eq. (22)).

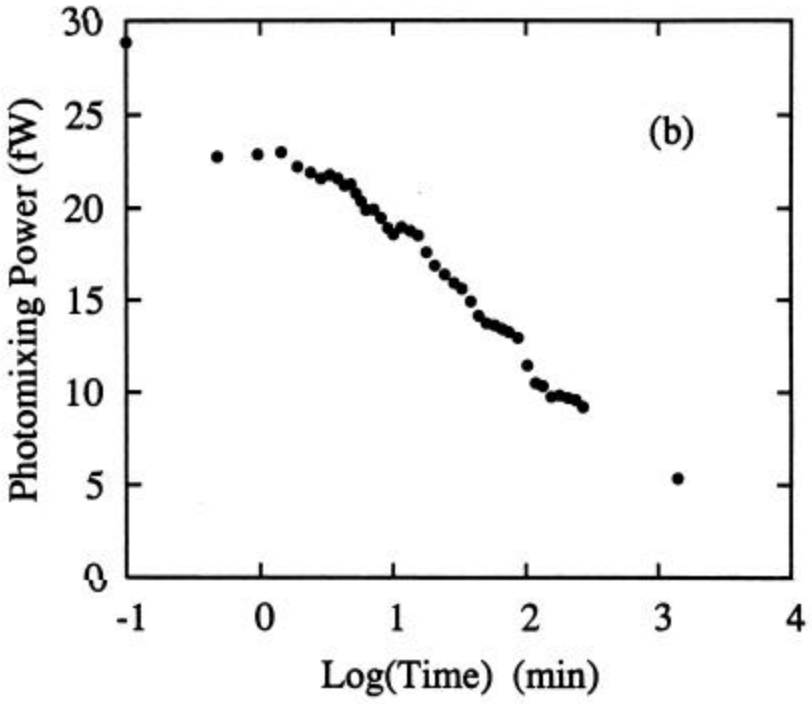

Figure 5(b). Power of the photomixing signal Pmi=5 for the intrinsic a-Si:H sample versus light soaking time.

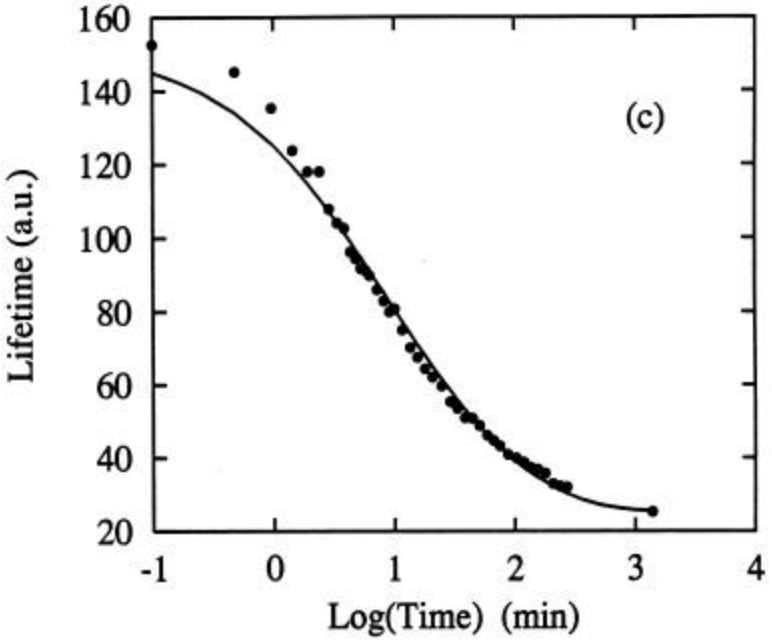

Figure 5(c). The lifetime t for the intrinsic a-Si:H sample versus light soaking time. The solid line is curve fit to the stretched exponential law (Eq. (22)).

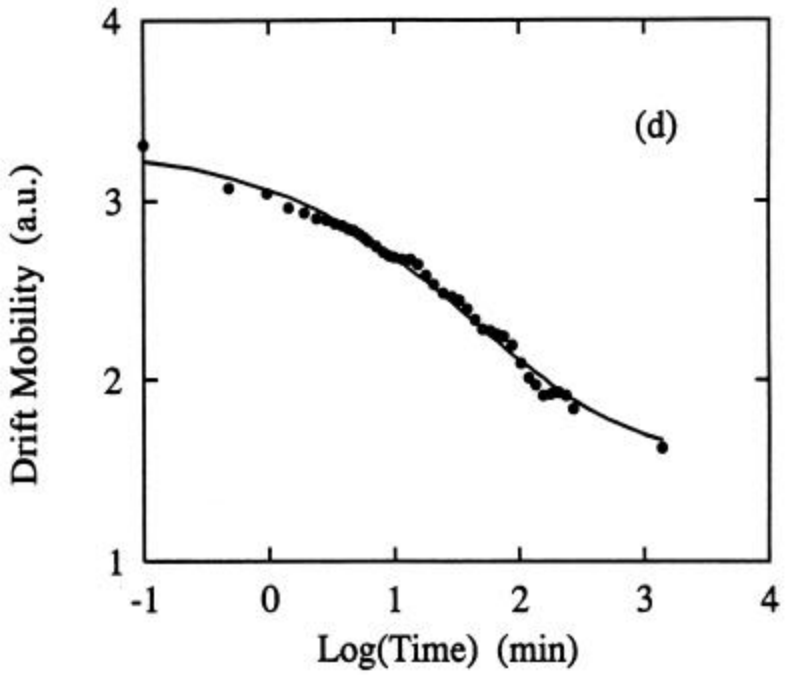

Figure 5(d). The drift mobility md for the intrinsic a-Si:H sample versus light soaking time. The solid line is curve fit to the stretched exponential law (Eq. (22)). In addition to the decay of the dc photoconductivity and lifetime, continuous decay of the drift mobility can be seen due to light soaking. Different stretched exponential parameters were found, which are shown in Table I. The drift mobility md was determined by Eq. and was determined by Pmix.

where N_r, N_s are the effective concentrations of the recombination and the scattering centers, s_r, s_s are the effective recombination and scattering cross sections, and ν is the thermal velocity of charge carriers.

The solid lines in Fig. 5 are curve fit to the following stretched exponential law:

$$N = N_s - (N_s - N_0)\exp[-(t/t_0)^b], \tag{22}$$

by replacing N with $1/\sigma_{dc}$, $1/\tau$ and $1/\mu_d$ respectively, where N is the defect concentration at time t, N_0 and N_s are the initial and saturated defect concentrations, β is the stretching parameter, and τ_0 is the time constant. The results from curve fit are listed in Table I.

Table I. Summary of results from curve fitting for a-Si:H.

	β	τ_0 (min)
From dc Photoconductivity	0.65	300
From lifetime	0.64	130
From Drift Mobility	0.49	160

As can be seen from the above table, different stretched-exponential parameters for photoconductivity, lifetime and drift mobility were obtained, which indicates the generation of defects with different generation kinetics upon light soaking. Our studies so far do not reject any existing microscopic models[10,11,12-17] for the Staebler-Wronski effect, such as weak bond breaking[12-15] and charge trapping[16] models. Rather our studies indicate that combinations of different models may be necessary to explain the generation of defects with different characteristics. The recombination centers for electrons are most likely positively charged or neutral defects, whereas the scattering centers for electrons can be either negatively or positively charged defects. Upon light soaking, in addition to the generation of defects, the defects that serve as deep trapping or recombination centers can be charged, since electrons and holes are trapped to them. This results in enhanced scattering and thus the decay of the drift mobility for electrons. The charged defects may become quasi-stable through some relaxation processes and can also form certain long-range potential fluctuations,[18-22] if they are not spatially correlated.

All the above statements are also supported by the light soaking experiments on the aSiC:H sample. Decay of photoconductivity lifetime and drift mobility upon light soaking were found (Fig. 6 a-c). The solid lines are the curve fit according to the stretched exponential law. The increase for the drift mobility at t~100min during light soaking is probably due to an increase of the sample temperature upon light illumination. Table II shows the results from the curve fit according to the stretched exponential law (Eq. (22)). Different parameters were found for different decay processes.

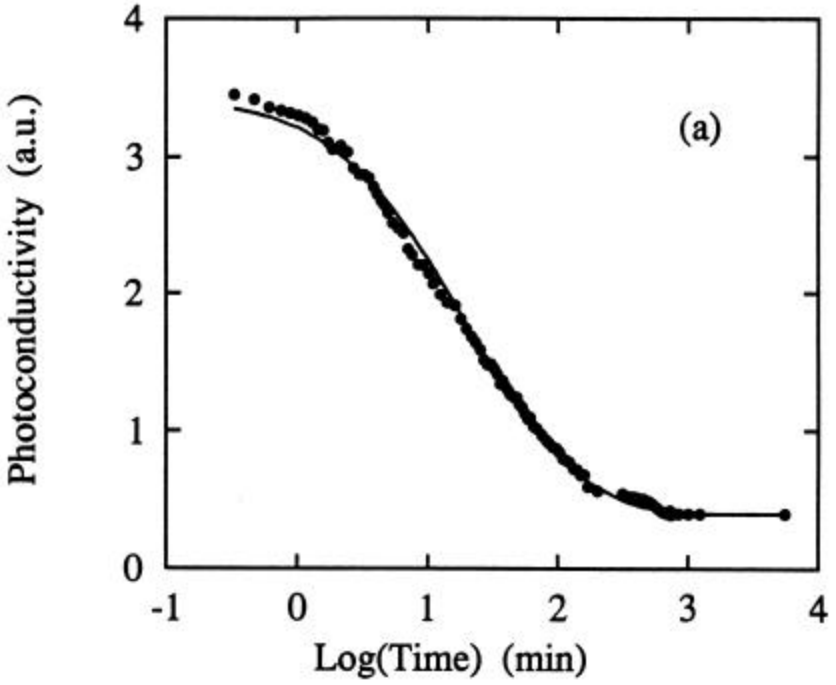

Figure 6(a). The dc photoconductivity for the a-SiC:H sample versus light soaking time. The solid line is curve fit to the stretched exponential law (Eq. (22)).

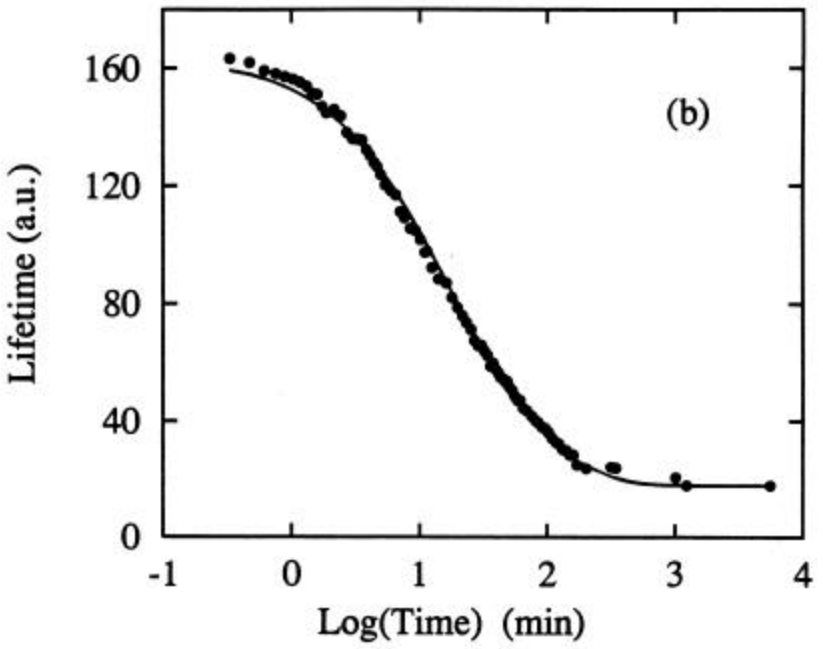

Figure 6(b). The lifetime τ for the a-SiC :H sample versus light soaking time. The solid line is curve fit to the stretched exponential law (Eq. (22)). Different stretched exponential parameters were found, which are shown in Table II.

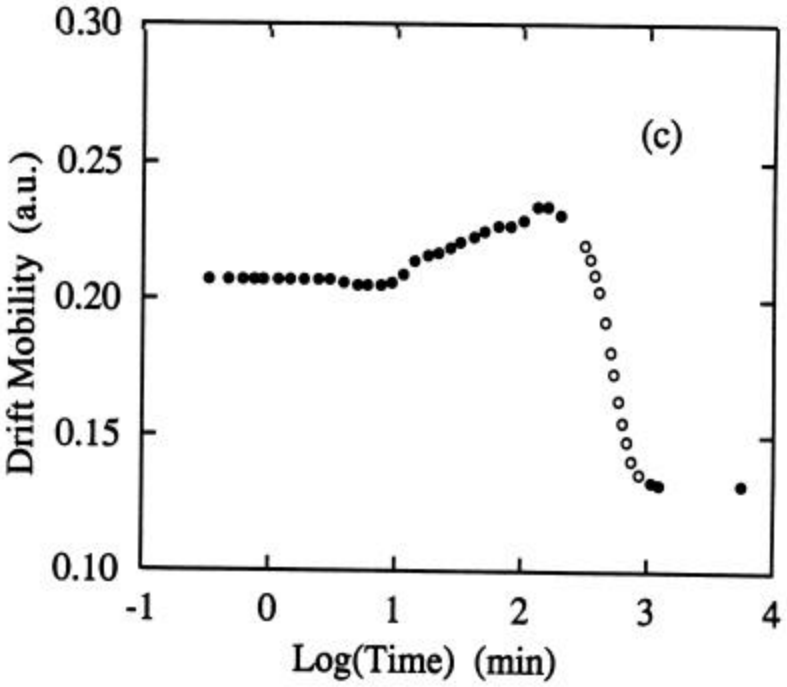

Figure 6(c). The drift mobility μ_d for the a-SiC :H sample versus light soaking time. In addition to the decay of the dc photoconductivity and lifetime, decay of the drift mobility can be seen due to light soaking. The increase for the drift mobility at t~100min during light soaking is probably due to an increase of the sample temperature upon light illumination and the open circles for the drift mobility were obtained from the dc photoconductivity and curve-fitted lifetime data.

It should be pointed out that in some Time-Of-Flight (TOF) measurements the decay of drift mobility due to light soaking was not found[23-24]; while a light soaking effect was found using the traveling wave technique[25]. This basically results from the facts that the photomixing process is a fast process with an equivalent time scale of 630 ps and is close to the steady state limit, since the ac generation rate is only about 14% of the total generation rate, which allow it to study the transport of electrons about 0.1eV below the conduction band edge.[2,3] Therefore, the photomixing measurements are very sensitive to changes in the extended state transport path, such as the change in the profile of scattering centers and long-range potential fluctuations, whereas on the other hand, the drift mobility measured by TOF, which is a slower process with a time scale of about 10 ns, is mainly limited by the trapping and thermal emission processes and thus may not be sensitive to changes in the extended state transport path. In addition, the difference between TOF and photomixing maybe due to the differences in the generation rates employed by the two techniques.

Table II. Summary of results from the curve fit for a-SiC :H.

	β	τ_0 (min)
From dc Photoconductivity	0.87	200
From Lifetime	0.93	170

2. Effects of deposition conditions on transport properties of intrinsic a-Si:H and a-SiC:H

Extensive studies on effects of the deposition conditions, such as deposition temperature (Ts)[26-31] and hydrogen dilution ratio (R)[32,33], on the structural and electronic properties of a-Si:H and a-SiC:H films have been performed in attempt to improve the quality of these films for solar cell applications.[26-33] The experimentally available transport data for these films, however, are normally limited to conductivities and $\mu\tau$ products which are convolutions of a few separate physical parameters. With the unique advantage of the photomixing technique of being able to experimentally determine both the drift mobility (μ_d) and lifetime (τ), we report here the drift mobility (at 480 K), lifetime (at 480 K) and the Urbach energy (e) of a-Si:H and a-SiC:H films as a function of deposition temperature (T_s) and hydrogen dilution ratio (R), respectively. The sample were obtained from the Wronski group.

The intrinsic a-Si:H films[29-31] were prepared by RF glow discharge at deposition temperatures (T_s) of: 200 C, 220 C, 240 C, 265 C, and 280 C. The a-SiC:H films[32,33] were prepared by RF glow discharge with hydrogen dilution ratio ($R = H_2/(CH_4+SiH_4)$) of: 0 (T_s = 250 C), 20 (T_s = 250 C), and 25 (T_s = 305 C). Most of these samples were provided and fully characterized by the Wronski group at Penn. State University.[29-33]

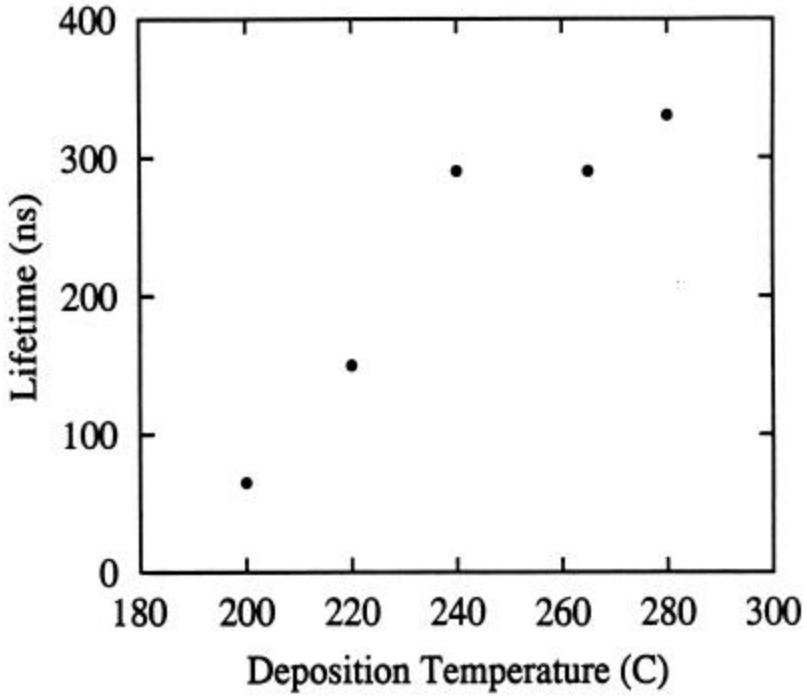

Figure 7. Lifetime (at 480 K) of a-Si:H films as a function of deposition temperature.

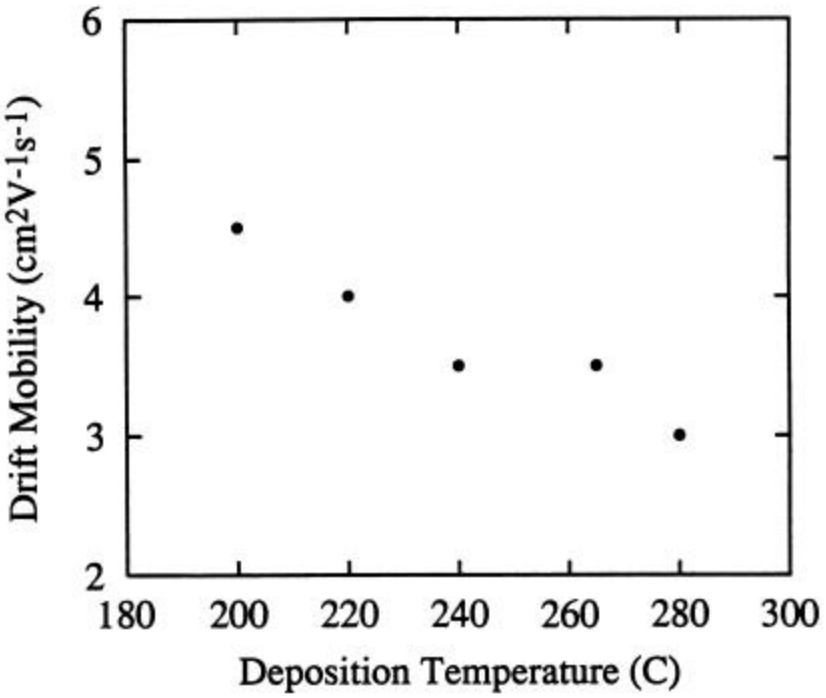

Figure 8. Drift Mobility (at 480 K) of a-Si:H as a function of deposition temperature.

For the a-Si:H films with increasing deposition temperature (T_s), the lifetime (at 480 K) increases (Fig. 7), the drift mobility (at 480 K) decreases (Fig. 8), and the Urbach energy decrease, except for the sample with T_s = 200 C (Fig. 9). The decrease of the Urbach energy (Fig. 9) indicates that the Urbach edges get sharper and the atomic structure of the films gets closer to that of crystalline Si. This is consistent with previous results indicating that the monohydride and dihydride content, and the void fraction all decrease with increasing deposition temperature.[31] The $\mu\tau$ product (at 480 K) of these films increases as the deposition temperature (T_s) increases to 240 C, and converges to a constant value at higher T_s. This is also consistent with previous results.[31]
It is important to note that the decrease of the monohydride and dihydride content, and the void fraction in these a-Si:H films as a result of increasing deposition temperature (T_s) actually results in an increase in the subgap absorption, i.e., higher density for the midgap defects.[31] Nevertheless, the lifetime for electrons (as they are the dominant photoconductive charge carriers in intrinsic a-Si:H films) still increases with increasing T_s (Fig. 7). All these indicate that with increasing deposition temperature (T_s), the density of defects with relatively large deep trapping and recombination cross sections for electrons, such as positively charged and neutral defects, must decrease, whereas the density of defects with relatively small deep trapping and recombination cross sections for electrons, such as negatively charged defects, must increase to account for the increase of the subgap absorption. The increase of charged defects with increasing Ts is also evidenced by the decrease of the drift mobility (Fig. 8), as the charged defects can enhance the scattering of electrons, especially if they form certain long range potential

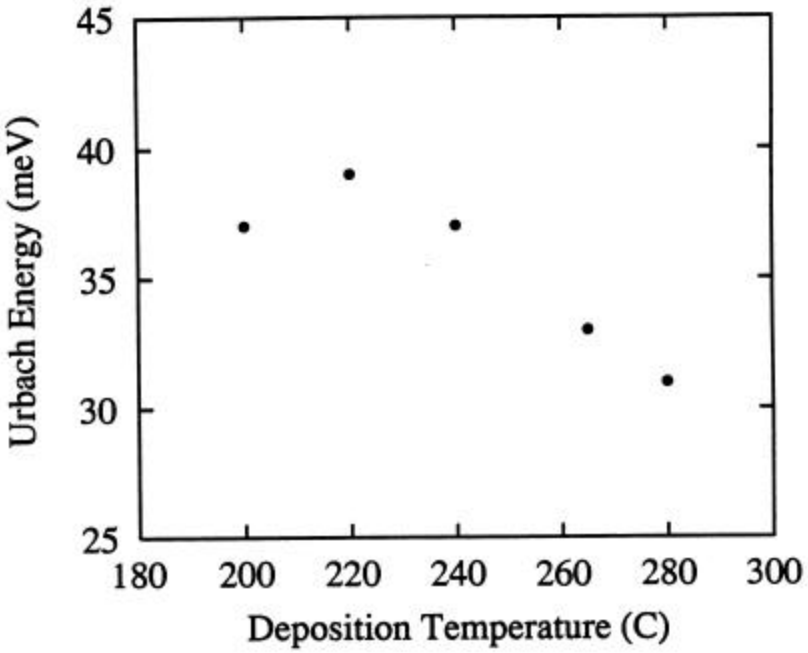

Figure 9. Urbach energy of a-Si:H films as a function of deposition temperature .

fluctuations.[18-22] In other words, the change in the deposition temperature (T_s) not only affects the density of midgap defects, but also, more importantly, affects the charge state profile of midgap defects.

For the a-SiC:H films with increasing hydrogen dilution ratio, both the lifetime (at 480 K) (Fig. 10) and the drift mobility (at 480 K) (Fig. 11) increase, and the Urbach energy shows a tendency to decrease (Fig. 12). These results are consistent with previous results indicating that with increasing hydrogen dilution ratio, both the voids fraction and the density of midgap defects decreases,[32,33] and further indicate that the density of positively charged, negatively charged, and neutral defects all shows a tendency to decrease with increasing hydrogen dilution ratio.

3. Mobility and lifetime in annealed and light soaked conditions for glow discharge and hot wire intrinsic a-Si:H

We have utilized the capabilities of our photomixing technique to separately determine the mobility and lifetime under annealed and under light soaked conditions on samples prepared by various groups. Since it has been reported that higher stabilized cell efficiencies has been achieved utilizing i-layers grown under hydrogen dilution conditions our goal was to characterize such samples by our techniques and gain insight to the factors which determine the properties of these films.

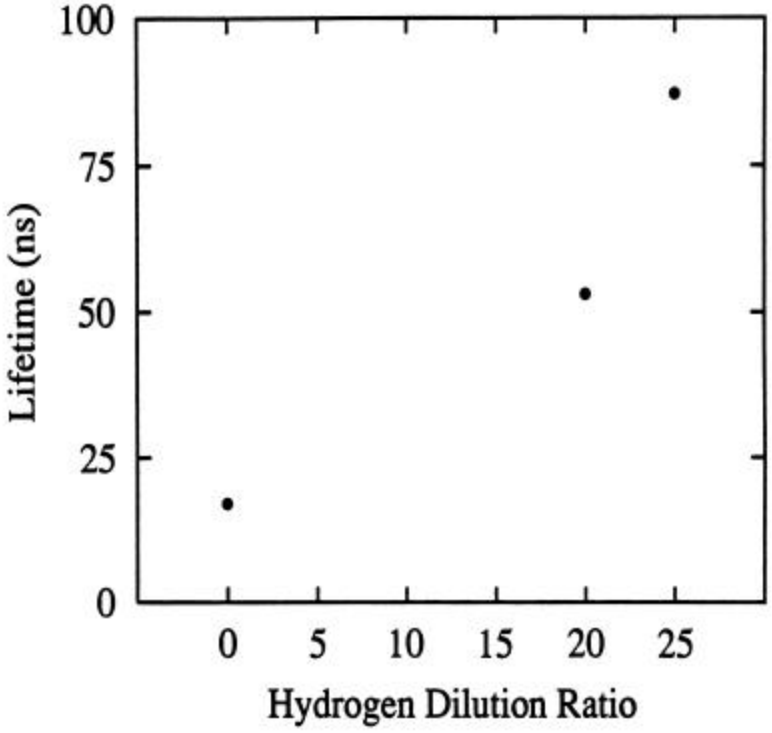

Figure 10. Lifetime (at 480 K) of a-SiC :H films as a function of hydrogen dilution ratio.

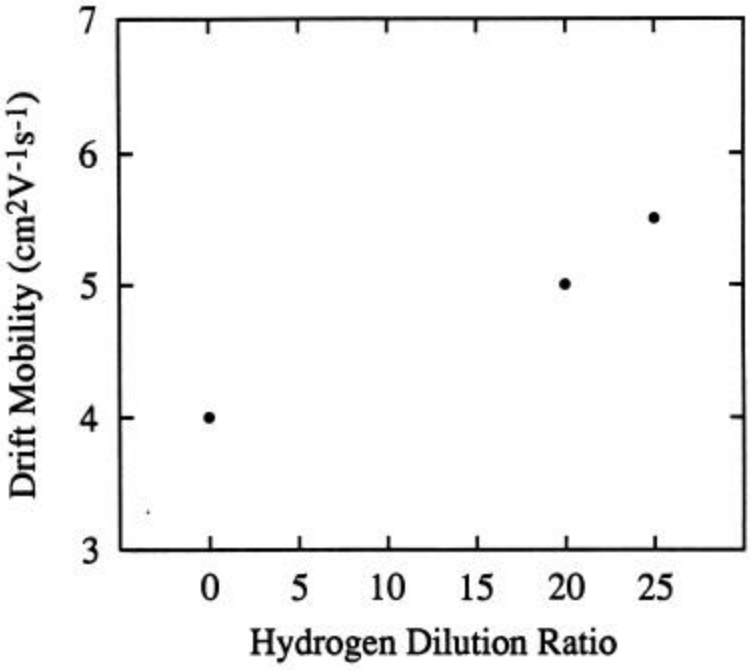

Figure 11. Drift mobility (at 480 K) of a-SiC :H films as a function of hydrogen dilution ratio.

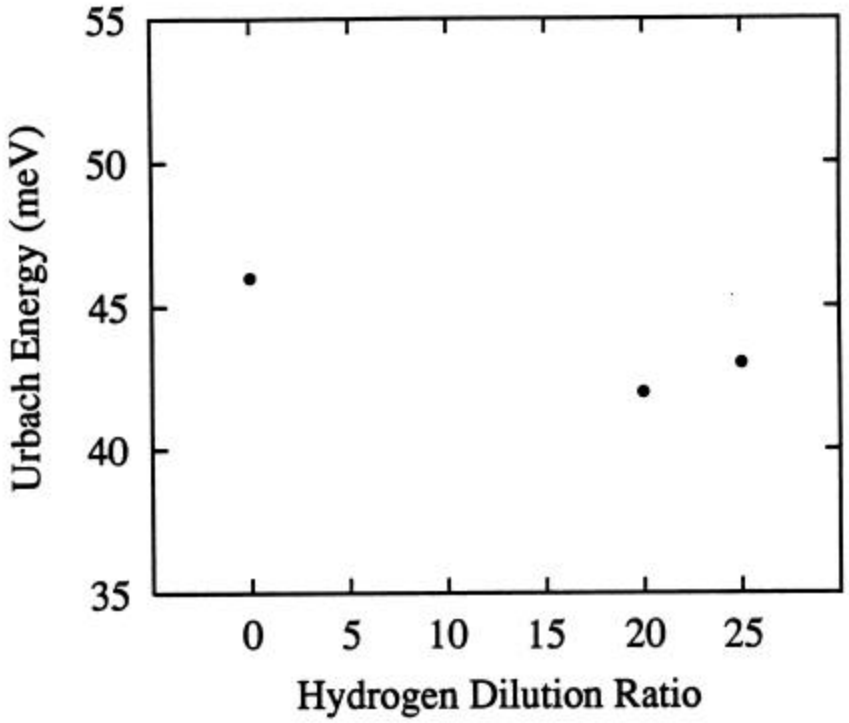

Figure 12. Urbach energy of a-SiC:H films as a function of hydrogen dilution ratio.

Intrinsic a-Si:H films produced by the glow discharge (provided by NREL and Solarex) and the hot wire techniques (provided by NREL) were investigated with the photomixing technique. The sample characterizations are as follows.

Table III. Sample Characterization

Sample ID	Preparation	Provider	H Content (%)	Ts(C)	Thickness (μm)	Other
THD15	Hot wire	NREL	1	600	2.2	
THD16	Hot wire	NREL	11	350	2.0	
S#127I	GD	NREL	No H dil.		0.46	
BK#1	GD	NREL	10		0.59	
D1203-2	GD	Solarex	With H dil.		1.2	Light soaked (LS) for 600 hrs
D1203-3	GD	Solarex	No H dil.		1.5	LS for 600 hrs

The mobility and lifetime were determined on the above samples under the conditions of *in situ* light soaking and under annealed conditions as a function of electric field and as a function of light intensity.

In the *in situ* light soaking measurements, which were performed with a He-Ne laser with about 4 sun intensities for 4 and 7 hours, mobility decays were found in various fashions. In general, the mobility decays for the hot wire samples (<20%) (Fig.13) were found less

than those of the glow discharge samples (~40%) (Fig. 14). This supports the findings that some hot wire samples are more stable than glow discharge samples under light soaking.

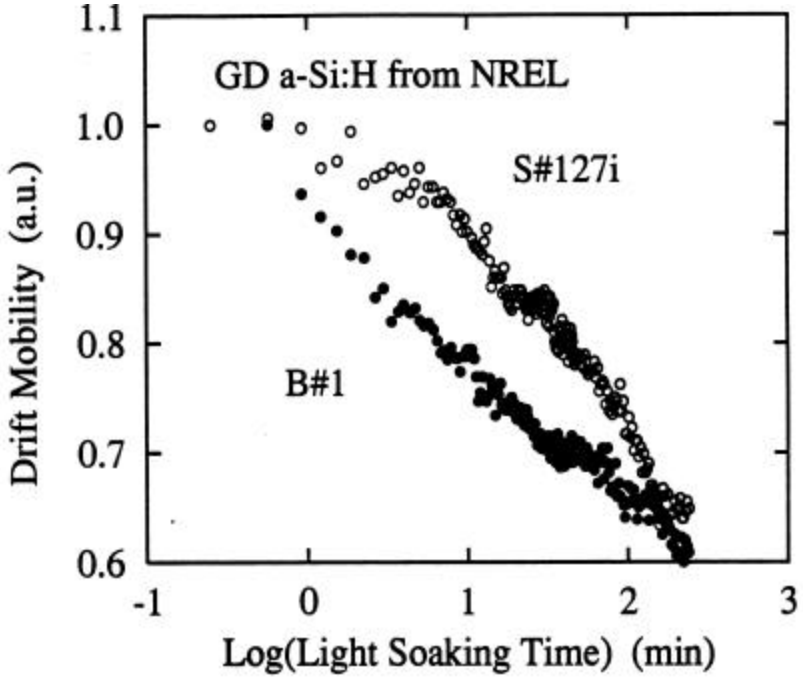

Figure 13. Drift mobility versus light soaking time for the hot wire samples at 4 sun light intensity.

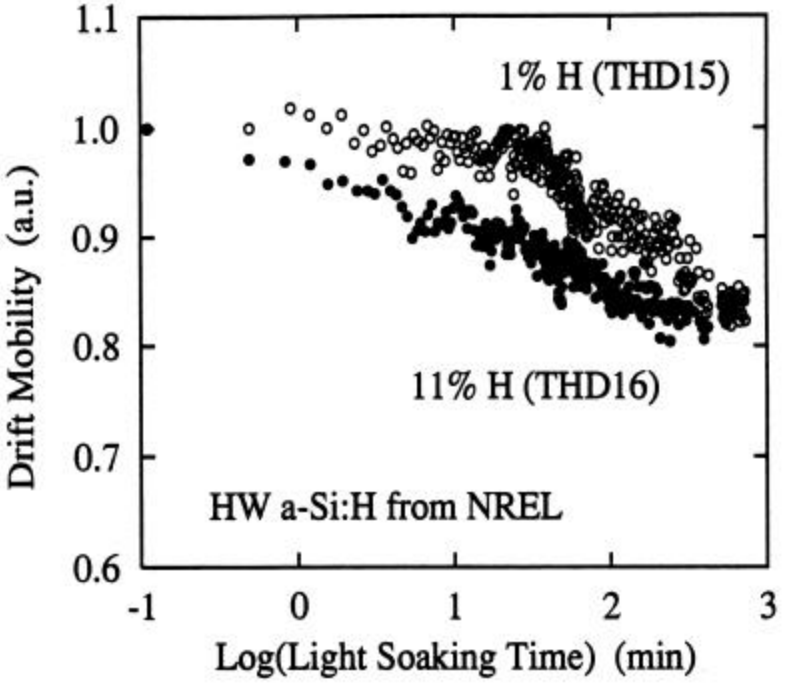

Figure 14. Drift mobility versus light soaking time for the glow discharge samples at 4 sun light intensity.

4. Electric field dependence measurements of mobility

We employed our photomixing technique to measure the field dependence of the mobility and lifetime with the following results.

In the dc bias dependence measurements with the applied electric field ranging from 2000V/cm to 9000V/cm, the mobilities were found increasing and the lifetimes decreasing with increasing dc bias, while the mt products remain essentially independent of the dc bias.

Four a-Si:H thin film samples provided by the National Renewable Energy Laboratory (NREL) were investigated by the photomixing technique. Samples THD15 and THD16 were produced by the hot wire process, with hydrogen contents about 1% and 11%, deposition temperatures of 600 C and 350 C, and thicknesses of 2200 nm and 2000 nm, respectively. Samples S#127i and B#1 were produced by the glow discharge process, with hydrogen content about 10% and thicknesses of 460 nm and 590 nm.

The electric field dependence of the drift mobility (μ_d) and the lifetime (τ) of these samples were measured both in the annealed state (4 hours at 180 C) and in the light soaked state (4 hours at 4 sun intensity). It was found that the drift mobility (μ_d) increases with increasing electric field, while the lifetime (τ) decreases with increasing electric field, and the mt product is essentially independent of the electric field in the range from 2000 V/cm to 9000 V/cm. The fact that the lifetime decreases while the drift mobility increases indicates the existence of the diffusion limited transport and recombination[34] in all the samples in both the light soaked as well as the annealed states. It should be pointed out that in this case, the increase in μ_d with increasing field as well as the increasing in μ_d with increasing carrier density due to light illumination, which can possibly be explained by long-range potential fluctuations,[35-42] is compensated by the corresponding decrease in τ, which can result in a field independent $\mu\tau$ or the commonly observed ohmic behavior of the photocurrent. In the presence of long range potential fluctuations, one would expect m to increase with increasing electric field and with increasing carrier concentration.[43,46] Such increase in the drift mobility do not necessarily lead to an increase in the photoconductivity, since one commonly observes a corresponding decrease in τ.

Fig. 15 and Fig. 16 show the electric field dependence of the drift mobility of these samples. The open dots and the solid dots are the experimental data in the annealed state and the light soaked state, respectively. The solid lines were obtained through a curve fitting procedure which will be discussed later. It is important to point out that the field dependence of the drift mobility is less in the light soaked state than that in the annealed state (Fig. 15 and Fig. 16).

It is clear from Fig. 16 that a greater field dependence of the drift mobility of an a-Si:H film occurs in the annealed state This indicates that the amount of light induced degradation is controlled by the generation of defects which are responsible for controlling the field

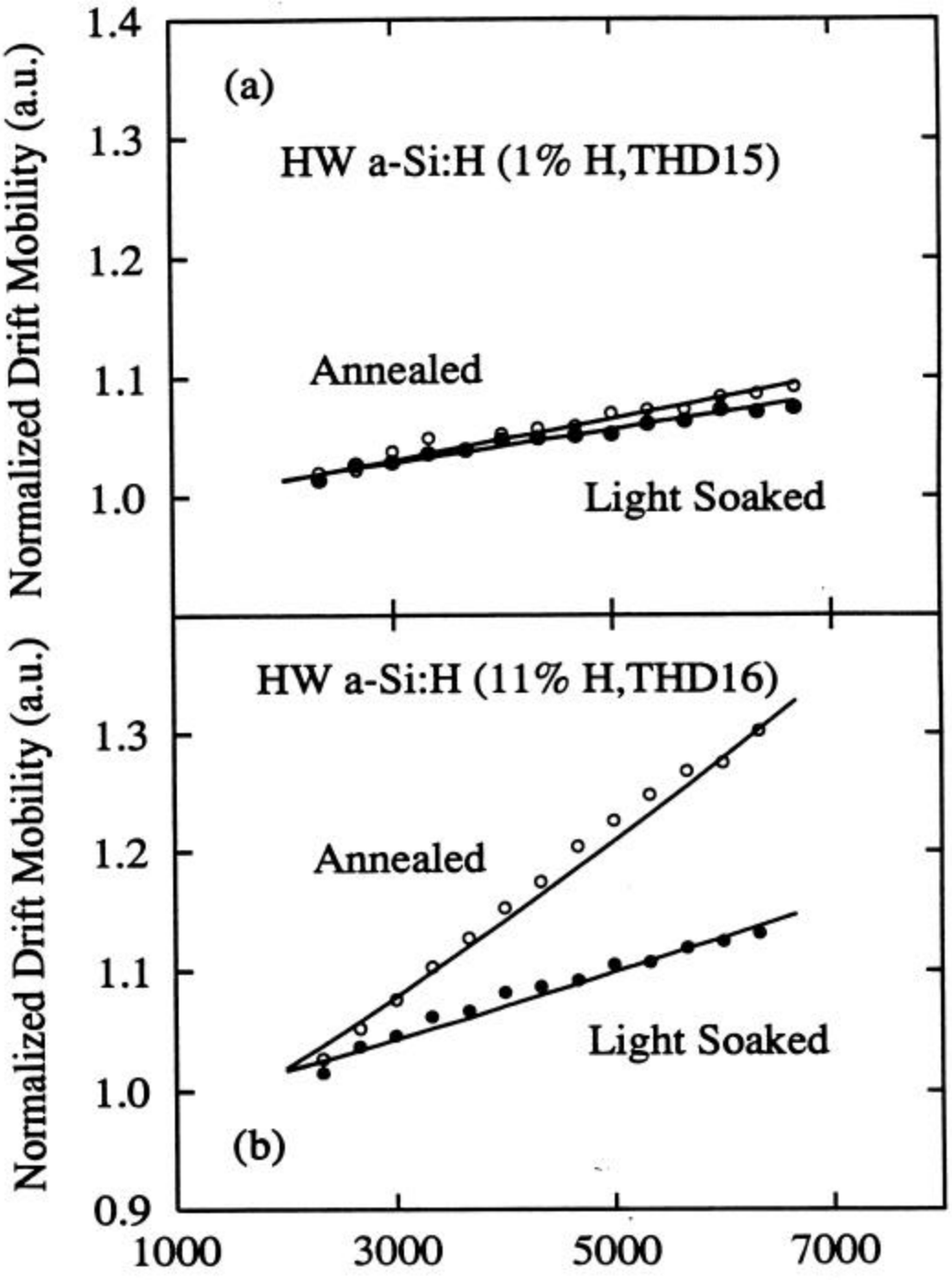

Figure 15. Drift mobility versus applied electric field for the hot wire samples THD15 (1% H) (a) and THD16 (11% H) (b). Open and solid dots represent the data in the annealed and light soaked state respectively. Solid lines are curve fitting according to Eq. (25).

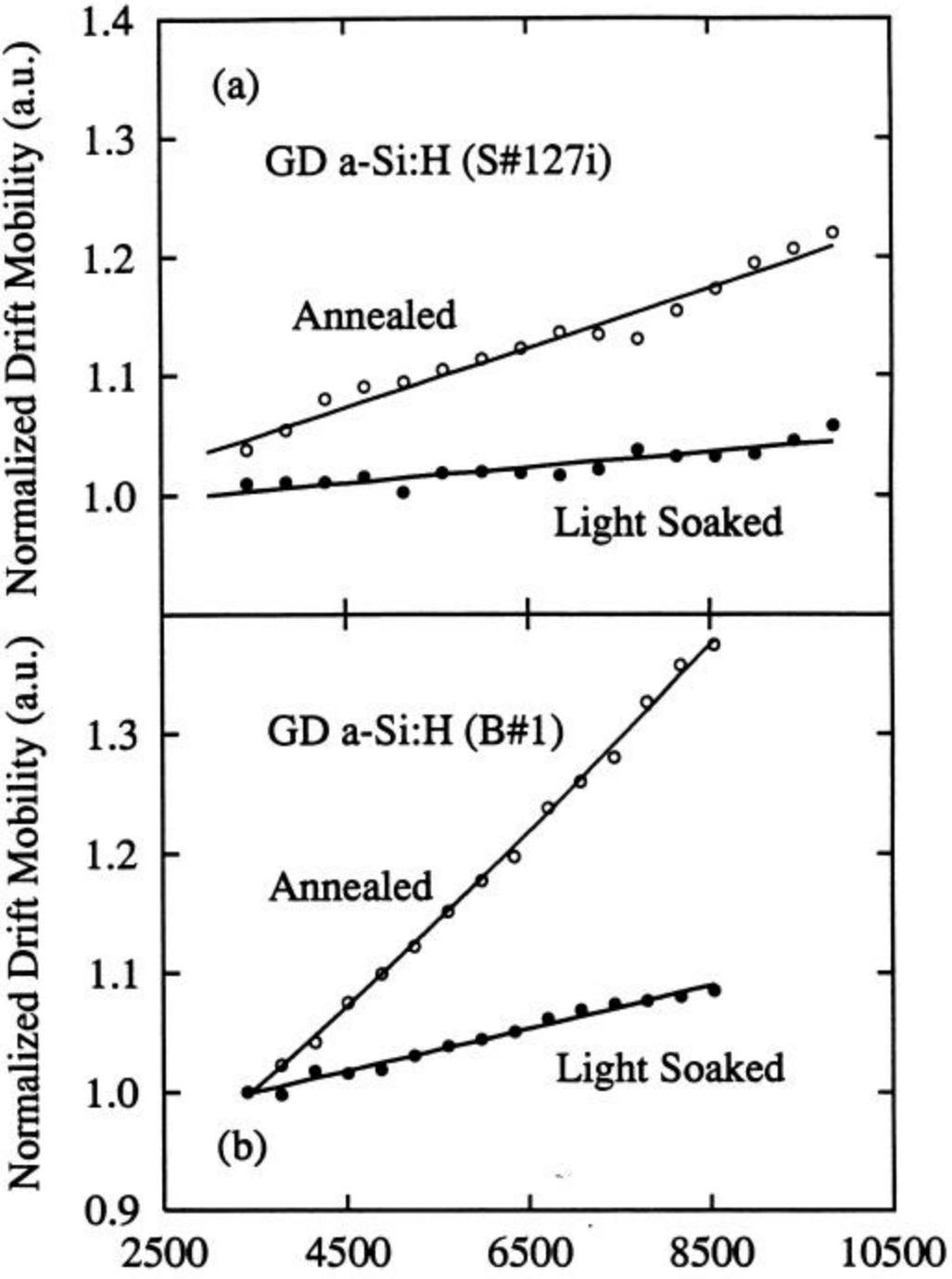

Figure 16. Drift mobility versus applied electric field for the glow discharge samples S#127i (a) and B#1) (b). Open and solid dots represent the data in the annealed and light soaked state respectively. Solid lines are curve fitting according to Eq. (25).

dependence of the drift mobility in the annealed state. The light induced defects as well as the native defects, which serve as recombination centers and trapping centers, can be charged and can form certain potential barriers or fluctuations. In the transport process, the charged carriers can either go over the potential barrier through thermal activation or go around the potential barrier through scattering. If the former dominates the latter, then through simple statistical calculations one can obtain the following electric field (E) dependence of the drift mobility $\mu_d(E)$:[44]

$$m_d(F) = m_d^0 \exp(-\frac{eV_P}{kT}) \frac{eLF}{kT[1-\exp(\frac{eLF}{kT})]} \qquad (if \quad |LF| \leq V_P), \tag{23}$$

By normalizing the values for the drift mobility to the values at the lowest electric field we obtain:

$$\frac{m_d(F_i)}{m_1(F_1)} = \frac{F_i}{F_1} \times \frac{1-\exp(-\frac{eLF_1}{kT})}{1-\exp(-\frac{eLF_i}{kT})}, \tag{24}$$

From curve fitting to this expression, we can determine the range L. The results, obtained from fits to the normalized values of the drift mobility, for the range of the long range potential can then, subsequently, be used to fit the original data according to equation 1 to obtain the depth of the potential V_p, the magnitude (V_P) of the potential fluctuations has a tendency to increase, whereas the range (L) of the potential fluctuations has a tendency to decrease. But because of the long range nature of the potential fluctuations, the potential fluctuations should be spatially nondegenerate. Therefore, during the light soaking process, the magnitude (V_P) of the potential fluctuations should not increase as significantly as the range (L) of the potential fluctuations decreases. This is partially evidenced by the experimental results that the field dependence of the drift mobility is less in the light soaked state than that in the annealed state (Fig. 15 and Fig. 16).

It is reasonable to assume that the charged defects are responsible for the long-range potential fluctuations. In a-Si:H, a reasonable candidate for the charged defects is the charged dangling band state ($T_3^{+/-}$). Just as in the case of neutral dandling bonds (T_3^0), a fraction of the charged dangling bonds ($T_3^{+/-}$) is stable, while another fraction in metastable, i.e., the density of the latter increases upon light soaking and decreases upon annealing. The existence of the stable and metastable charged dangling bonds ($T_3^{+/-}$) has been attributed to the local dipole potential fluctuations.[38] In the present context, it is not important to differentiate whether a $T_3^{+/-}$ defect is newly created or it is converted from a T_3^0 defect. Assuming that the density (n) of the $T_3^{+/-}$ defects is determined by:[40,41]

$$n \mu V_P / L, \tag{25}$$

we can estimate the lower limit of the ratio of the defect densities in the light soaked state (n_{LS}) and that in the annealed state (n_{AN}) can be estimated by $n_{LS} / n_{AN} = L_{AN} / L_{LS}$ where

L_{AN} and L_{LS} (Table I) are the ranges of the potential fluctuations in the annealed and light soaked states, respectively. The results of such ratios are also included in Table IV.

Table IV. Experimental and curve fitting results for electric dependence of mobility

Sample ID	Preparation	H Content (%)	$(\mu\tau)_{AN}/(\mu\tau)_{LS}$	L_{AN}(A)	L_{LS}(A)	N_{LS}/n_{AN}
THD15	Hot wire	~1	1.8	82	64	1.3
THD16	Hot wire	~11	5.3	345	133	2.6
S#127I	GD	~10	4.8	128	33	3.9
B#1	GD	~10	9.1	383	92	4.2

In conclusion, by using the photomixing technique we have found that the drift mobility (μ_d) of intrinsic hydrogenated amorphous silicon (a-Si:H) films produced by both glow discharge and hot wire techniques increases with increasing electric field; The results can be analyzed employing the model of the long-range potential fluctuations. It should be pointed out that our results suggest that the light induced charged dangling bonds may not affect $\mu\tau$ by increased recombination, but rather by affecting md through controlling potential fluctuations in the sample. It has been found that upon light soaking both τ and μ_d decease following different stretched exponential laws.

5. Electric field dependence of mobility of compensated a-Si:H samples

We have previously determined the drift mobility and recombination lifetime in a series of compensated a-Si:H by photomixing that had been measured earlier by the time-of-flight technique by the Xerox group. We had found that the drift mobilities decreased as the compensation increases and could be accounted for by existence of long-range potential fluctuations. To further extend our understanding of the electric field dependence of the drift mobility as influenced by long-range potential fluctuation, we performed the photomixing measurements as a function of electric field on several compensated samples in the field regime from 2000 V/cm to 10000 V/cm. These compensated a-Si:H samples were provided by Dr. R. A. Street of Xerox and were made by plasma deposition of SiH_4 with equal volume concentrations of B_2H_6 and PH_3. The samples employed had the following concentration ratios of B_2H_6 and PH_3 to SiH_4 in the deposition gas: 10^{-4} and 10^{-3}, which will be referred to as the compensation concentration. In order to measuring the quite low mixing signal of compensated samples, a lock-in amplifier was used.

Fig. 18 and Fig. 19 show the electric field dependence of the drift mobility for compensation 10^{-4} and 10^{-3} respectively. The open dots are the experimental points while the solid lines were obtained through a curve fitting procedure of a statistical model for the electric field dependence of mobility which we will describe later on. The ranges of the potential fluctuations derived from curve fitting are 570 Å and 360 Å for the samples with compensation concentration 10^{-4} and 10^{-3} respectively. This results can be explained that raising the doping concentrations will reduce the range and increase the magnitude of the potential fluctuations.

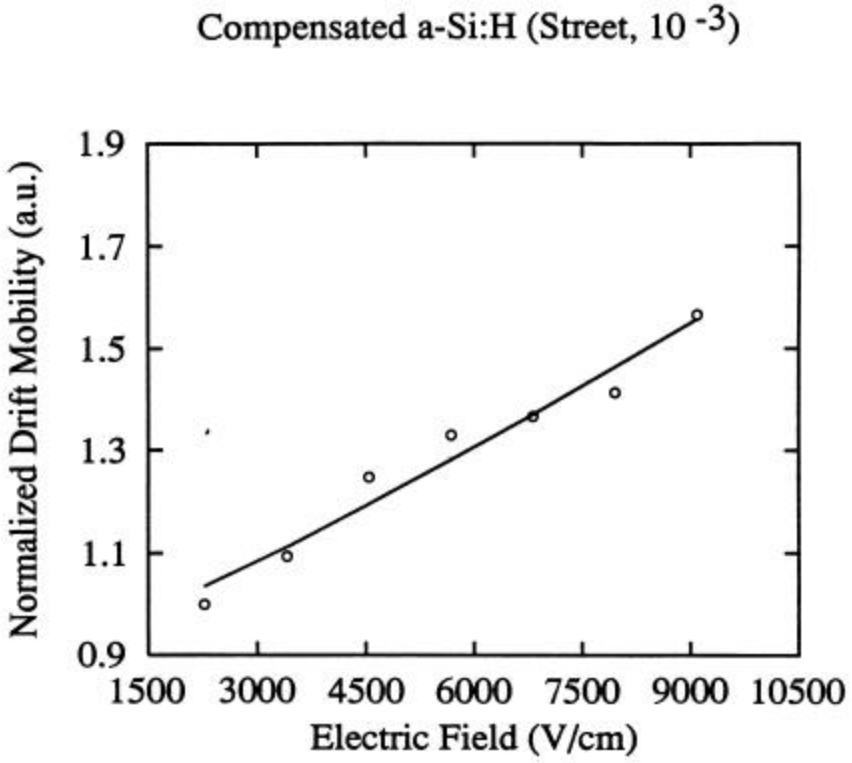

Figure 17. Drift mobility of compensated a-Si:H film with compensation level of 10^{-4} versus electric field.

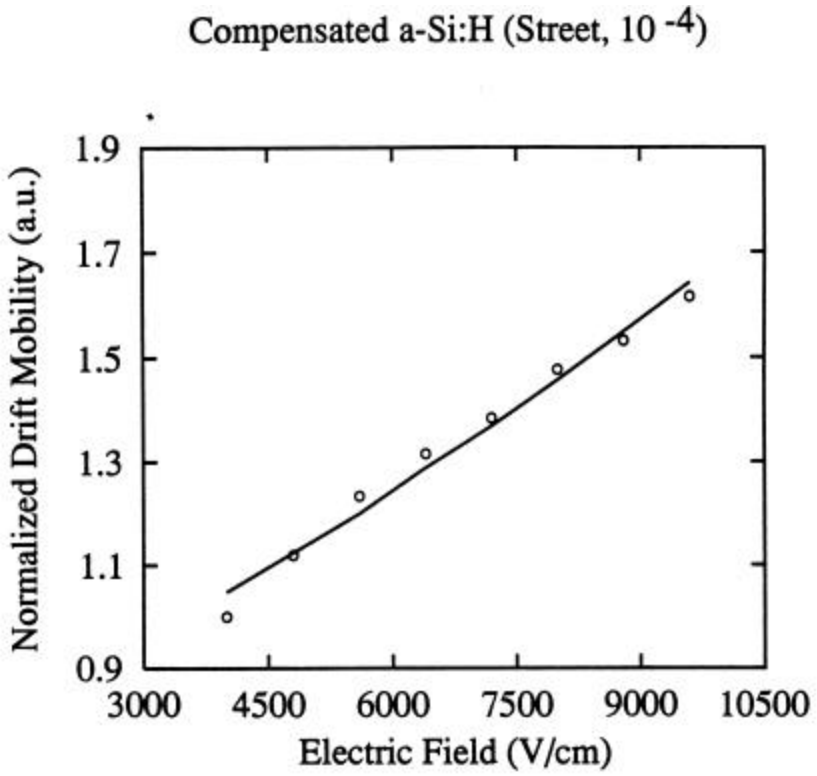

Figure 18. Drift mobility of compensated a-Si:H film with compensation level of 10^{-3} versus electric field.

6. Photoelectron emission in air from amorphous semiconductors and transparent conducting oxides

It is well established that photoelectron spectroscopy is a method to determine near surfaces electronic properties of amorphous semiconductors and detecting chemical impurities on surfaces; however the technique usually requires an ultrahigh-vacuum environment and is not readily adaptable to analytic procedures which can ultimately be used on the production line.

If photoemission measurements could be performed in air, it would prove to be a useful technique that would be readily adaptable for the detection of surface contaminants and monitor cleanliness in the production environment; in addition, if the photoemission yield could be scanned over small as well as large areas and non-uniformities detected, micro-shunting problems in solar cells could be identified.

We have available in our laboratory an apparatus that can perform optically stimulated electron emission from semiconductors surfaces in air. The principle of the technique consists of the following:

When metal or semiconductor surfaces are illuminated with ultraviolet light with the proper wavelength, electrons are emitted from the surface. The emitted and subsequently scattered electrons can be collected across an air gap. By maintaining the surface collector distance relatively constant, changes in the measured photocurrent (which is of the order of 10^{-10} to 10^{-12} A) can provide information about the surface, e.g., electronic structure and chemical composition. Any contaminant on the surface, depending on its photoemission, can either enhance or attenuate the inherent emission from a clean surface. In addition, the probe can be scanned over the surface and thus provide a two dimensional display of the surface characteristic. The excitation source consists of a Hg lamp with the 5eV and the 6.7eV lines which are adequate for photoemission from metals and semiconductors of interest for photovoltaic cell production.

We have performed photoemission measurements on a-Si:H films produced at NREL. Figure 24 shows the results for a 4 inch by 4 inch sample indicating the non-uniformity due to possible inhomogeneity of composition and the positioning of the sample substrate in the glow discharge.

We obtained a series of transparent conducting oxide (TCO) films from S. Hegedus of University of Delaware, Institute of Energy Conversion, to perform Optically Stimulated Electron Emission (OSEE) measurements. They are consisted of TCO films of SnO2 and ZnO both textured and untextured and films of a-SiC:H on ZnO. Some of the TCO films were virgin and others were exposed to index matching organic liquids for optical measurements and then subsequently subjected to degreasing and cleaning with TCE and Freon. This apparatus enables us to profile the barrier height on a surface up to 4 inches by 4 inches in area in air; thus it can be employed under normal production environment conditions to monitor possible in-process surface changes of barrier heights. In our

previous report we presented results on a-Si:H films produced by NREL which revealed some non-uniformity of barrier height due possibly to inhomogeneity of composition, due perhaps to the positioning of the sample substrate in the glow discharge. We also referred to some results on TCO samples supplied by Steven Hegedus. We will now present more detailed data on the TCO samples as well as photoemission from a range of substances that maybe of general interest to other teams.

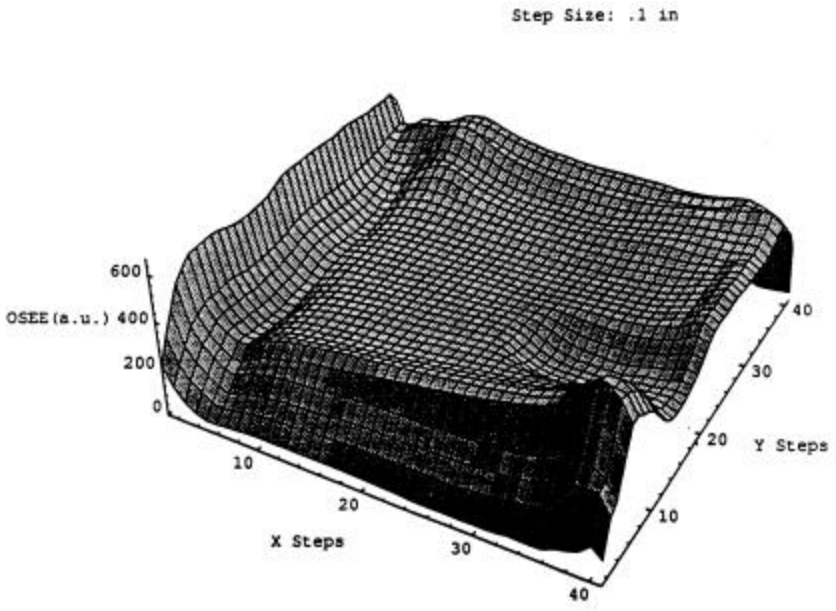

Figure 19. Inhomogeneity of NREL a-Si:H film detected by the Optical Stimulated Electron Emission (OSEE) technique.

The TCO samples described by S. Hegedus are as follows: The TCO surfaces were cleaned with TCE, freon, and DI water before sending them to us since on index matching liquid was applied to perform optical measurements on the textured surfaces. In addition a few identical pieces that had not been exposed to the index matching liquid were run to compare the effect of the degreasing and cleaning in the TCE and freon. All textured TCO layers were 0.8-1.0 mm thick. The TCE 4375 and 4376 series were exposed to an organic fluid and then cleaned in TCE and freon. The following is the description of the samples:

Number	Sample description
4375-11	text. SnO_2 from Solarex (standard device substrate)
4375-12	text. ZnO from Solarex
4375-21	text. ZnO from Utility PV Group (UPG)
4375-22	text. ZnO from Harvard (Prof. Gordon's Group)
4376-11	200 Å a-SiC p-layer deposited at IEC on 4375-11
4375-12	200 Å a-SiC p-layer deposited at IEC on 4375-12
4376-21	200 Å a-SiC p-layer deposited at IEC on4375-21
4376-22	200 Å a-SiC p-layer deposited at IEC on4375-22

A	virgin sample of 4375-11
B	virgin sample of 4375-12
C	virgin sample of 4375-21

91539-21	1000 Å specular ZnO (no texture) sputtered at IEC
91552-17	200 Å specular ZnO sputtered on text. SnO_2
91554- 04	1000 Å specular ZnO sputtered on text. SnO_2
E	1000 Å specular SnO_2 grown on text. ZnO (Harvard)

Results:

The following figures are the results of the photoemission from the various combinations of samples described in the above table. The photoemission in air was obtained using a Hg lamp as the illuminating source and collecting the electrons across a narrow air gap. The light source and the collector were scanned over the surface of the sample using stepping motors. The x-steps and y-steps were at intervals of 0.05 inches and the optically stimulated electron emission (OSEE) in arbitrary units is displayed on the z-axis. The photocurrents were of the order of 10^{-11} to 10^{-12} amps and provide information about the barrier heights or any contaminants on the surface. Any containments on the surface can either enhance or attenuate the inherent emission from a clean surface.

Figure 20 through 27 show the results for samples 4376-11, 4376-21, 4376-12 and 4376-22 respectively. These were 200A a-SiC p-layers deposited by IEC on textures substrates 4375-11, 4375-21, 4375-12, and 4375-22 respectively. The sources of the substrates are shown in the above. These figures show a spatial variation in the electron yield which may be due to the surface or the interface between the TCO and the a-SiC layers. The dominant Hg lines responsible for the photoemission are the 5 eV and the 6.7 eV lines. The optical measurements on these samples have been recently supplied by Steven Hegedus which will allow us to ascertain surface or volume penetration.

Figure 27 shows the yield from sample 4375-11, the textured SnO_2 film, which was coated with an organic index matching layer for optical measurement and then was cleaned with TCO, freon and DI water as compared to sample A which is a virgin sample of 4375-11, the textured SnO_2 film from Solarex. It is clear that the cleaning procedure leaves no residue.

Figure 25 is a comparison of samples 4375-12, 4375-22 and sample B. From the yeild of the samples, it is clear the cleaning procedures leaves no residue.

Figure 26 compares samples 91539-21, 91552-17, 9153-04 and sample E which are 1000Å specular ZnO (no texture) sputtered at IEC, 200 Å specular ZnO sputtered on textured SnO_2 , 1000 Å specular ZnO sputtered on textured SnO_2 and 1000 Å specular SnO_2 grown on textured ZnO from Harvard. The barrier heights are relatively the same on all these samples.

Finally Figure 27 compares sample A the virgin sample of 4375-11, the textured SnO_2 from Solarex with sample C the virgin sample of 4375-21, the textured ZnO sample from Utility PV Group (UPG). It should be noted that for sample 4375-21 two regions of stripped increased yield were observed. Visual examination indicates a yellow discoloring in this region relative to the rest of the film. Hegedus has indicated that he would be interested in obtaining the absolute values of the barrier heights of the TCO films after various treatments; we are looking into this matter.

It should be noted that for all the TCO samples have less yields than the p-layers of a-SiC:H deposited on the TCO films. This is probably due to that the a-SiC:H films have lower bandgaps than the TCO films. The optical data supplied by S. Hegedus is being analyzed to answer this question.

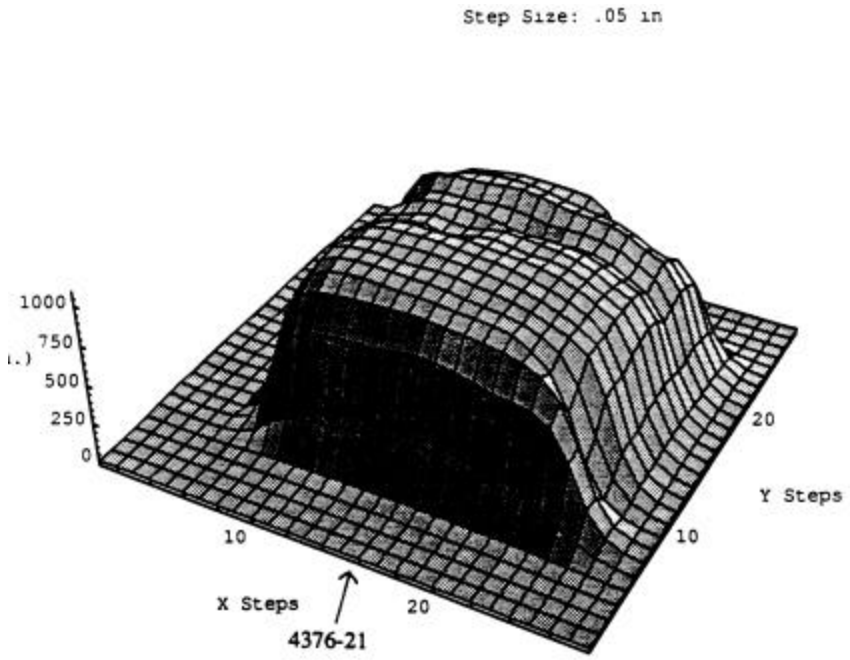

Figure 20. Photoemission in air from sample 4376-21: 200 Å of a-SiC p-layer deposited at IEC on layer 4375-22, texture ZnO from Harvard (Prof.Gordon's Group).

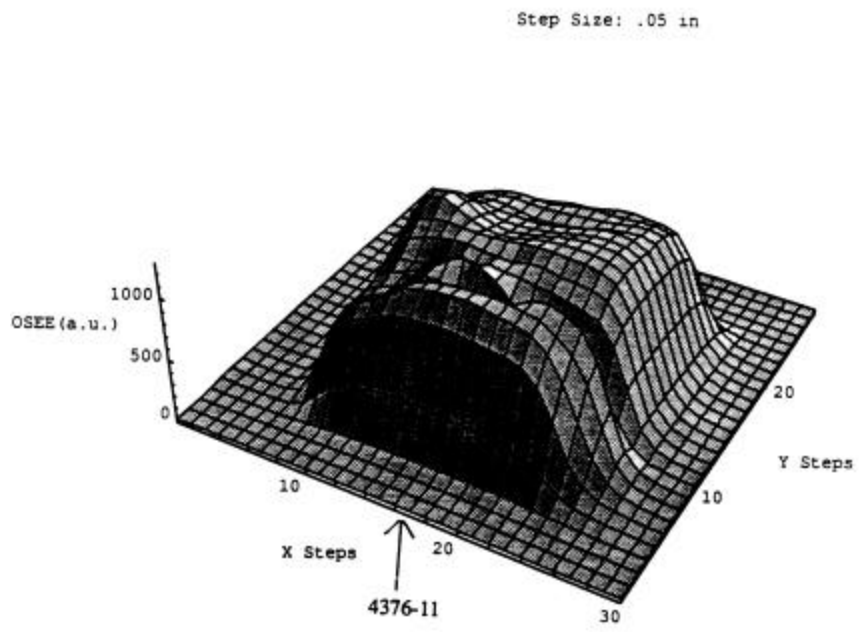

Figure 21. Photoemission in air from sample 4376-11: 200 Å of a-SiC p-layer deposited at IEC on sample 4375-11, textured SnO_2 from Solarex (standard device substrate).

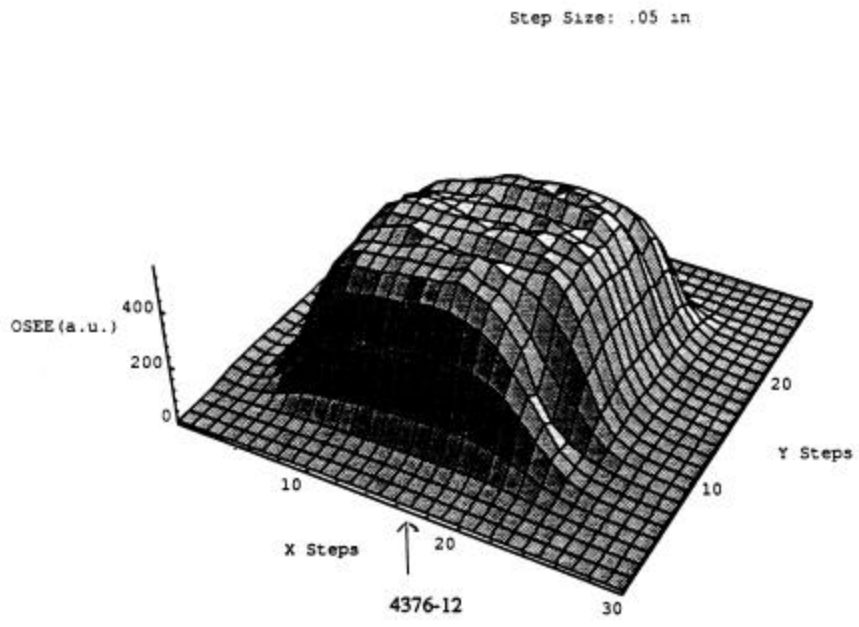

Figure 22. Photoemission in air from sample 4376-12: 200 Å a-SiC p-layer deposited at IEC on layer 4375-12, textured ZnO from Solarex.

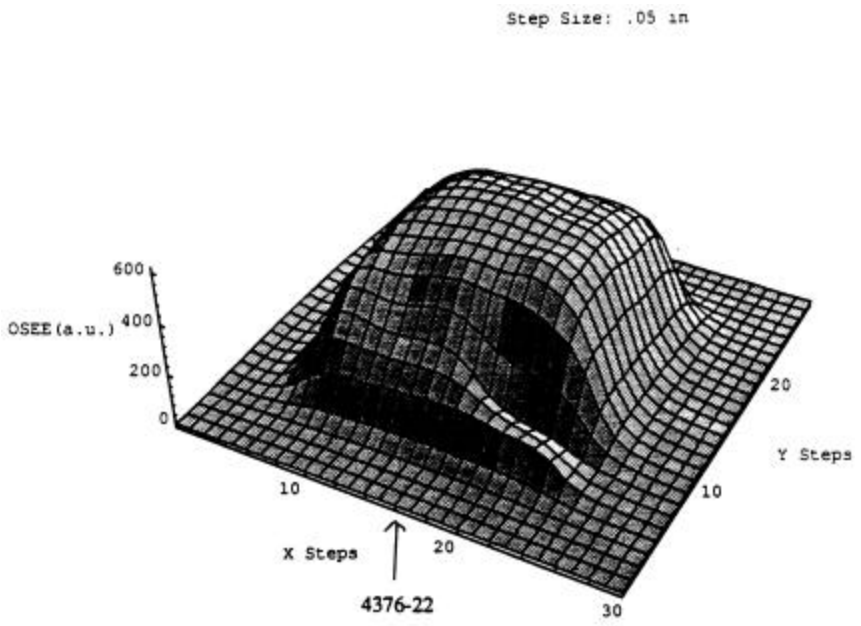

Figure 23. Photoemission in air from sample 4376-22: 200 Å a-SiC p-layer deposited at IEC on 4375-22, textured layer ZnO from Harvard (Prof. Gordon's Group).

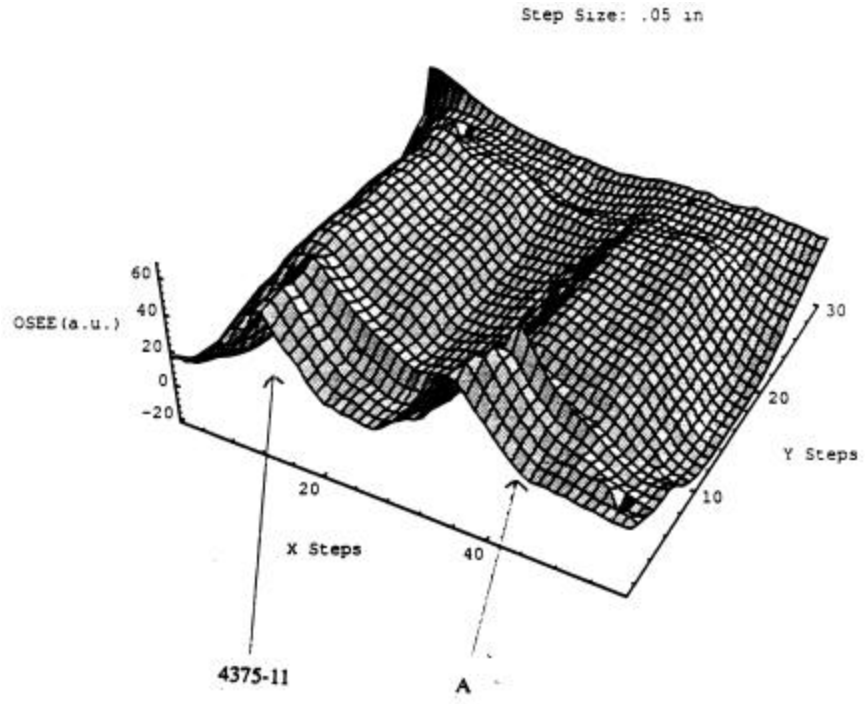

Figure 24. Comparison of the photoemission in air between samples: 4375-11: textured SnO_2 from Solarex (standard device substrate) and A: virgin sample of 4375-11.

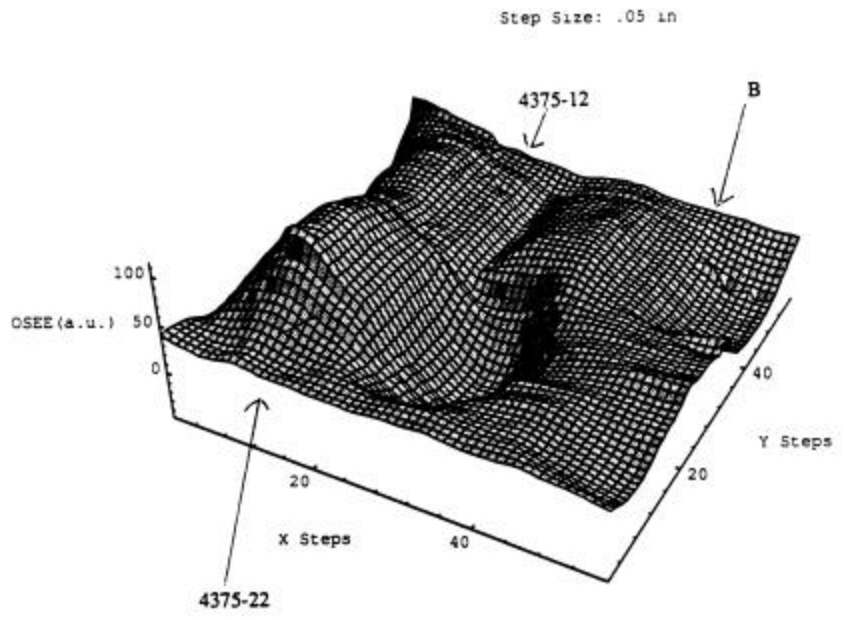

Figure 25. Comparison of the photoemission in air between samples: 4375-12: textured ZnO from Solarex, 4375-22: textured ZnO from Harvard (Prof. Gordon's Group), and B: virgin sample of 4375-21.

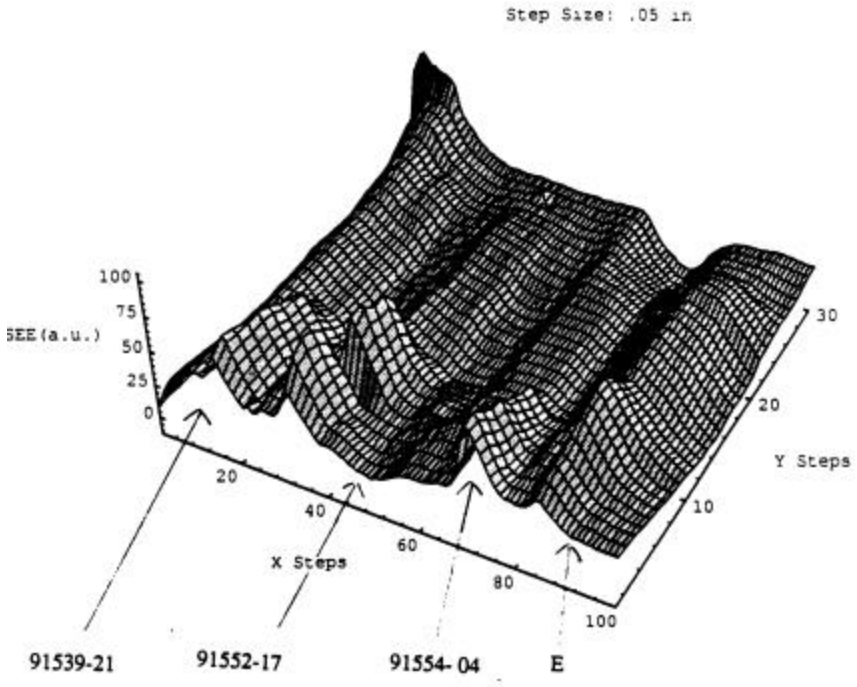

Figure 26. Comparison of the photoemission in air between samples of: 91539-21: 1000 Å, specular Zn0 (no texture) sputtered at IEC, 91552-17: 200 Å, specular ZnO sputtered on textured SnO_2, 91554-04: 1000 Å, specular ZnO sputtered on textured SnO_2 and E: 1000 Å, specular SnO_2 grown on textured ZnO (Harvard).

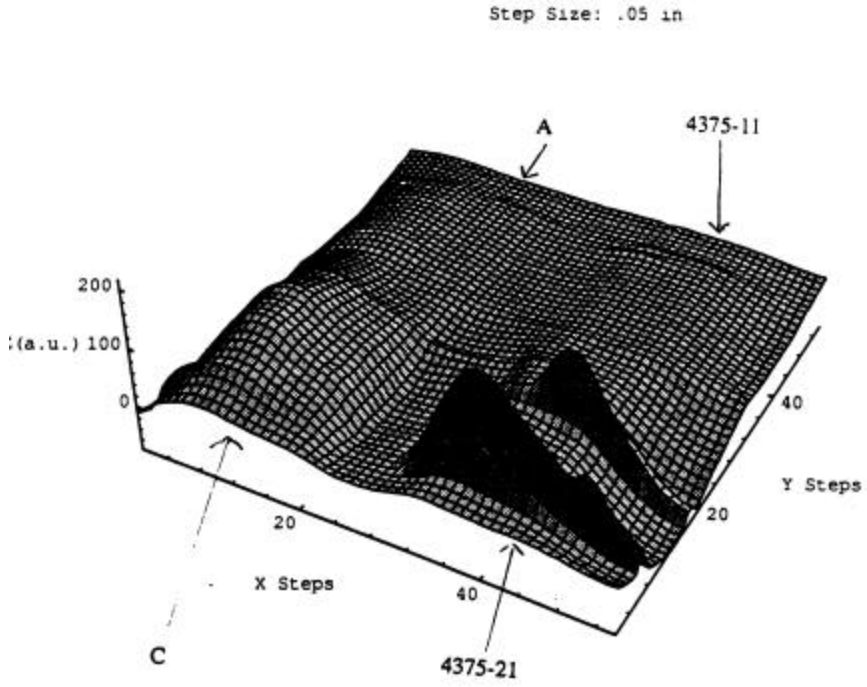

Figure 27. Comparison of the photoemission in air between samples: A: virgin sample of 4375-11, C: virgin sample of 4375-21, 4375-11: textured SnO_2 from Solarex (standard device sample), and 4375-21: textured ZnO from Utility PV group (UPG).

7. Light induced degradation and continuous decay of photoconductivity, lifetime and drift mobility in hot-wire intrinsic a-Si:H

The intrinsic a-Si:H samples, provided by the National Renewable Energy Laboratory (NREL), were deposited by hot-wire technique[45] on Corning 7059 glass. The basic properties of samples of two batches produced at different times are listed as follow:

Table V. Sample characterization of samples THD58-61 and THD 82-83.

Sample ID	Substrate Temp.(C)	Heater Temp. (C)	H Content (%)	Thickness (μm)	Production date
THD59	290	350	10-12	2.100	4/19/95
THD60	325	425	7-9	2.098	4/19/95
THD58	360	500	2-3	2.038	4/19/95
THD61	400	575	<1	1.930	4/19/95
THD82		475		2.400	12/18/95
THD83		504		1.950	12/18/95

Light induced degradation studies were performed on the series of hot-wire samples employing the photomixing technique to determine the dc photoconductivity σ_{dc}, lifetime τ and the drift mobility μ_d as a function of illumination time. The mixing and the light soaking were performed in situ employing a He-Ne laser with an intensity of 4 suns.

Figs. 28-30 show the decay of the dc photoconductivity σ_{dc}, lifetime τ and the drift mobility μ_d as a function of illumination time for sample THD82 due to light soaking. Similar results were obtained on the other samples. The open dots are the experimental points while the solid lines are fitted to the stretched exponential law (Eq. (22)).

As can be seen from the table VI, different stretched-exponential parameters for photoconductivity, lifetime and drift mobility were obtained, which indicates the generation of defects with different generation kinetics upon light soaking. Our studies so far do not reject any existing microscopic models[11,12,13-18] for the Staebler-Wronski effect, such as weak bond breaking[13-16] and charge trapping[17] models. Rather our studies indicate that combinations of different models may be necessary to explain the generation of defects with different characteristics. The recombination centers for electrons are most likely positively charged or neutral defects, whereas the scattering centers for electrons can be either negatively or positively charged defects. Upon light soaking, in addition to the generation of neutral defects, defects that serve as deep trapping or recombination centers are introduced. This results in enhanced scattering and thus the decay of the drift mobility for electrons. The charged defects may become quasi-stable through some relaxation processes and can also form certain long-range potential fluctuations[19-22], if they are not spatially correlated.

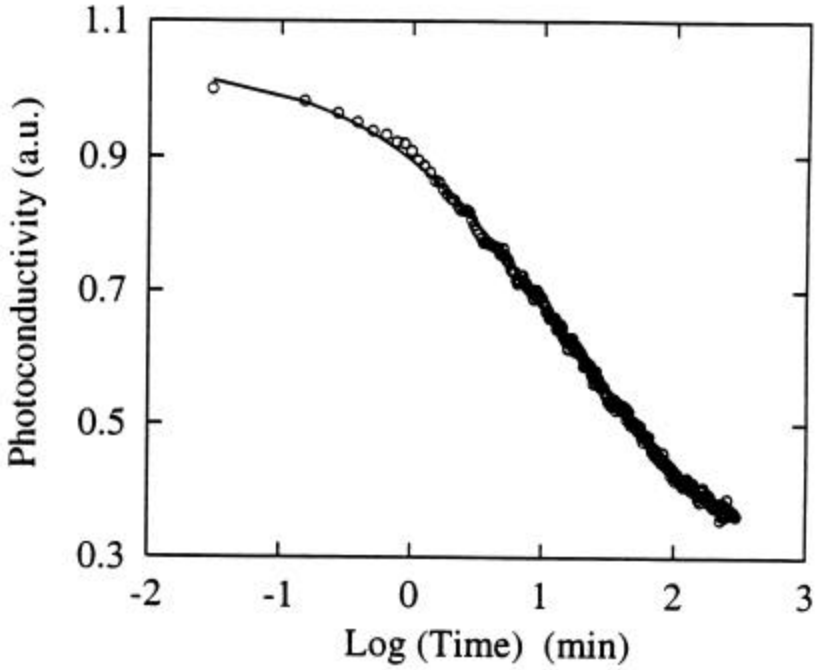

Figure 28. Photoconductivity decay vs. light soaking time for sample THD82.

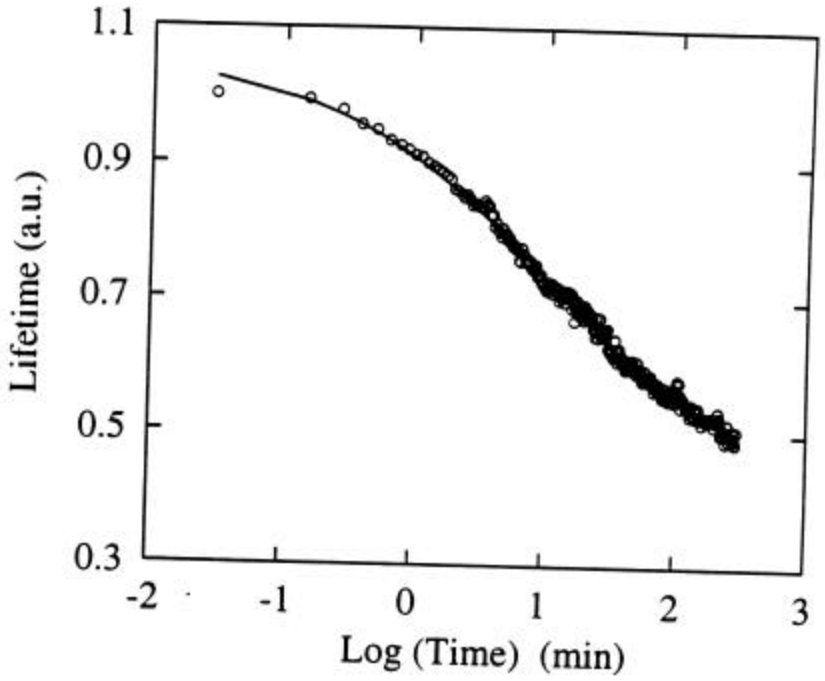

Figure 29. Lifetime decay vs. light soaking time for sample THD82.

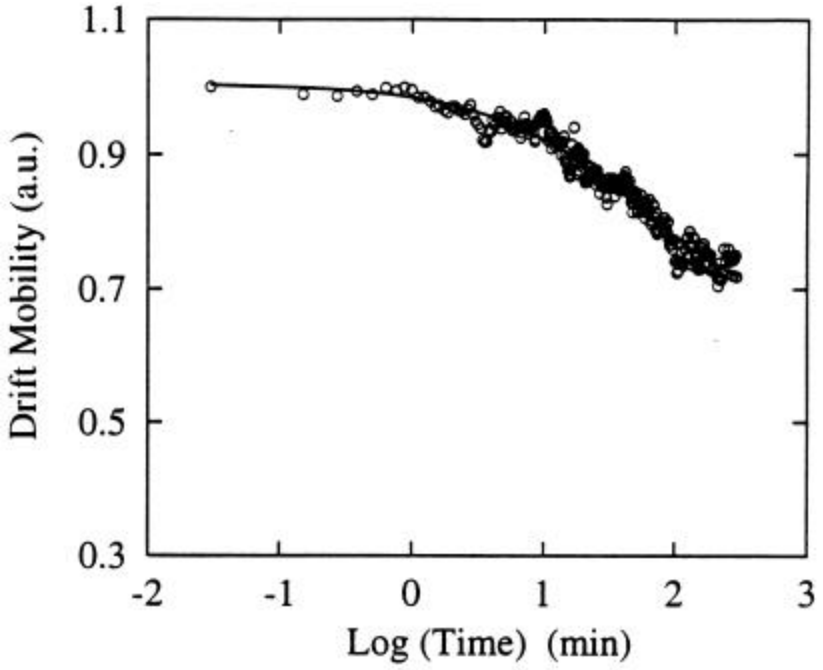

Figure 30. Drift mobility vs. light soaking time for sample THD82.

The results from curve fitting are listed in Table VI.

Table VI. Summary of results from the curve fitting of degradation measurement

Sample ID	Curve fitting from	β	τ_0 (min)
THD59	Photoconductivity	0.66	83
THD60	Photoconductivity	0.64	75
THD58	Photoconductivity	0.88	60
THD61	Photoconductivity	0.77	76
THD82	Photoconductivity	0.56	105
THD83	Photoconductivity	0.63	174
THD59	Drift mobility	0.51	23
THD60	Drift mobility	0.49	36
THD58	Drift mobility	0.88	70
THD61	Drift mobility	0.72	76
THD82	Drift mobility	0.66	95
THD83	Drift mobility	0.67	297
THD59	Lifetime	0.76	95
THD60	Lifetime	0.64	74
THD58	Lifetime	0.63	163
THD61	Lifetime	0.62	105
THD82	Lifetime	0.50	51
THD83	lifetime	0.67	258

8. Temperature dependence measurements and Urbach Energy of intrinsic a-Si:H films produced by the hot-wire technique

Extensive studies on effects of the deposition conditions, such as deposition temperature (Ts) on the structural and electronic properties of these samples have been performed in attempt to improve the quality of these films for solar cell applications.

By measuring the dc and the ac photoconductivities at a single photomixing frequency as a function of temperature, the capture rate K, and the spread of the band tail e can be determined by curve fitting the expression for the drift mobility μ_d by employing Eq. (19) and (18).

Figure 31 shows the dc photoconductivity as a function of temperature for THD 59. Figure 32 shows the temperature dependence of the drift mobility μ_d for THD59; the open circles are the experimental values while the smooth curves are curve fitted employing equation mentioned above. Similar results were obtained from the other samples (THD 58, 60, 61). The values of room temperature dc photoconductivity and drift mobility μ_d, as a function of the substrate temperature of the sample preparation, i.e. hydrogen concentration, are shown in Figures 33-34 (at 250 K) and the derived parameters ε as a function of the substrate temperature of the sample preparation, i.e. hydrogen concentration, are shown in Figures 35. (The nominal substrate temperatures are given in these figures, since we did not know the exact deposition temperatures.)

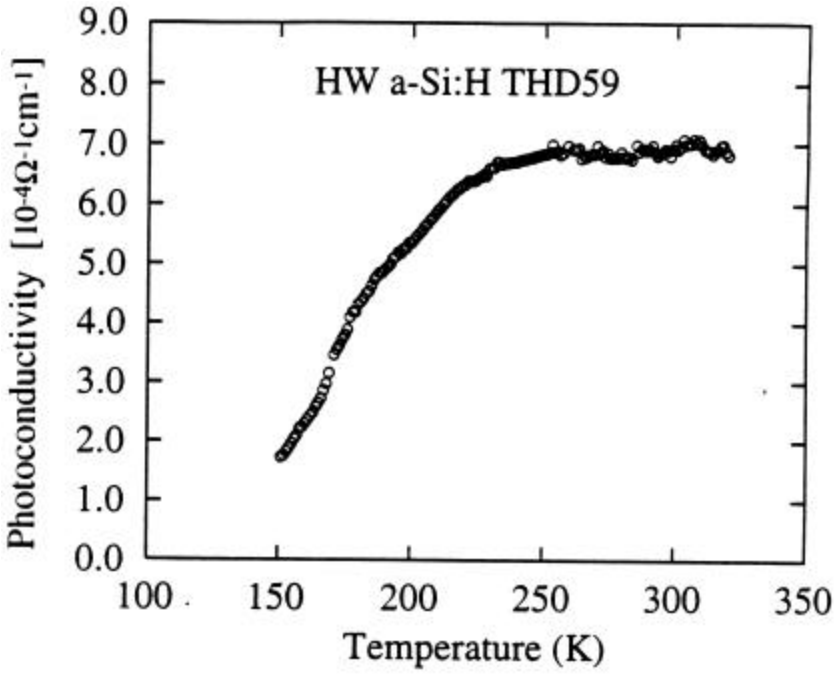

Figure 31. The dc photoconductivity as a function of measurement temperature for sample THD59.

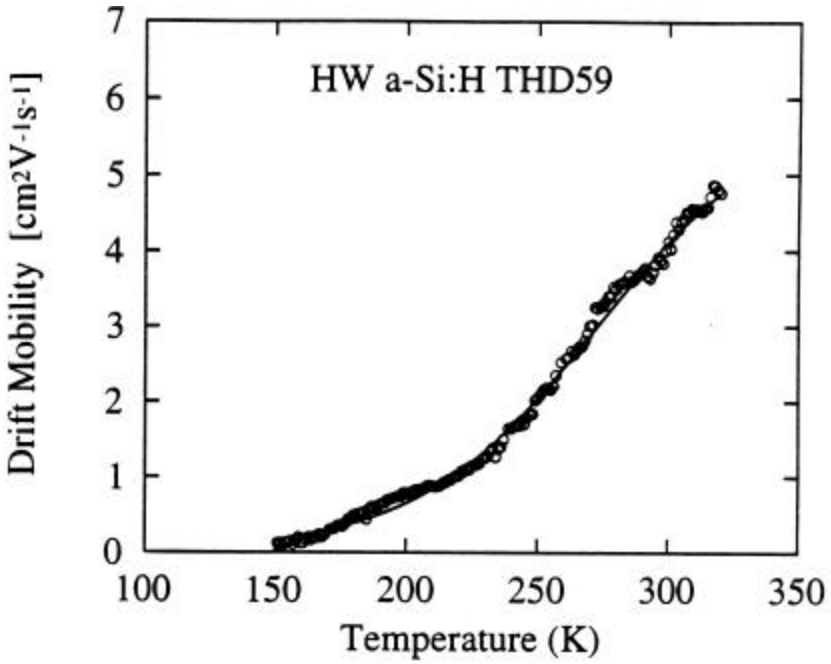

Figure 32. The drift mobility as a function of measurement temperature for sample THD59.

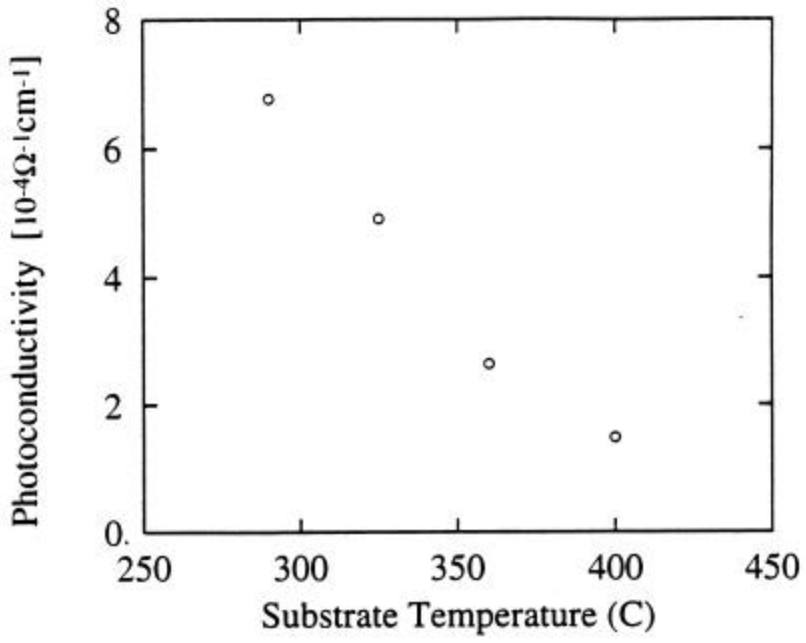

Figure 33. The photoconductivity as a function of the substrate temperature for the samples THD 58 - 61.

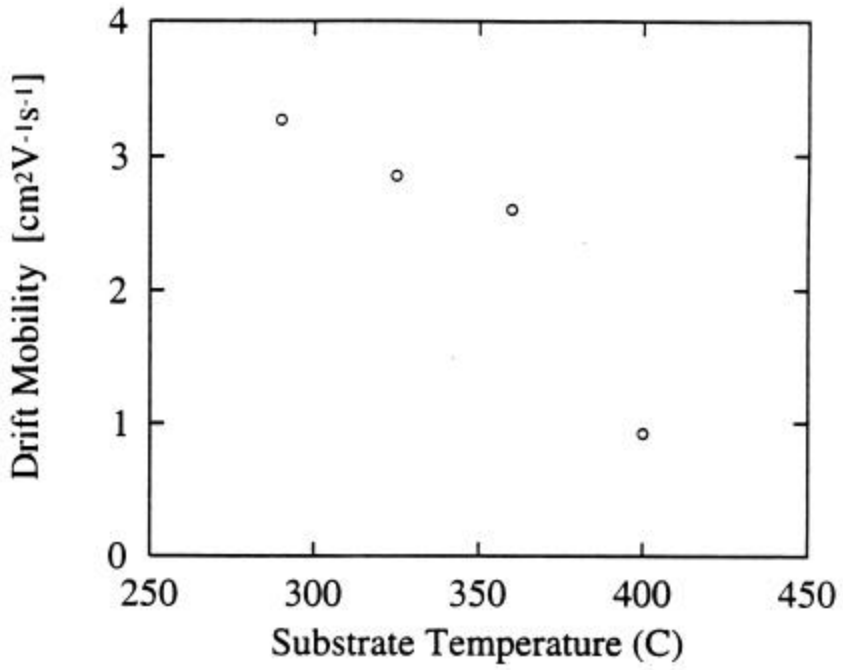

Figure 34. The drift mobility as a function of the substrate temperature for the samples THD 58 - 61.

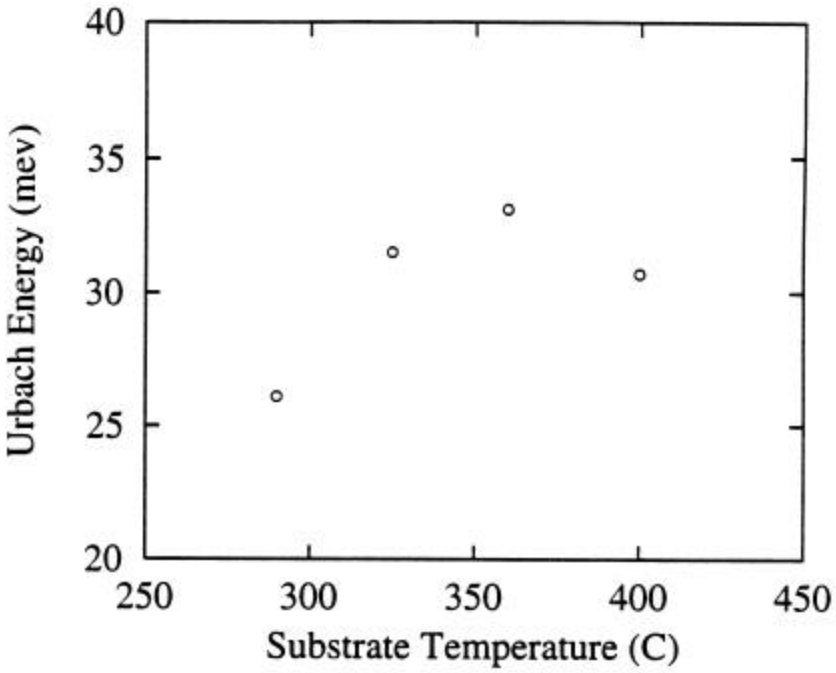

Figure 35. The Urbach energy as a function of the substrate temperature for the samples THD 58 - 61.

Because the hydrogen content of hot-wire a-Si:H films increase with the deceasing deposition (or substrate temperature), both of dc photoconductivity and drift mobility decease with the deceasing of the hydrogen content as expected, while, the Urbach energy increases with the deceasing of the hydrogen content, which is predicted by the equation 6. An exception seems to be the sample THD61.

9. Mobility and lifetime in as-grown, annealed and light soaked conditions of hot-wire intrinsic a-Si:H

We have utilized the capabilities of our photomixing technique to separately determine the mobility and lifetime under as-grown, annealed and under light soaked conditions on these samples. The samples THD58 - 61 were produced at NREL on 4/19/95 and the samples THD82 -83 were produced on 12/18/95 by Brent Nelson and Eugene Iwaniczko. Samples were prepared in a special "Hot Wire"deposition chamber attached to the doping section of NREL's "T" deposition system. It might thus be possible that different trace amounts of dopants could be present in the two sets of samples. Our goal was to characterize such samples by our techniques and gain insight into the factors which determine the properties of these films.

After light soaking for 5 hours at 4 sun intensity, all samples were annealed at 150 ^{o}C for one hour and cooled down to room temperature, whose characteristics are given in tables 7 through 9. where the drift mobility, lifetime and dc photoconductivity (σ_{dc}) are shown for given field (6050 V/cm) for the as-grown, annealed state and light soaked state.

For samples THD82-83, the values of σ_{dc} are almost the same both in the annealed and as-grown states, but the magnitude of μ_d tends to decrease, meanwhile the magnitude of τ tends to increase in the annealing process (see table 7). As a comparison, another batch of samples, THD58-61, show different behavior, as we reported early (see table 9). The values of the drift mobility in the annealed state obviously are much larger than that in the as-grown state, meanwhile, the lifetime become smaller as compared with that in the as-grown state. It indicates that the concentration or nature of the defects in the as-grown and in the annealed states could be different which depend on the process of production.

Table VII. μ_d, τ and σ_{dc} for THD82-83 (produced on 12/18/95).

Sample ID	Substrate Temp (C)	State	μ_d $cm^2V^{-1}s^{-1}$	τ ns	σ_{dc} $10^{-4}\Omega^{-1}cm^{-1}$
THD82	475	As grown	2.06	47.1	2.8
THD83	504	As grown	1.79	34.7	2.2
YHD82	475	Annealed	1.98	56.2	3.25

Table VIII. μ_d, τ and σ_{dc} for THD82-83 in all states (produced on 12/18/95).

Sample ID	Substrate Temp (C)	State	μ_d $cm^2V^{-1}s^{-1}$	τ ns	σ_{dc} $10^{-4}\Omega^{-1}cm^{-1}$
THD82	475	Annealed	1.51	46.1	2.51
THD83	504	l.s.	0.89	41.1	1.07
YHD82	475	l.s.	1.3	27.4	1.27

Table IX. μ_d, τ and σ_{dc} for THD58, 60 and 61(produced on 4/19/95).

Sample ID	Substrate Temp (C)	State	μ_d $cm^2V^{-1}s^{-1}$	τ ns	σ_{dc} $10^{-4}\Omega^{-1}cm^{-1}$
THD60	425	As grown	1.85	103.9	6.1
THD58	500	As grown	1.61	49.9	2.9
THD61	575	As grown	0.81	67.2	2.0
THD60	425	Annealed	2.23	78.3	5.8
THD58	500	Annealed	2.3	41.9	3.0
THD61	575	Annealed	1.11	45.7	1.7
THD60	425	l.s.	1.62	36.4	2.0
THD58	500	l.s.	1.36	30.5	1.5
YHD61	575	l.s.	0.84	43.8	1.3

The absolute mobility values determined in the above table depend upon the proper impedance match of the sample to the input of the spectrum analyzer.

10. Electric field dependence of mobility in hot-wire intrinsic a-Si:H films

The electric field dependence of the drift mobilities (μ_d) and the lifetimes (τ) of these samples were measured in the as-grown state, the annealed state (1hours at 150 C) and in the light soaked state (5 hours at 4 sun intensity). It was found that the drift mobility (μ_d) increases with increasing electric field, while the lifetime (τ) decreases with increasing electric field, and the $\mu\tau$ product is essentially independent of the electric field in the range from 1,000 V/cm to 10,000 V/cm. The fact that the lifetime decreases while the drift mobility increases indicates the existence of the diffusion limited transport and recombination[31] in all the samples in the light soaked as well as the as grown and the annealed states. It should be pointed out that in this case, the increase in μ_d with increasing field as well as the increasing in μ_d with increasing carrier density due to light illumination, can possibly be explained by the existence of long-range potential fluctuations. The increase in μ_d is compensated by the corresponding decrease in τ, which can result in a field independent $\mu\tau$ or the commonly observed ohmic behavior of the photocurrent. In the presence of long range potential fluctuations, one would expect m to increase with increasing electric field and with increasing carrier concentration. Such increase in the drift mobility do not necessarily lead to an increase in the photoconductivity, since one commonly observes a corresponding decrease in τ.

Figures 36-41 show the electric field dependence of the drift mobility for the hot-wire samples. The solid diamonds, open dots and solid dots are the experimental points for the annealed, the as-grown and light soaked state respectively. The solid curves were obtained by a curve fitting procedure to a model of transport through potential barriers which we presented in the paper we published[5] and described in the early sections of this report employing equations (23) and (24).

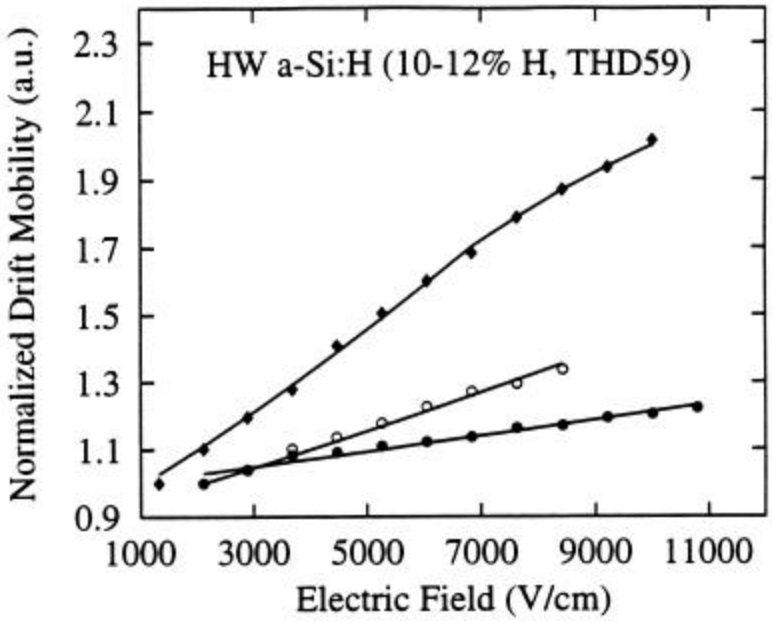

Figure 36. The normalized drift mobility versus electric field for sample THD59.

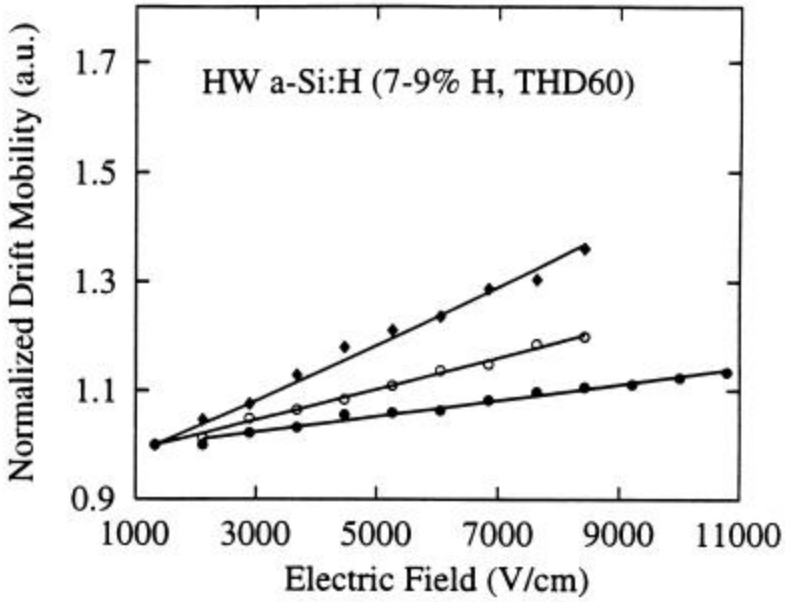

Figure 37. The normalized drift mobility versus electric field for sample THD60.

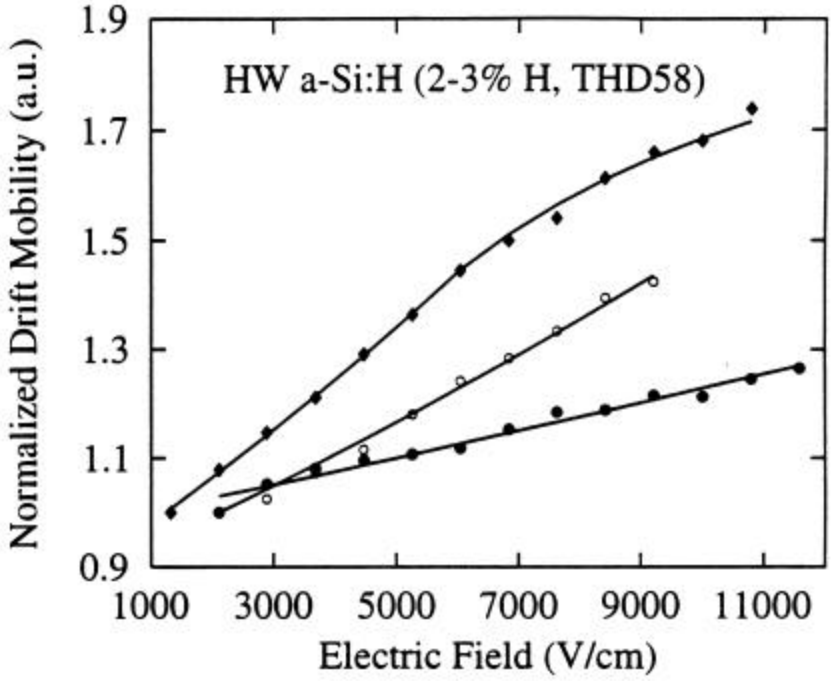

Figure 38. The normalized drift mobility versus electric field for sample THD58.

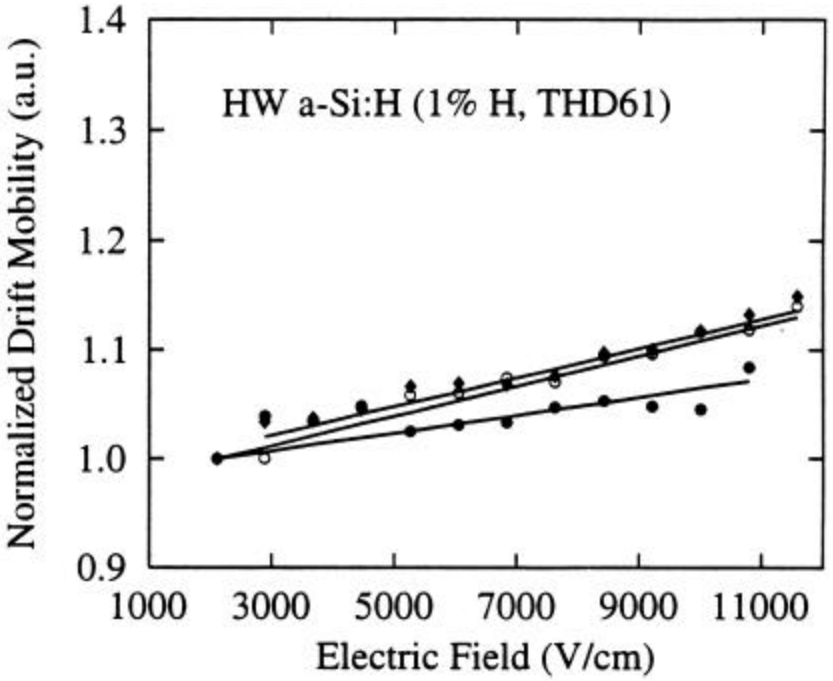

Figure 39. The normalized drift mobility versus electric field for sample THD61.

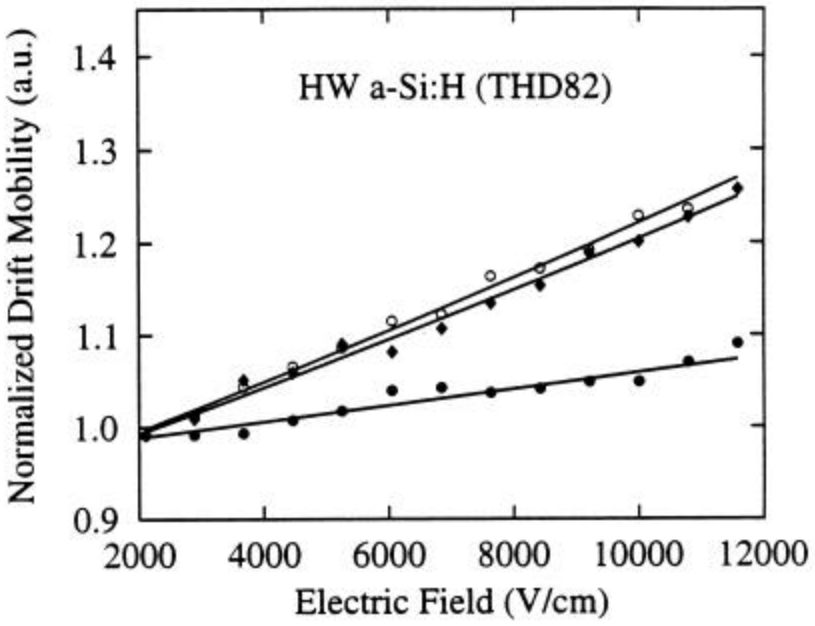

Figure 40. The normalized drift mobility versus electric field for sample THD82.

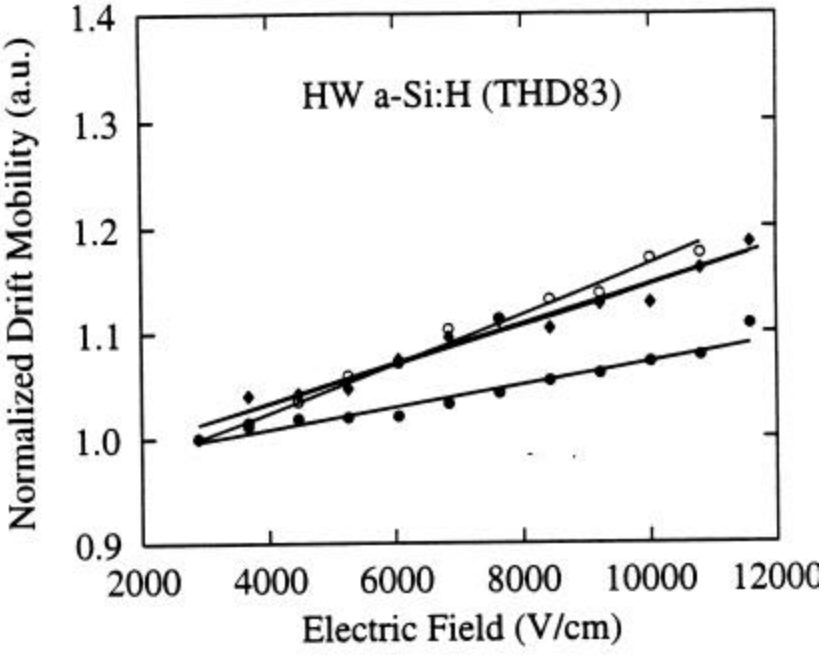

Figure 41. The normalized drift mobility versus electric field for sample THD83.

11. Photomixing measurement on solar cell devices

Photomixing measurement have been performed on two Schottky structure samples fashioned on PEVCD (TPni48) and hot-wire (THDni50) films respectively from NREL (Crandall, Mahan, Nelson). A neutral density filter was used to reduce the light intensity of the He-Ne laser. Golden spring contact was used for the electric contact. The dc dark current, dc photocurrent and mixing power versus reverse bias were measured.

Figures 42 and 43 show reverse bias dark I-V data for TPni48 and THDni50 respectively. Open circles are experimental data, solid line is a fitting curve according the empirical diode equation[46]:

$$I = I_0 \exp(qV/(nkT))(1-\exp(-qV/(kT))), \tag{26}$$

Where n is the ideality factor. A semilog plot of I/(1-exp(-qV/(kT)) versus reverse bias is a linear relation and the factor n can be obtained from the slope. The n value is 1.02 for both of these two samples.

Figures 19 and 20 shows dc photocurrent versus reverse bias for TPni48 and THDni50 respectively. Open circles are experimental data. The solid line is fitting curve employing the equation[47]:

$$J = qF(1-\exp(-aW)/(1+aL_P)) + (qP_0D_P)/D_P, \tag{27}$$

Where a: the absorption coefficient.
W: the thickness of the depletion layer.
L_P: diffusion length.
P_0: the equilibrium hole density.
D_p: the diffusion coefficient for holes.
F: the incident photon flux.

aW and aL_P can be obtained from curve fitting. When the voltage across the depletion layer is 1 volt for sample TPni48, aW and aL_P are 2.52 and 0.01, respectively. For sample THD50 aW and aL_P are 0.48 and 0.076 respectively.

Figures 46 and 47 are the square root of mixing power as a function of reverse bias. Open circles are experimental data. The solid line is fitting curve using modified Gartner's formula; Gartner discussed the transit time effects at high modulation frequencies and proposed a formula to describe the ac current vs. voltage relationship which assume all series resistances and capacitances to be negligible. We suppose that the square root of mixing power is proportional to the ac photocurrent, and assume that there is not only a surface generation. The ac photo current may be expressed as in the following equation:

$$I_{ac} \mu j\frac{ewV_D}{W} + q\Phi(\frac{1-\exp(-jw\,t_0)}{jw\,t_0} - \frac{1-\exp(-aW)\exp(-jw\,t_0)}{aW + jw\,t_0}), \qquad (28)$$

Where ε is the dielectric constant, ω is the mixing (or modulation) frequency, V_D the voltage across the depletion layer, t_0 is the transit time of carriers through the depletion layer.

The transit time of carriers through the depletion layer t_0 can be obtained from above curve fitting. They are 1.6×10^{-8} sec. and 2.3×10^{-8} sec. for TPni48 and THDni50 respectively.

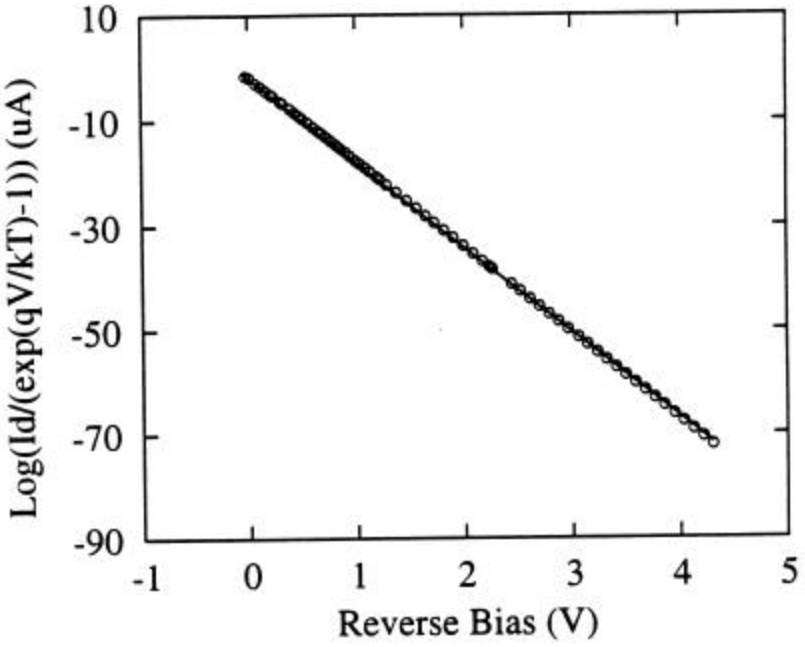

Figure 42. The dark current vs. reverse bias for Schottky sample.

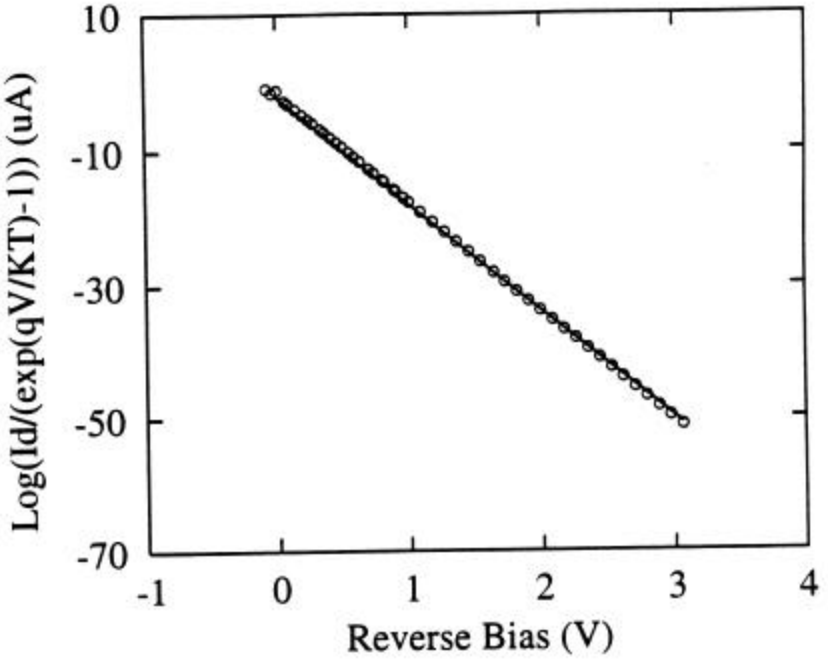

Figure 43. The dark current vs. reverse bias for Schottky sample THDni50.

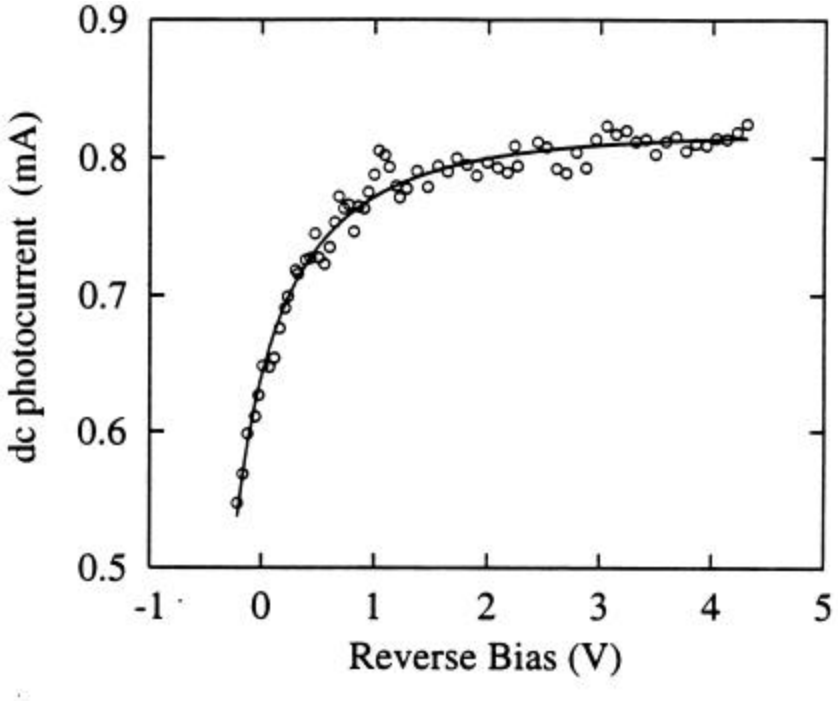

Figure 44. The dc photo current vs. reverse bias for Schottky sample TPni48.

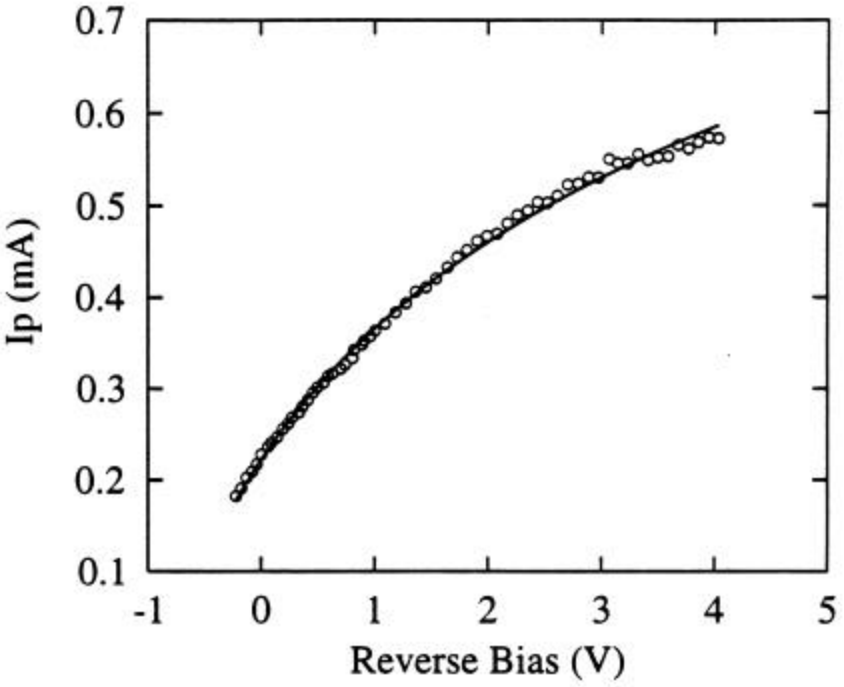

Figure 45. The dc photocurrent vs. reverse bias for Schottky sample THDni50.

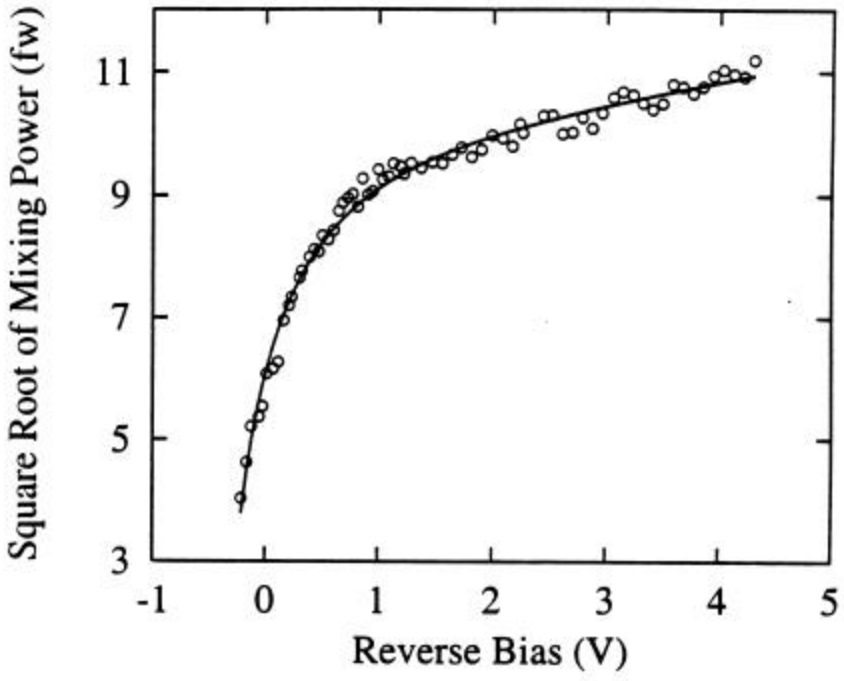

Figure 46. The mixing power vs. reverse bias for Schottky sample TPni48.

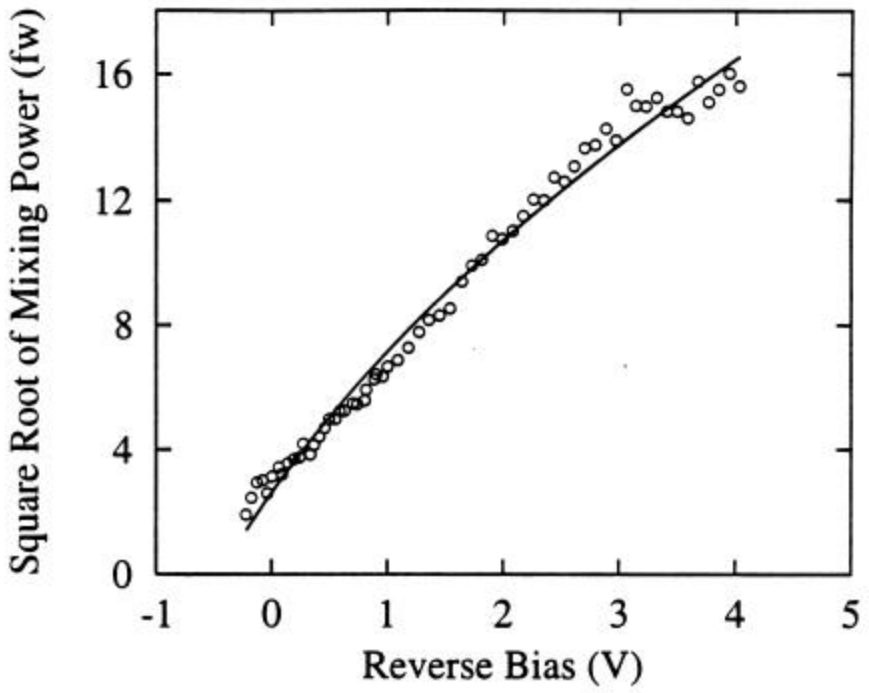

Figure 47, The mixing power vs. reverse bias for Schottky sample THDni50.

The above analysis of the Schottky barriers is preliminary; future work will extend the analysis to include the work on modulated photocurrent techniques.

12. Hot-Wire a-SiGe:H Alloys

Brent Nelson supplied us with a series of samples of a-SiGe:H alloys prepared by the hot-wire technique using varying growth parameters to explore the parameter space between pure a-Si:H and pure a-Ge:H to produce a-SiGe:H alloys to optimize the transport parameters within the two bandgap regimes: 1.40-1.45 eV and 1.60-1.65 eV. Since the number of collisions a reactive species makes before impinging on the substrate is an important deposition parameter, the chamber pressure and the distance from the filament were varied. For each composition, four samples were prepared which represented five different deposition parameters. The photoconductivity, mobility and lifetime were determined and in addition the electric field dependence of the mobility was measured enabling a determination of the range and the depth of the long range potential fluctuations for all the samples and positions. We selected the position which yielded the largest photoresponse.

Figures 48-52 show the photoconductivity, drift mobility, lifetime and range of the long-range potential fluctuations, the depth of the potential respectively as a function of the Tauc gap and therefore as a function of composition. It is significant to notice that the decrease in the photoconductivity from the a-Si:H endpoint as a-Ge:H is added to the alloy system is due primarily to the decrease in mobility while the lifetime remains constant. This decrease in mobility results from the decrease in range and the increase in the depth of the long range potential fluctuations. For a-Si:H, the presence of long-range potential fluctuations can arise from random charges which are not fully screened by free charge and result in the statistical deviation in the average charge within a volume of material yielding a spatially varying potential; in addition, other sources of potential fluctuations can be structural inhomogeneties such as voids or clusters of hydrogen bonds. The monotonic increase in the depth and the decrease in the range of the long-range potential fluctuations with increase in Ge in this alloy system suggest that compositional disorder may play a role in the long-range potential fluctuations. This point will be pursued in more detail once larger area homogeneous films are available which should be in the near future as indicated by Brent Nelson. It should also be significant to perform light-soaking measurements on the a-SiGe:H alloy system to determine the change in the range and depth of the long-range potential fluctuations.

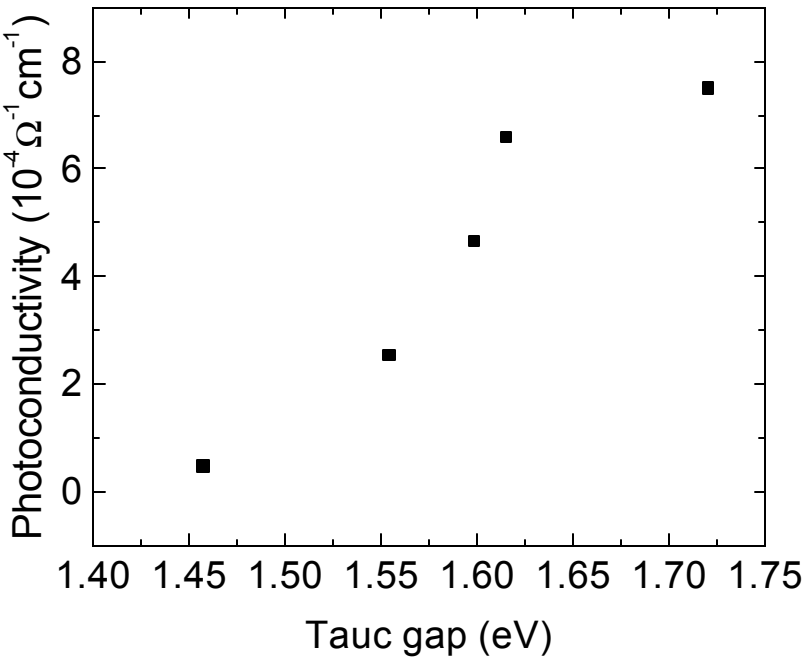

Figure 48. The dependence of the photoconductivity on the Tauc gap.

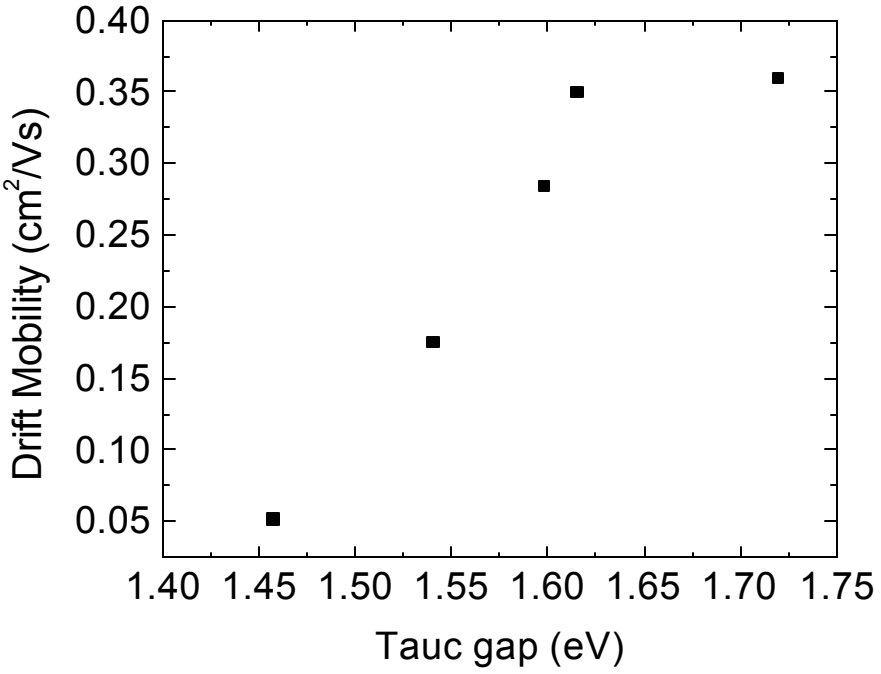

Figure 49. The dependence of the drift mobility on the Tauc gap.

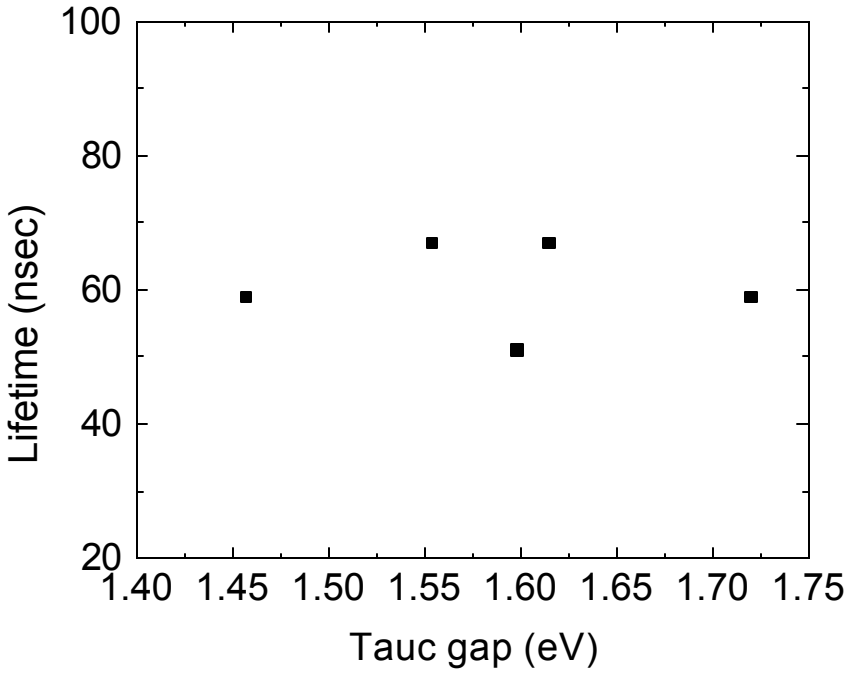

Figure 50. The dependence of the lifetime on the Tauc gap.

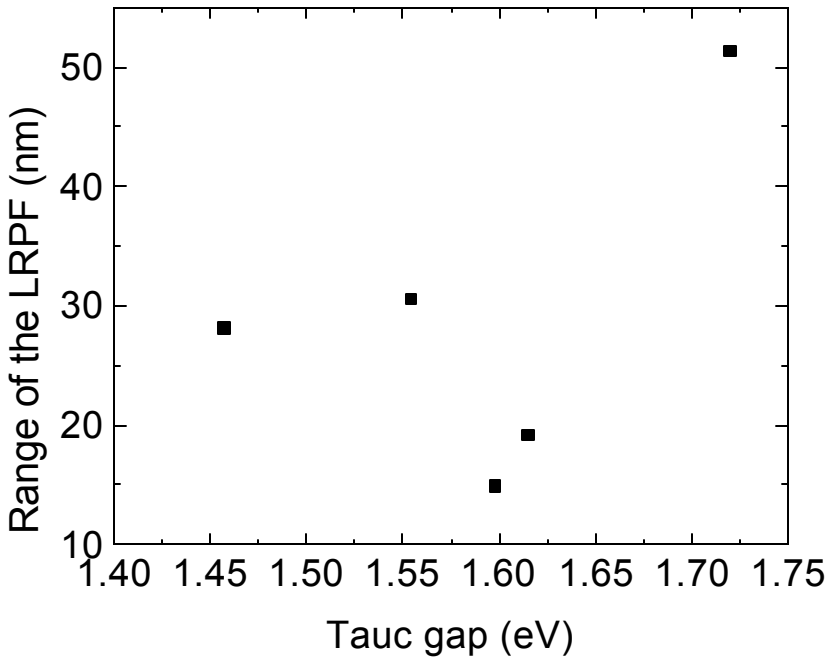

Figure 51. The dependence of the range of the long range potential fluctuation on the Tauc gap.

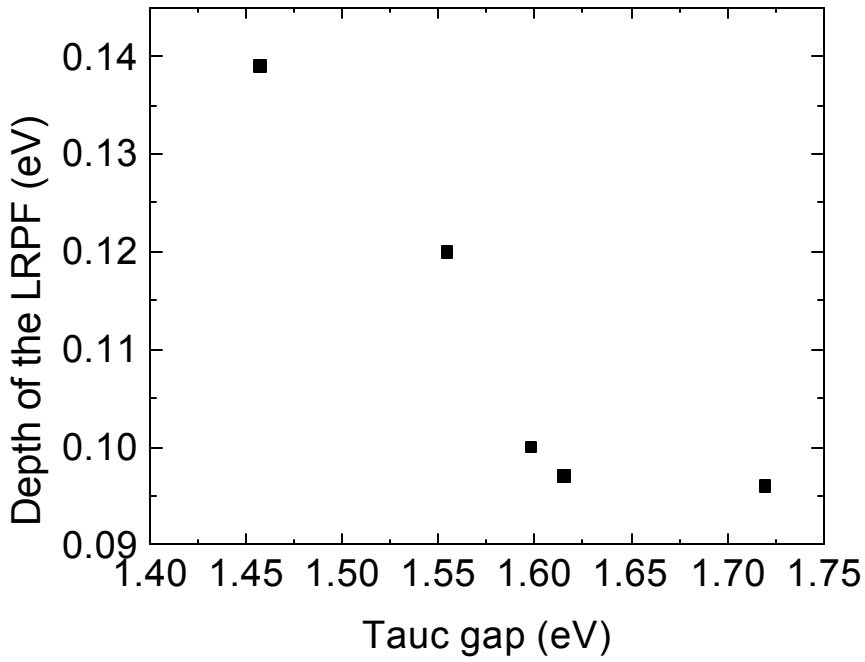

Figure 52. The dependence of the depth of the long range of potential fluctuation on the Tauc gap.

13. Atomic Force Microscopy study of the surface morphology of hot-wire a-Si:H and its correlation with the electrical properties

The morphology of thin film is of great scientific and technological importance. Evidence has been accumulating that the surfaces of a-Si:H exhibit a granular morphology for the various growth techniques. There is evidence that particles are produced in glow discharges which can be incorporated in the films during growth. This leads to the question as to whether the surface morphology is imprinted into the bulk film during growth and so influences the charge transport properties of the material.

Since we recently completed a detailed study of the charge transport properties of a-Si:H with a hydrogen content ranging from 12% to less than 1%, which were produced by the hot-wire technique varying the deposition substrate temperature, $290^0C<T_s<400^0C$ and determined the photoconductivity, mobility, and the range of the long-range potential fluctuations, it was of interest to study the morphology of the surfaces by AFM. We initiated a study with Dr. David Braunstein of the Parks Scientific to employ AFM to study systematically the surfaces of hot-wire a-Si:H. We employed a Parks Scientific Autoprobe CP in the intermitant contact mode employing a tip of 50 Angstroms.

The samples employed in this study were produced at NREL by the hot-wire assisted chemical vapor deposition technique using a filament temperature of approximately 1990^0C. A SiH_4 flow rate of 20sccm, and a chamber pressure low enough to minimize gas collisions before the film precursors hit the substrate. The films were deposited on 7059 Corning glass. [The photomixing transport measurements results on these samples were reported in S. Dong, Y. Tang, J. Liebe, R. Braunstein, R.S. Crandall, B.P. Nelson, and A.H. Mahan, J. Appl. Phys. 82, 702 (1997).]

Figure 53a shows an AFM scan of 1µm by 1µm area of a-Si:H produced at a substrate temperature of 345^0C with a hydrogen content of 6-7%. Figure 53b shows a histogram of the height distribution; analysis yields the rms roughness=17.8 Angstroms.

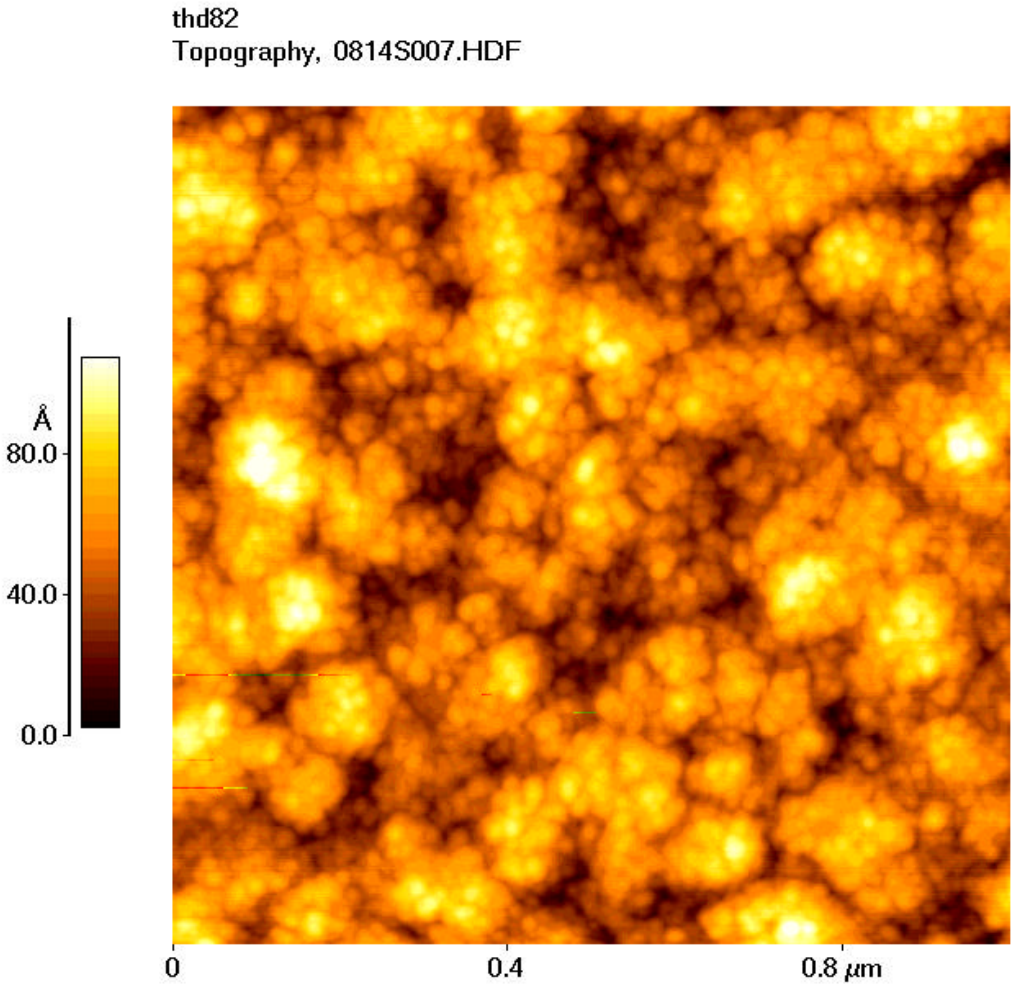

(a)

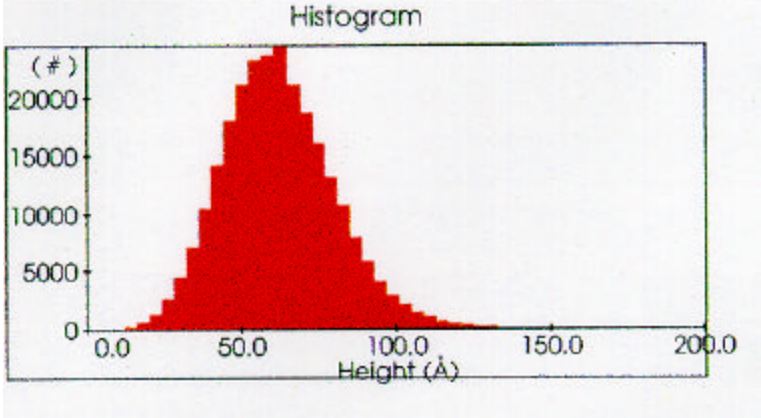

(b)

Figure 53. (a) An AFM scan of 1µm by 1µm area of a-Si:H produced at 345^{0}C; (b) A histogram of the height distribution; analysis yields the rms roughness=17.8 Angstroms.

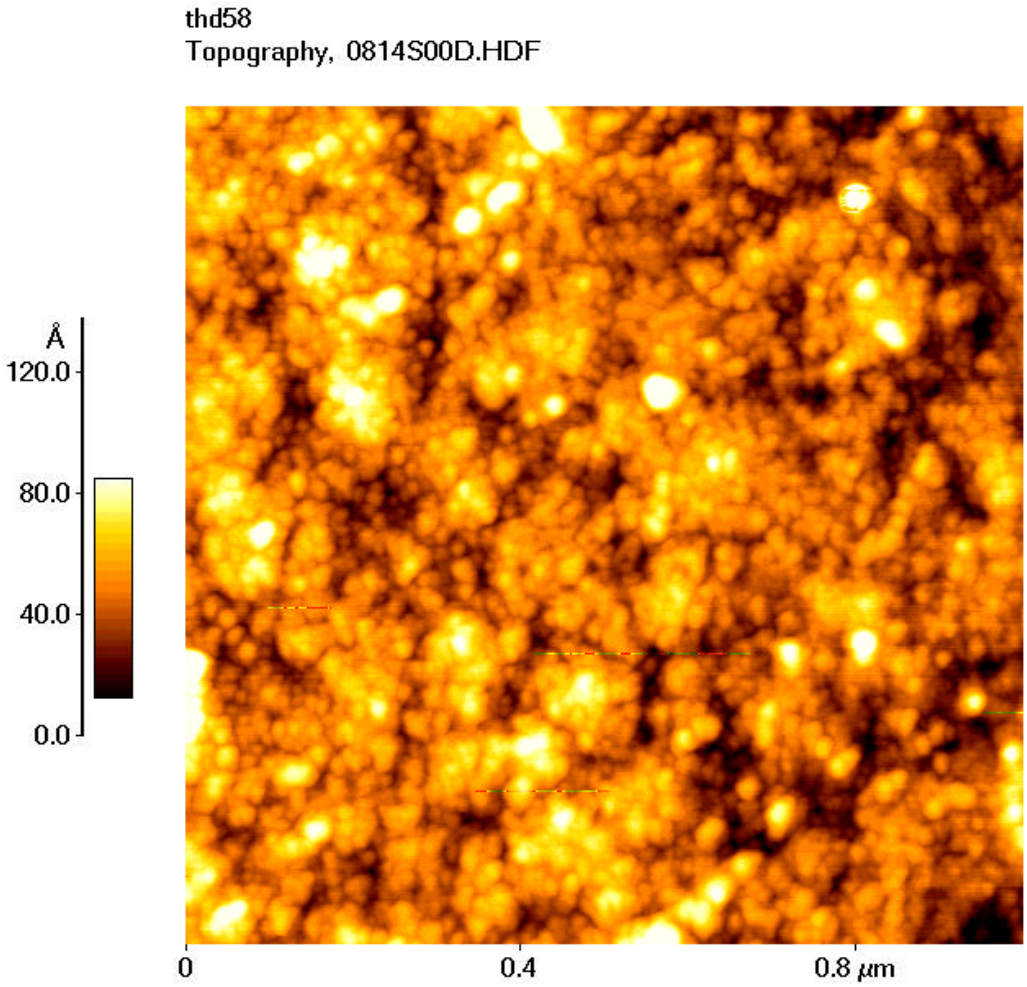

(a)

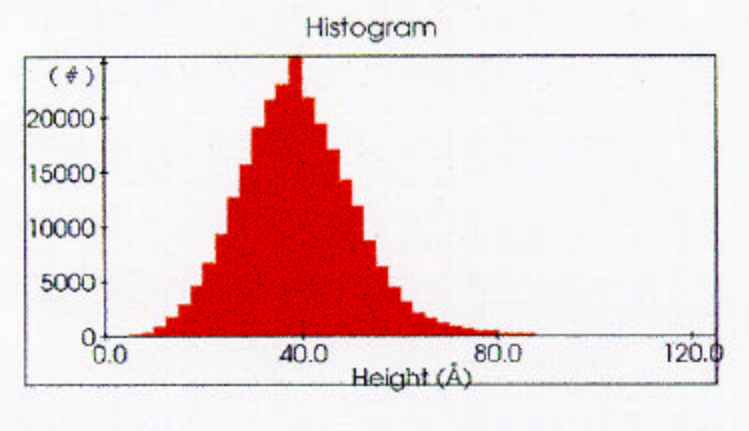

(b)

Figure 54.(a) shows an AFM scan of 1µm by 1µm area of a-Si:H produced at 360^{0}C; (b) A histogram of the height distribution; analysis yields the rms roughness=13.0 Angstroms.

Figure 54a shows an AFM scan of 1µm by 1µm area of a-Si:H produced at a substrate temperature of 360^{0}C with a hydrogen content of 2-3%. Figure 54b shows a histogram of the height distribution; analysis yields the rms roughness=13.0 Angstroms.

Table X shows the deposition substrate temperature, hydrogen content, and the rms surface roughness of the hot-wire samples.

Table X. Sample characteristics.

Sample ID	Substrate temp (^{0}C)	RMS rough (A)	H content (%)
THD59	290	20.7	10-12
THD60	325	20.0	7-9
THD82	345	18.7	6-7
THD58	360	13.0	2-3
THD83	360	12.0	2-3
THD61	400	10.4	<1

A plot of rms surface roughness as a function of substrate temperature is shown in Figure 22. It should be noted that the surface roughness decreases with increasing substrate temperature. It is tempting to interpret the surface roughness as a measure of grain size but this is not correct and the analysis of grain size has to await a fractal analysis of the AFM images which will be performed.

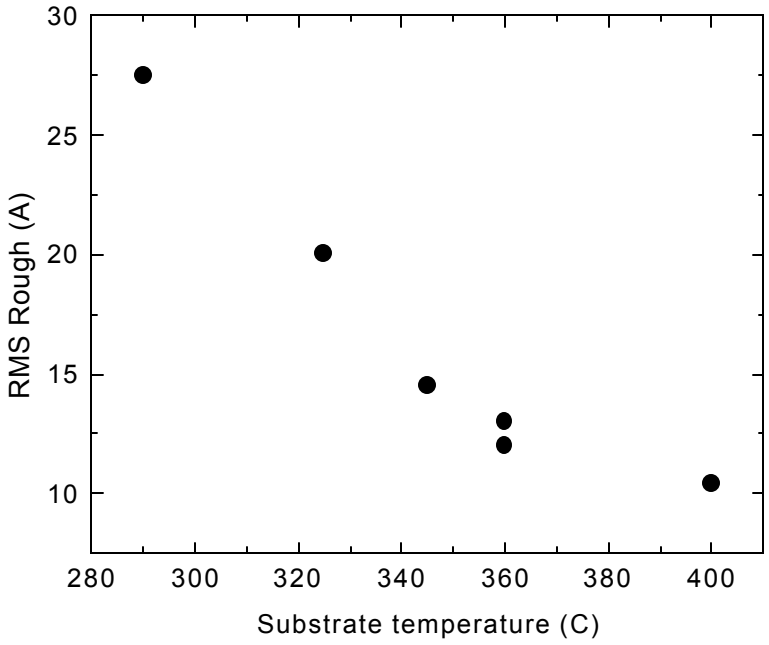

Figure 55. The RMS rough as a function of the substrate temperatures.

Figures 56, 57 and 58 show the photoconductivity, the mobility and the range of the long-range potential respectively as a function of substrate temperature. The decrease in the photoconductivity, mobility and range of the long-range potential fluctuations as the deposition substrate temperature is increased appear to be correlated with the decrease in surface roughness! If we were to interpret the decrease in the surface roughness as the decrease in grain size in the bulk of the films, we would conclude that the smaller grain sizes scatter more and are responsible for the decrease in the range of the range-range potential fluctuations! Further correlation of the surface morphology with bulk structural inhomogeneties and the relationship with charge transport must await the fractal analysis to obtain the grain size. The correlation of the surface roughness with substrate temperature indicates that the morphology of films is intrinsic to the growth process and is not due to particulates in the deposition stream.

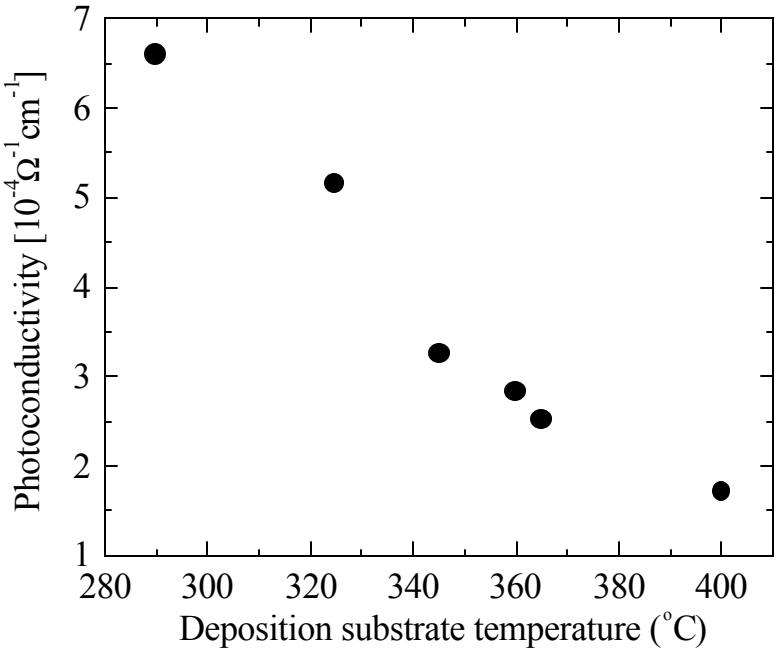

Figure 56. The annealed state photoconductivity as a function of the substrate temperatures.

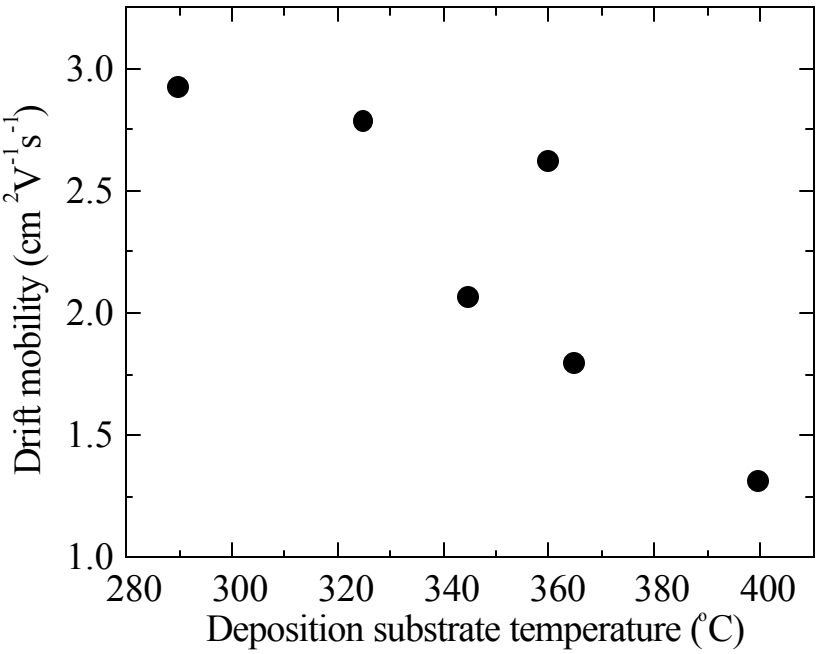

Figgure 57. The annealed state drift mobility as a function of the substrate temperatures.

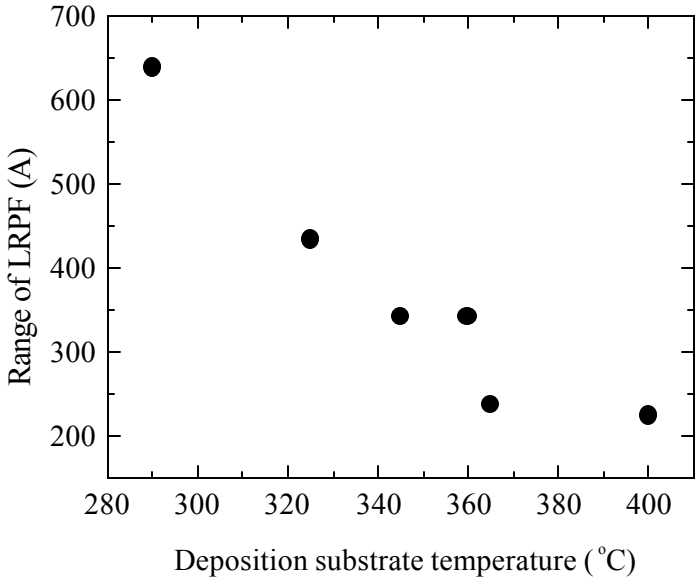

Figure 58. The range of potential fluctuations in annealed state as a function of the substrate temperatures.

14. Diluted, Undiluted and Electron Cyclotron Resonance (ECR) Produced a-Si:H

Figure 59 shows the results obtained for the diluted and undiluted samples of a-Si:H from the Wronski group. It should be noted that for the undiluted sample the lifetime and the mobility decay at approximately the same rate; while for the diluted sample the drift mobility decays more rapidly than the lifetime Table XI compares the characteristics of the diluted and undiluted samples.

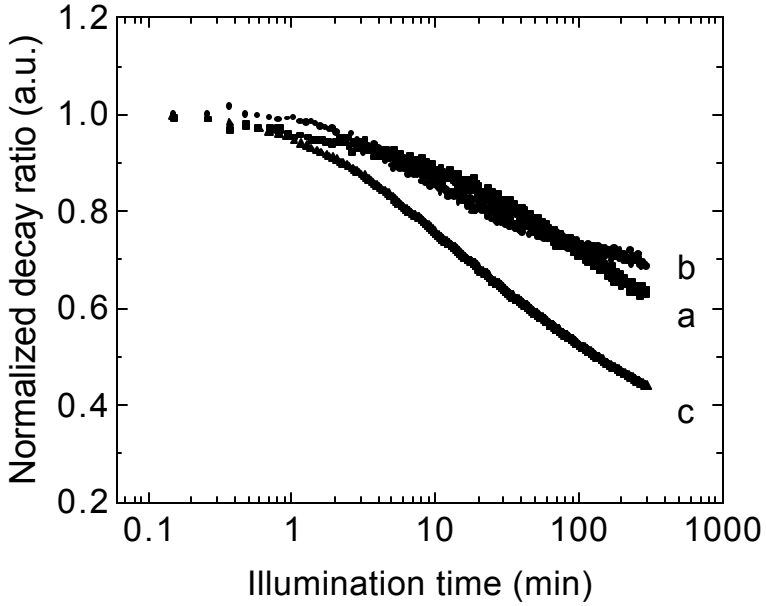

Figure 59. The decay of photoconductivity (c), lifetime (a), and drift mobility (b) as a function of illumination time with 4 suns intensity of a He-Ne laser line for undiluted a-Si:H.

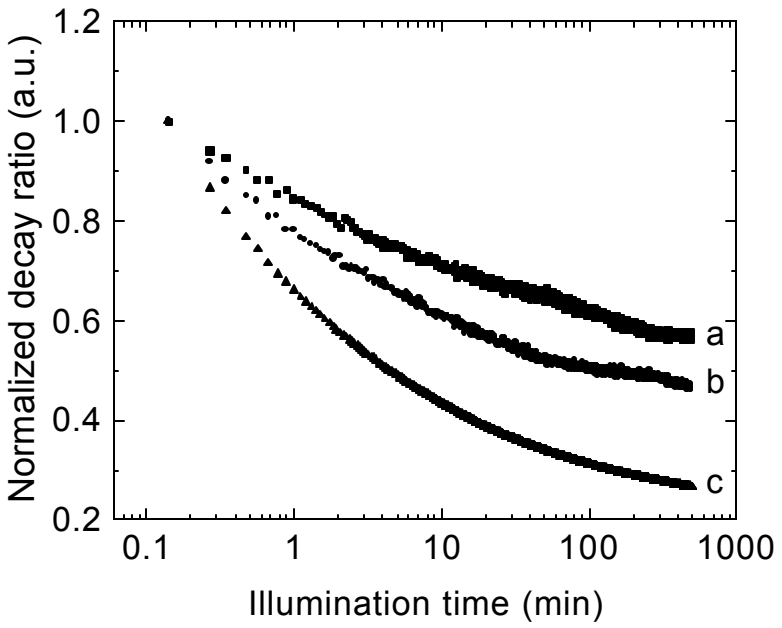

Figure 60. The decay of photoconductivity (c), lifetime (a), and drift mobility (b) as a function of illumination time with 4 suns intensity of a He-Ne laser line for diluted a-Si:H: dilution ratio 10:1 H_2 SiH_4.

Table XI. Characteristic comparison of diluted and undiluted a-Si:H samples.

	Undiluted		Diluted	
Parameters	Annealed	Light-soaked*	Annealed	Light-soaked*
σ_{pc} (10^{-4} $\Omega^{-1}cm^{-1}$)	8.94	3.93	14.94	4.05
τ (nsec)	71.37	46.80	102.4	57.36
μ (cm^2/Vs)	0.68	0.45	0.788	0.381
Range (nm)	30.27	30.14	33.07	23.4
Depth (eV)	0.0730	0.0884	0.0877	0.0926

* The light-soaked state was obtained by in situ employing the He-Ne laser with an intensity of 4 suns over a period of 5 hours illumination.

The measurement of ECR samples of a-Si:H from Dalal group are shown in Figure 61.

It should be noted that for this case the mobility decays at a slower rate than the lifetime. This is different from the case for the diluted a-Si:H shown in Figure 60 where the mobility decays more rapidly than the lifeyime. The drift mobility and liftime decay at different rates depending upon the sample preparation. Since the lifetime is generally determined by the number of neutral defects while the mobility is determined by the

charged defects, it is indicated that during light-soaking, the rates of production of neutral and charged centers differ for different samples.

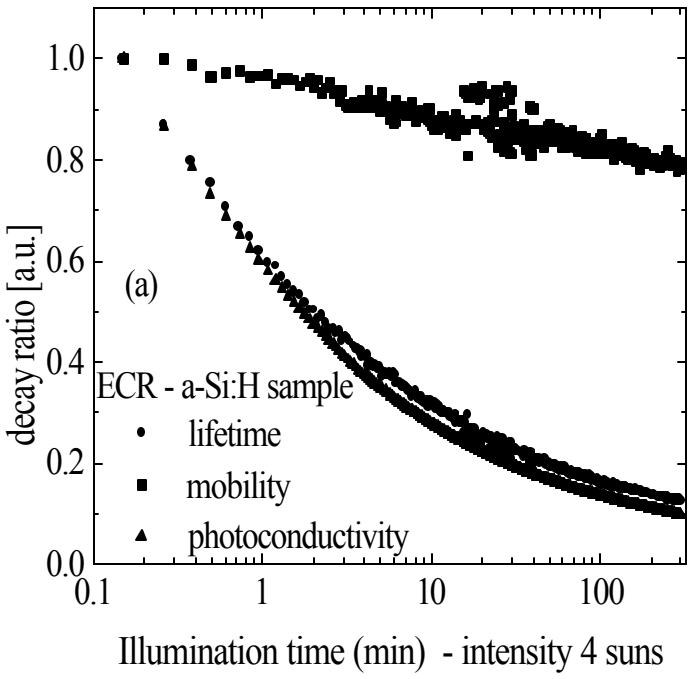

Figure 61. The decay of mobility (μ), lifetime (τ), and photoconductivity (σ).

15. Spacial dependence of lifetime, photoconductivity, range, and depth of potential fluctuations in annealed diluted a-Si:H.

Measurement of lifetime, mobility, and photoconductivityas a function of position for a diluted a-Si:H were measured for four positions separated by 5 mm along a straight line. Despite the photoconductivity being the same for all positions, the mobilities and lifetimes differed indicating inhomogeneous rate of production of neutral and charged defects during light-soaking. The results are shown in Figure 62 and Table XII.

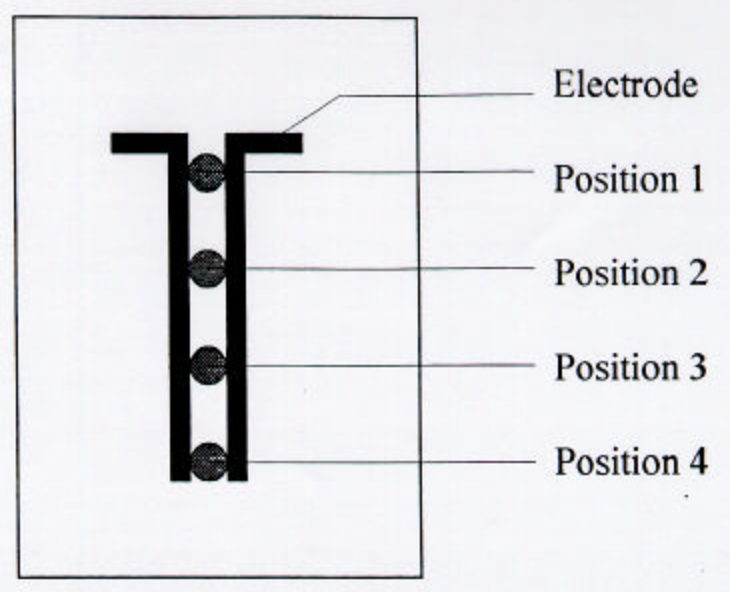

Figure 62. Schematic representation of the positions on the diluted a-Si:H sample to measure the lifetime, mobility and photoconductivity and their decays during light-soaking, separately. The separation between positions is about 5mm.

Table XII: Changes of lifetime (τ), mobility (μ), photoconductivity (σ_{PC}), range and depth of the potential in the annealed state with the relative positions on the sample.

Parameter	Position 1	Position 2	Position 3	Position 4
τ (nsec)	102.4	122.0	157.6	216.2
μ ($cm^2/V.s$)	0.788	0.712	0.579	0.378
σ_{PC} ($10^{-4}\Omega^{-1}cm^{-1}$)	14.94	16.08	16.90	15.14
Range (nm)	30.27	25.01	20.01	9.37
Depth (eV)	0.073	0.089	0.099	0.103

16. Determination of the Built-in Electric Field near Contacts to $CuInSe_2$

The built-in electric field in polycrystalline $CuInSe_2$ (CIS) near gold co-planar contact was quantitatively revealed for the first time by the photomixing technique. A He-Ne Laser beam was focused locally on the CIS sample near one of its contacts. While both dc dark and photocurrents showed ohmic behavior, the high frequency (252MHz) photomixing current showed significant non-ohmic behavior, as it was non-zero under applied dc bias, which reveals a built-in electric field ~1000V/cm. The capability of the photomixing technique to probe local charge transport properties is expected to be very useful for, e.g., the quantitative evaluation of the quality of ohmic contacts and the investigation of electric field induced p-n junction formation in CIS and related materials.

SUBCONTRACT SUPPORTED PUBLICATIONS

R. Braunstein and Yi Tang, "Charge Transport Measurements in Amorphous Semiconductors by Photoconductive Frequency Mixing", 21st International Conference on the Physics of Semiconductors, World Scientific, **Vol 1, 269** (1992)

Yi Tang, R. Braunstein and Bolko von Roedern, "Photomixing Determination of Mobility and Lifetime in Intrinsic a-Si:H", Mat. Res. Soc. Symp. Proc. **258**, 735 (1992)

Yi Tang, R. Braunstein, Bolko von Roedern and F. R. Shapiro, "Determination of Drift, Extended State Mobility and Recombination Lifetime in Compensated a-Si:H by Photomixing", Mat. Res. Soc. Symp. Proc. **297**, 407 (1993)

Yi Tang, R. Braunstein and Bolko von Roedern, "Determination of Drift Mobility and Lifetime for Dominant Charge Carriers in Polycrystalline $CuInSe_2$", Appl. Phys. Lett. **63**, 2393 (1993)

Yi Tang and R. Braunstein, "Effects of Deposition Conditions on the Transport Properties of Intrinsic Hydrogenated Amorphous Silicon and Hydrogenated Amorphous Silicon Carbide Films Investigated by the Photomixing Technique", Appl. Phys. Lett. **66**, 721 (1995)

Yi Tang, S. Dong, R. Braunstein, and Bolko von Roedern, "Effect of Light Induced Instability in Intrinsic Hydrogenated Amorphous Silicon Films by the Photomixing Technique", Appl. Phys. Lett. **68**, 640 (1996)

Yi Tang and R. Braunstein, "Continuous Decay of Drift Mobility in Intrinsic a-Si:H and a-SiC:H Upon Light Soaking Investigated by the Photomixing Technique", J. Appl. Phys. **79**, 850 (1996)

J. Liebe, K. Heinemann, K. Baerner, I. V. Medvedeva, Yi Tang, S. Dong, and R. Braunstein, "Transient Ambipolar Charge Distribution in Amorphous and Crystalline Semiconductors", Materials Science and Engineering **B** (1997)

S. Dong, Y. Tang, J. Liebe, R. Braunstein, R. S. Crandall, B. P. Nelson, and A. H. Mahan, "Transport Properties of Intrinsic Hydrogenated Amorphous Silicon Produced by the Hot-Wire Technique Investigated by the Photomixing Technique", J. Appl. Phys. **82**, 702 (1997)

S. Dong, J. Liebe, Y. Tang, R. Braunstein, and B. von Roedern, "Potential Fluctuations in Intrinsic Hydrogenated Amorphous Silicon", Proc. 14th NREL/SNL PV Program Review Meeting, Lakewood, CO (American Inst. Of Physics Conf. Proc.)

References

1. E. R. Giessinger, R. Braunstein, S. Dong, and B. G. Martin, J. Appl. Phys. 69, 1469 (1991).

2. Yi Tang, R. Braunstein, and B. von Roedern, Mat. Res. Soc. Symp. Proc. 258, 735 (1992).

3. Yi Tang, R. Braunstein, B. von Roedern, and F. R. Shapiro, Mat. Res. Soc. Symp. Proc. 297, 407 (1993).

4. R. Braunstein and Yi Tang, Proceedings of the 21st International Conference on Physics of Semiconductors (August 1992), Beijing, China, 1, 269.

5. Yi Tang, R. Braunstein, and B. von Roedern, Appl. Phys. Lett. 63 (17), 2393 (1993).

6. R. Brüggemann, C. Main, J. Berkin, and S. Reynolds, Phil. Mag. B 62, 29 (1990).

7. H. Oheda, J. Appl. Phys. 52, 6693 (1981).

8. M. Stutzmann, W. B. Jackson, and C. C. Tsai, Phys. Rev. B 32, 23 (1985).

9. T. J. McMahon and J. P. Xi, Phys. Rev.B 34, 2475 (1986).

10. D. Redfield and R. H. Bube, Phys. Rev. Lett. 65, 464 (1990).

11. R. Biswas, I. Kwon, and C. M. Soukoulis, Phys. Rev. B 44, 3403 (1991).

12. M. Stutzmann, Phil. Mag. B 56, 63 (1987).

13. M. Stutzmann, Phil. Mag. B 60, 531 (1989).

14. J. Kakalios, R. A. Street, and W. B. Jackson, Phys. Rev. Lett. 59, 1037 (1987).

15. W. B. Jackson, Phys. Rev. B 41, 10257 (1990).

16. D. Adler, Solar Cells 9, 133 (1982).

17. R. H. Bube, L. Benatar, and D. Redfield, J. Appl. Phys. 75, 1571 (1994).

18. H. Fritzsche, J. Non-Cryst. Solids 6, 49 (1971).

19. H. Overhof and W. Beyer, Phil. Mag. B 43, 433 (1981).

20. H. M. Branz and M. Silver, Phys. Rev. B 42, 7420 (1990).

21. B. von Roedern and A. Madan, Phil. Mag. B 63, 293 (1991).

22. H. Overhof, Mat. Res. Soc. Symp. Proc. 258, 681 (1992).

23. R. A. Street, Appl. Phys. Lett. 42, 507 (1983).

24. Q. Wang, H. Antoniadis, and E. A. Schiff, Appl. Phys. Lett. 60, 2791 (1992).

25. J. Takada and H. Fritzsche, Phys. Rev. B 36, 1706 (1987)

26. P. G. LeComber, A. Madan, and W. E. Spear, J. Non-Cryst. Solids 11, 219 (1972).

27. R. H. Klazes, M. H. L. M. Van Den Broek, J. Bezemer, and S. Radelaar, Phil. Mag. 45, 377 (1982).

28. M. H. Brodsky, M. A. Frisch, J. F. Ziegler, and W. A. Lanford, Appl. Phys. Lett. 30, 561 (1977).

29. R. W. Collins, in Amorphous Silicon and Related Materials, edited by H. Fritzsche (World Scientific, Singapore, 1988), P. 1003.

30. C. R. Wronski, R. M. Dawson, M. Gunes, Y. M. Li, and R. W. Collins, Mat. Res. Soc. Symp. Proc. 297, 443 (1993).

31. R. M. A. Dawson, C. M. Fortmann, M. Gunes, Y. M. Li, S. S. Nag, R. W. Collins, and C. R. Wronski, Appl. Phys. Lett. 63, 955 (1993).

32. Y. -M. Li, A. Catalano, and B. F. Fieselmann, Mat. Res. Soc. Symp. Proc. 258, 923 (1992).

33. Y. Lu, I. An, M. Gunes, M. Wakagi, C. R. Wronski, and R. W. Collins, Mat. Res. Soc. Symp. Proc. 297, 31 (1993). Yi Tang, R. Braunstein, Appl. Phys. Lett. 66 (6), 721 (1995).

34. M. Silver and R. C. Jarnagin, Mol. Cryst. 3, 461 (1968).

35. H. Fritzsche, J. Non-Cryst. Solids 6, 49 (1971).

36. H. Overhof and W. Beyer, Phil. Mag. B 43, 433 (1981).

37. D. Han and H. Fritzsche, J. Non-Cryst. Solids 59-60, 398 (1983).

38. H. M. Branz and M. Silver, Phys. Rev. B 42, 7420 (1990).

39. B. von Roedern and A. Madan, Phil. Mag. B 63, 293 (1991).

40. H. Overhof and P. Thomas, "Electronic Transport in Hydrogenated Amorphous Semiconductors" (Berlin, Springer-Verlag), 114, 108 (1989).

41. S. D. Baranovskii and M. Silver, Phil. Mag. Lett. 61, 77 (1990).

42. J. A. Howard and R. A. Street, Phys. Rev. B 44, 7935 (1991).

43. C. Witt, U. Haken, M. Hundhausen, and L. Ley, Verhandlungen DPG (VI), 30, HL 26.2, Physik Verlag (1995).

44. The statistical model is based on the idea that the drift mobility is proportional to the probability of a carrier going over the potential barrier through thermal activation. The role of the external field is to change the density of states inside the potential well, thus to change the probability and the mobility. The density of states is assumed to be proportional to the spacial range inside the potential well.

45. A.H. Mahan, J. Carapella, B.P. Nelson, R. S. Crandall and I. Baberg,J. Appl. Phys. 69, 6728 (1991)

46. E. H. Rhoderich and R. H. Williams, Metal- Semiconductor Contacts, (1988)

47. Wolfgang W. Gartner,Phys. Rev. 116, 84 (1959).

REPORT DOCUMENTATION PAGE

Form Approved
OMB NO. 0704-0188

1. AGENCY USE ONLY (Leave blank)	2. REPORT DATE	3. REPORT TYPE AND DATES COVERED
	May 1999	Final Subcontract Report, 7 May 1994–30 April 1998

4. TITLE AND SUBTITLE
Photocharge Transport and Recombination Measurements in Amorphous Silicon Films and Solar Cells by Photoconductive Frequency Mixing; 7 May 1994–30 April 1998

5. FUNDING NUMBERS
C: XAN-4-13318-10
TA: PV905001

6. AUTHOR(S)
R. Braunstein, Y. Tang, S. Dong, J. Liebe, G. Sun, and A. Kattwinkel

7. PERFORMING ORGANIZATION NAME(S) AND ADDRESS(ES)
Department of Physics
University of California
Los Angeles, CA 90024-1406

8. PERFORMING ORGANIZATION REPORT NUMBER

9. SPONSORING/MONITORING AGENCY NAME(S) AND ADDRESS(ES)
National Renewable Energy Laboratory
1617 Cole Blvd.
Golden, CO 80401-3393

10. SPONSORING/MONITORING AGENCY REPORT NUMBER
SR-520-26127

11. SUPPLEMENTARY NOTES
NREL Technical Monitor: B. von Roedern

12a. DISTRIBUTION/AVAILABILITY STATEMENT
National Technical Information Service
U.S. Department of Commerce
5285 Port Royal Road
Springfield, VA 22161

12b. DISTRIBUTION CODE

13. ABSTRACT (Maximum 200 words)

This report describes work performed during this subcontract by the University of California. Thephotoconductivity, lifetime, and drift mobility of intrinsic hydrogenated amorphous silicon (a-Si:H), hydrogenated amorphous silicon carbide (a-SiC:H), and hydrogenated amorphous silicon germanium (a-SiGe:H) were determined using aphotomixing technique in the as prepared and light-soaked states. In addition to the decay of thephotoconductivity and electron lifetime, continuous decay of the electron drift mobility was found during the light-soaking process (Staebler-Wronski effect). Experimental data were fitted to a stretched exponential law. Different stretched-exponential parameters for photoconductivity, lifetime, and drift mobility were obtained, which indicates the production of defects with different generation kinetics upon light soaking. The transport properties of intrinsic a-Si:H samples (which were produced by the hot-wire technique at NREL at different substrate temperatures such that the hydrogen content ranged from >10% to <1%), were systematically studied. It was found that with increasing substrate temperature, the lifetime, the drift mobility, and thephotoconductivity decreased, but the Urbach energy (~ 0.1 eV below the conduction band) increased. These results indicate that for the a-Si:H films with increasing deposition temperature, the density of positively charged, negatively charged, and neutral defects all show a tendency to increase, in agreement with the results observed by other workers employing other measurement techniques. Researchers also found that the drift mobility of these samples increases and the lifetime decreases with increasing electric field, while the $\mu\tau$ product is essentially independent of the electric field in the range of 1,000–10,000 V/cm. The electric field dependence of mobility $(\Delta\mu)/\mu_0/(\Delta E)$ in the as-grown or/and annealed states are always larger than that in the light-soaked state. This electric field dependence of mobility can be explained by the existence of long-range potential fluctuations.

Photoemission measurements in air were performed on a-Si:H, a-SiC:H, and transparent conducting oxide layers, and revealed inhomogeneities of composition or surface contamination.

14. SUBJECT TERMS
photovoltaics ; photocharge transport ; recombination measurements ; amorphous silicon films ; solar cells ; photoconductive frequency mixing

15. NUMBER OF PAGES
85

17. SECURITY CLASSIFICATION OF REPORT	18. SECURITY CLASSIFICATION OF THIS PAGE	19. SECURITY CLASSIFICATION OF ABSTRACT	16. PRICE CODE
Unclassified	Unclassified	Unclassified	